MOMENTUM BROADENING AND COLLINEAR RADIATION IN A NON-EQUILIBRIUM QUARK-GLUON PLASMA

SIGTRYGGUR HAUKSSON

Department of Physics
McGill University
Montreal, Quebec

September 2021

A thesis submitted to McGill University in partial fulfillment of the requirements for the degree of Doctor of Philosophy

I dedicate this thesis to my family, and to the Mukusho Zen Dojo in Montréal.

Dans l'eau de l'esprit, sans souillure,
Le reflet de la lune...
Même les vagues se brisent
Et deviennent lumière...

— Dogen Zenji (1200 - 1253)

ABSTRACT

Heavy-ion collisions produce high-temperature strongly interacting matter known as the quark-gluon plasma. The plasma is out of thermal equilibrium at all stages of its evolution and thus provides a window into transport coefficients and hydrodynamization of non-equilibrium quantum chromodynamics (QCD): the theory of the strong force. Jets and photons are two experimental probes that are particularly sensitive to the evolution of the plasma, including its non-equilibrium properties. In order to use these probes to study non-equilibrium QCD, a thorough understanding of the physics of jets and photons in a non-equilibrium plasma is needed. This includes transverse momentum broadening of jet partons, as well as the collinear bremsstrahlung of photons and gluons.

In this thesis, we evaluate the rate of transverse momentum broadening of a parton in a non-equilibrium plasma. This is done by calculating the occupation density of soft gluons radiated by medium particles which are assumed to be anisotropically distributed in momentum space. Our results show that momentum broadening is reduced relative to a plasma in equilibrium because of increased screening. We furthermore establish that spurious divergences in the rate of momentum broadening are due to plasma instabilities and are cured when time evolution of the plasma is taken into account. To do this we evaluate analytically the time evolution of two-point gluon correlators in an unstable plasma. Finally, we analyze collinear bremsstrahlung of photons and gluons in a non-equilibrium plasma. Our calculation includes the Landau-Pomeranchuk-Migdal effect. We develop numerical methods to calculate the bremsstrahlung rate in an anisotropic plasma and show that the rate of photon production is reduced compared with thermal equilibrium, especially at higher photon momenta.

RÉSUMÉ

Les collisions relativistes de noyaux atomiques créent une matière à haute température dominée par l'interaction forte. Cette matière est connue sous le nom de plasma de quarks et de gluons (QGP). Le plasma est hors d'équilibre thermique pendant toute la durée de son évolution et donne ainsi accès aux coefficients de transport et d'hydrodynamization de la chromodynamique quantique (QCD) hors d'équilibre: la théorie de l'interaction forte. Deux variables expérimentales qui sont particulièrement sensibles à l'évolution hors d'équilibre du plasma sont les jets et les photons. Une étude complète des jets et des photons est nécessaire pour utiliser ces observables pour comprendre la QCD hors d'équilibre. Une telle étude inclut l'élargissement transversal de la quantité de mouvement des jets, ainsi que le bremsstrahlung collinéaire des photons et des gluons.

Dans cette thèse, nous calculons le taux de l'élargissement transversal de la quantité de mouvement d'un particule dans un plasma non-équilibré. Ce calcul est basé sur l'évaluation de la densité des gluons de basse énergie qui sont émis par des particules du plasma dont la distribution de la quantité de mouvement est anisotrope. Nos résultats montrent qu'il y a moins d'élargissement de la quantité de mouvement que dans un plasma équilibré, à cause d'un écrantage plus élevé. En outre, nous montrons que des divergences artificielles dans le taux de l'élargissement se produisent à cause des instabilités dans le plasma et disparaissent en incluant l'évolution temporelle du plasma. Dans ce but, nous calculons analytiquement l'évolution temporelle des propagateurs des gluons dans un plasma instable. Finalement, nous analysons le bremsstrahlung collinéaire des photons et des gluons dans un plasma hors d'équilibre. Ce calcul inclut l'effet Landau-Pomeranchuk-Migdal. Nous développons des méthodes numériques pour calculer le taux du bremsstrahlung dans un plasma anisotrope et montrons que le taux de productions des photons est plus bas que dans un plasma équilibré, surtout pour des photons énergétiques.

ACKNOWLEDGEMENTS

First and foremost, I'd like to thank my supervisor Charles Gale for his constant support during my PhD years. I am grateful for his countless suggestions, his technical assistance and his sound advice on physics and life in academia. I thank him for having helped me find my own research path.

I thank everybody that I have discussed with about physics generally and my work in particular during my PhD. In particular, I am indebted to Sangyong Jeon for all his helpful suggestions and for his patient explanation of complicated physics. I also thank Raju Venugopalan, Soren Schlichting, Kirill Boguslavski, Alina Czajka, Mayank Singh, Scott McDonald, and Shuzhe Shi, for helpful suggestions and useful conversations. I would particularly like to thank Stanisław Mrówczyński for his encouragement and interest. I furthermore thank everybody in my research group for their pleasant company and stimulating physics.

I thank FRQNT and Québec taxpayers for financial support during my PhD.

Finally, I thank all my friends and family for having made these years so interesting and for having been at my side in the ebb and flow of life. Most importantly, I thank my parents and sister: without their help this thesis would not have been completed.

STATEMENT OF ORIGINALITY

This thesis is based on [1], [2] and a manuscript that forms the basis of Ch. 5. These papers are all original work of the author.

In the following we describe the thesis in detail, highlighting original work. All sentences expressed in first person singular are original work.

- **Chapter 1:** A general introduction to heavy-ion collisions and hot QCD matter.
- **Chapter 2:** Sec. 2.1 is an introduction to HTL effective theory. The rest of the chapter is original work. In Sec. 2.2, I derive expressions for energy loss and momentum broadening in the real-time formalism, building on earlier work in thermal equilibrium, as well as classical treatment out of equilibrium. In Sec. 2.3, I derive the first full analytic expression of soft gluon rr correlator in anisotropic plasma.
- **Chapter 3:** All sections except Sec. 3.5 are original work. In Sec. 3.1, I provide estimates of divergences due to instabilities. In Sec. 3.2, I derive the retarded soft gluon correlator in an unstable plasma. In Sec. 3.3, I explain how parton energy loss should be evaluated in an unstable plasma, building on earlier work using classical methods. In Sec. 3.4, I derive for the first time the rr correlator in an unstable plasma. Sec. 3.5 is a literature review on instabilities in heavy-ion collisions. In Sec. 3.6, I propose a phenomenological prescription for instabilities when calculating momentum broadening in heavy-ion collisions.
- **Chapter 4:** All sections are original work and all numerical calculations are mine. In Sec. 4.1, I show how the anisotropic collision kernel depends on an IR momentum cut. In Sec. 4.2, I explore the kernel's dependence on anisotropy and provide a qualitative explanation. In Sec. 4.3, I calculate the rate of momentum broadening in different directions.

- **Chapter 5:** Sec. 5.1 is an overview of earlier work on collinear photon and gluon radiation. The rest of the chapter is original work and all numerical calculations are mine. In Sec. 5.2, I devise a numerical scheme to calculate the rate of photon production through bremsstrahlung in an anisotropic plasma. In Sec. 5.3, I use this scheme to evaluate the rate of photon production and discuss results.

CONTENTS

LIST OF FIGURES

Part I

INTRODUCTION

1

INTRODUCTION

1.1 STRONGLY INTERACTING MATTER

The strong interaction, also known as the strong nuclear force, is one of the four fundamental forces in the Universe, along with the electromagnetism, gravity and the weak interaction. It binds elementary particles known as quarks and gluons together in composite hadrons such as protons and neutrons. The complicated structure of hadrons as well as most of their mass is therefore due to the strong interaction. This interaction furthermore binds protons and neutrons into nuclei and explains nuclear reactions such as fusion and some types of nuclear fission.

Everyday phases of matter such as solids, liquids and gases, as well as some more exotic phases like superconductors and superfluids, arise from the electromagnetic interaction between electrons and ions. Matter interacting through the strong force may have the same richness of phases but is less explored. Such matter is particularly interesting because the mediator of the strong interaction, known as gluons, interact among themselves (see below) giving qualitatively different dynamics from electromagnetism. The different phases of strong matter can be characterized by the temperature T, and the baryon chemical potential μ_B which quantifies the imbalance between quark and antiquark number.

There are many examples of matter interacting through the strong force, see Fig. 1.1. Roughly $10\,\mu$s after Big Bang, our Universe was filled with a soup of particles at low baryon chemical potential and at an extreme temperature of roughly 10^{10} K to 10^{12} K. This matter is known as the quark-gluon plasma (QGP) and its dynamics is governed by the strong interaction between quarks and gluons. As the Universe expanded, the QGP cooled and quarks and gluons became confined in the protons and neutrons we see today. Another example of strongly-interacting matter are neutron stars, the final

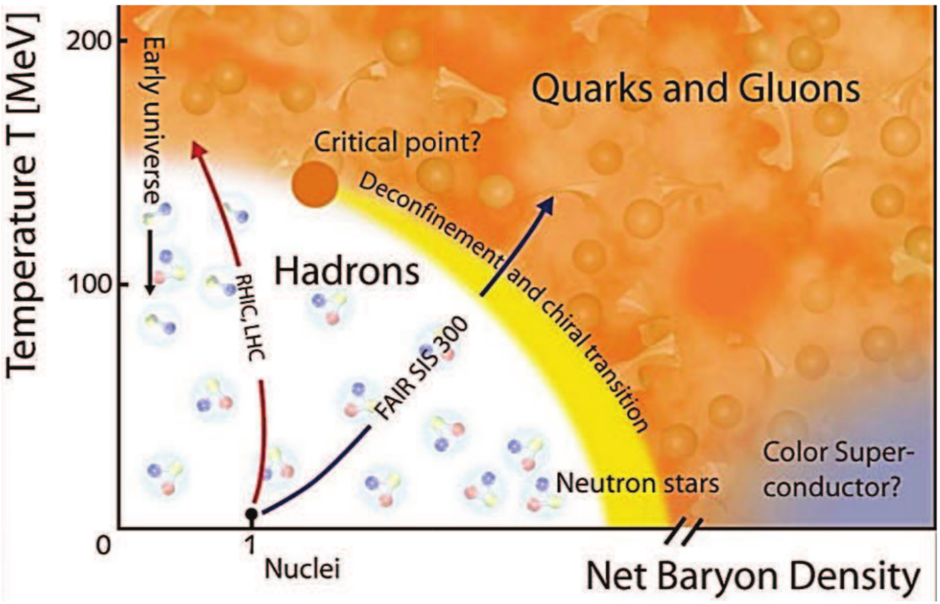

Figure 1.1: Phase diagram for QCD matter. Figure from [3].

stage in the evolution of heavy stars that do not form a black hole. Neutron stars are extremely dense clumps of nuclear matter at high baryon chemical potential. They are relatively cold as kinetic energy has escaped with neutrinos. Studying their properties is one of the main motivations for gravitational wave detection performed by LIGO [4].

Experiments are essential to understand the quark-gluon plasma and other phases of strongly-interacting matter. Since at least two decades, this has been made possible in heavy-ion collisions in which two heavy nuclei are made to collide at extremely high energies in particle colliders. The violent collisions convert kinetic energy into thermal energy of the nuclear matter which reaches temperatures high enough to form a small droplet of the QGP. Since a great abundance of quarks and antiquarks are created in these energetic collisions, the net chemical potential of the QGP is close to zero. [1] Focusing on heavy-ion collision at the highest available energy, there are two places in the world where experiments are performed: the Large Hadron Collider (LHC) in CERN and the Relativistic Heavy-Ion Collider (RHIC) at the Brookhaven National Laboratory in the

1 Heavy-ion collisions can also be used to study matter at high temperature and moderarely high baryon chemical potential. This is done by colliding nuclei at lower energy so that fewer pairs of quarks and antiquarks are produced. Then the initial quark content of the nucleons is more dominant and QGP at higher baryon chemical potential is created [5].

U.S., see [6] for a review. The LHC predominantly collides two Pb nuclei at energies of 2.76 TeV or 5.02 TeV per nucleon, while RHIC predominantly collides two Au nuclei at energies of 200 GeV per nucleon. Both experiments are capable of colliding other nuclei, as well as a nucleus and a proton.

In heavy-ion collisions, there is nothing containing the quark-gluon plasma. Therefore, the QGP droplet expands and its temperature drops, meaning that experiments gives access to different regions of the phase diagram of strong matter. As the temperature becomes sufficiently low, the QGP becomes a gas of hadrons which end up flying into detectors where their energy, momentum and species can be measured. The challenge in heavy-ion collisions is that the quark-gluon plasma cannot be manipulated like in condensed-matter experiments as it only exists for a time of the order of 10 fm $\sim 10^{-22}$ s.[2] Thus we must deduce properties of the QGP from measurements of probes emitted by the quark-gluon plasma, including the yield and angular correlation of final-stage hadrons.

There are multiple experimental probes of the quark-gluon plasma in addition to final-stage hadrons. Together they give a complete picture of heavy-ion collisions. For instance, photons are radiated by electrically charged quarks in the plasma and their yield and energy give an indication of the plasma's temperature, see [7] for a discussion. Even more important are jets which are collimated showers of high-energy particles, formed as two partons scatter at large angles in the initial collision of nuclei. As jets traverse the quark-gluon plasma, they lose energy and broaden, leaving them with detailed information about the QGP medium.

1.2 QCD AT FINITE TEMPERATURE

To understand the quark-gluon plasma and other phases of strongly interacting matter, the theory of the strong force is needed. This theory is quantum chromodynamics (QCD) which is a gauge theory with fermions known as quarks and gauge bosons known as gluons. In principle, QCD calculations should allow us to deduce thermodynamic prop-

2 We use units where $c = \hbar = k_B = 1$ and metric $g^{\mu\nu} = Diag(1, -1, -1, -1)$. Thus time can be expressed in units of length and temperature is expressed in units of energy.

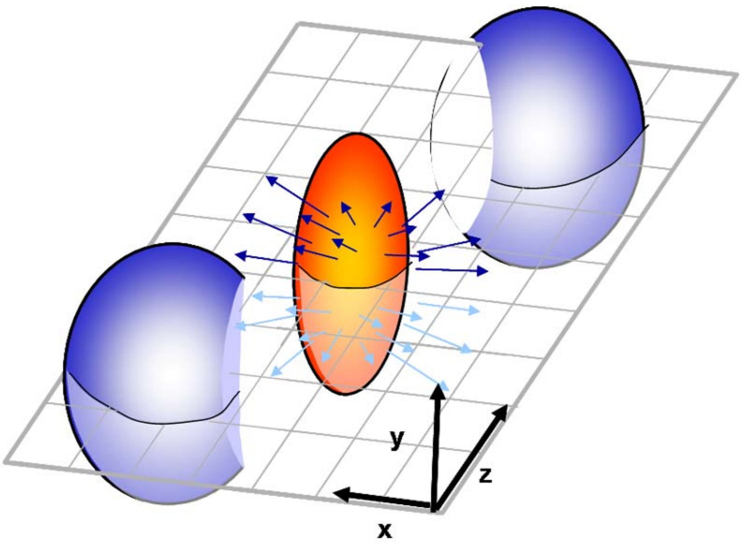

Figure 1.2: Schematic view of heavy-ion collisions. The beam axis is in the z-direction and the the transverse plane is the xy plane.

erties of the plasma, as well as its interaction with probes such as jets and photons. QCD is well established experimentally in high-energy experiments such as deep inelastic scattering and electron-positron annihilation, see [8] for an early review. In more recent years, QCD has been used to explain low-energy physics such as masses of light nuclei [9].

The dynamics of quarks and gluons in QCD is given by the Lagrangian

$$\mathcal{L} = \sum_j \bar{\psi}_j \left(i\not{D} - m_j \right) \psi_j - \frac{1}{4}\mathcal{F}_{\mu\nu}\mathcal{F}^{\mu\nu}, \tag{1.1}$$

see e.g. [10]. We have suppressed colour indices and reproduce the field strength tensor $F^{\mu\nu}$ below. The quarks ψ come in six different flavours known as up, dow, strange, charm, bottom and top, which we label as j. These flavours are different elementary particles with different masses m_j. The defining feature of QCD is that each quark has an intrinsic degree of freedom known as colour charge which is labelled by three indices sometimes referred to as red, green and blue. More precisely, the quarks are in the fundamental representation of the gauge group $SU(3)$, meaning that their colour charge is given by three complex numbers which transform as

$$\psi_a(x) \to \left(\exp(i\alpha^B(x)t^B) \right)_{ab} \psi_b(x). \tag{1.2}$$

under a local colour rotation which also acts as a gauge transformation. Here t^B are the eight generators of SU(3) that act on the fundamental representation, the functions $\alpha^B(x)$ specify the local colour rotation and a and b are colour indices of quarks.

The covariant derivative in the quark part of the QCD Lagrangian is

$$D_\mu := \partial_\mu - igA^B_\mu t^B \tag{1.3}$$

where g is the strong coupling constant. The gauge bosons A^B_μ transform under colour rotation in such a way that the quark part of the Lagrangian remains invariant,

$$A^B_\mu(x)t^B \to V(x)A^B_\mu(x)t^B\, V(x)^\dagger + \frac{i}{g}V(x)\partial_\mu V(x)^\dagger \tag{1.4}$$

with $V(x) = \exp(i\alpha^C(x)t^C)$. The first term shows that the gluons are in the adjoint representation of $SU(3)$. In essence, they have two colour indices each of which is rotated by the matrix $V(x)$ under colour rotation. The second term in Eq. (1.4) shows that the gluons are gauge bosons with colour rotation giving a change in gauge. The dynamics of the gluons is given by the field strength tensor

$$\begin{aligned} \mathcal{F}^B_{\mu\nu}t^B &:= \frac{i}{g}\left[D_\mu, D_\nu\right] \\ &= \partial_\mu A^B_\nu t^B - \partial_\nu A^B_\mu t^B + igA^C_\mu A^D_\nu \left[t^C, t^D\right] \end{aligned} \tag{1.5}$$

which transforms as $\mathcal{F}^B_{\mu\nu}(x)t^B \to V(x)\mathcal{F}^B_{\mu\nu}(x)t^B V(x)^\dagger$ under colour rotation. As gauge bosons, the gluons mediate the strong force between quarks. Unlike photons in electromagnetism, gluons interact with each other as can be seen in the last term in Eq. (1.5). This gives rise to much more complicated dynamics than in electromagnetism.

One of the striking features of QCD is asymptotic freedom, the fact that the strong coupling g grows weaker at shorter distances and higher momenta [11, 12]. This is quantified by the beta function, $\beta(g) = dg/d\log Q$, which describes how the coupling g changes as the energy scale Q increases. In QCD the beta function is negative. At leading order in the coupling constant it is

$$\beta(g) = -\frac{g^3}{(4\pi)^2}\left(11 - \frac{2}{3}n_f\right) \tag{1.6}$$

where n_f is the number of quark flavours below Q. At high enough energy, it is therefore possible to expand an observable as a Taylor series in g and in principle calculate it order by order, giving ever more refined answers. We will assume weak coupling throughout this thesis, which is justified at high enough temperature.[3] The rules for calculating Feynman diagrams in QCD in a weak-coupling expansion can be found in any number of textbooks [10].

The converse of asymptotic freedom is a large value of the coupling at low energy. At those energy scales, quarks and gluons are confined in colour-neutral hadrons. In a gluon dominated plasma this is quantified by the so-called Polyakov loop [14]. Furthermore, chiral symmetry is broken, , which roughly means that a condensate is formed which pairs quarks with left-handed polarization and antiquarks with right-handed polarization [10].

Ideally, we would like to predict the different phases of strong matter directly from the QCD Lagrangian in Eq. (1.1). The theoretical tool that comes closest to realizing this is lattice QCD, see [15, 16] for reviews. In lattice QCD one calculates directly the thermodynamic partition function

$$Z = \sum_n e^{-\beta E_n} = \mathrm{Tr}\left[e^{-\beta H}\right] \tag{1.7}$$

at finite temperature $\beta = 1/T$ where H is a QCD Hamiltonian. This is done by expressing the partition function as a path integral over different field configurations, including different color configuration,

$$Z = \int \mathcal{D}\bar{\psi}\mathcal{D}\psi\mathcal{D}A^\mu e^{\int_0^\beta d\tau \int d^3\mathbf{x}\mathcal{L}_{QCD}} \tag{1.8}$$

and evaluating the path integral numerically. The derivation of Eq. (1.8) is the same in vacuum except that the usual time variable has been Wick-rotated to $t \to -i\tau$ with $0 \leq \tau \leq \beta$ to account for the finite temperature in Eq. (1.7). Furthermore, field configurations must be the same for $\tau = 0$ and $\tau = \beta$ because of the trace in Eq. (1.7). (There is a relative minus sign between fermions at $\tau = 0$ and at $\tau = \beta$ [17].)

Fig. 1.3 shows lattice results for the temperature dependence of the energy density and pressure of QCD matter at $\mu_B = 0$. There is a rapid increase in both energy density and pressure around $T = 155\,\mathrm{MeV}$. This is the crossover region between two phases with very different properties. The low-temperature phase is known as hadronic gas in

3 At finite temperature, there is a limit to how high an order one can calculate quantities. This is due to unscreened magnetic modes [13].

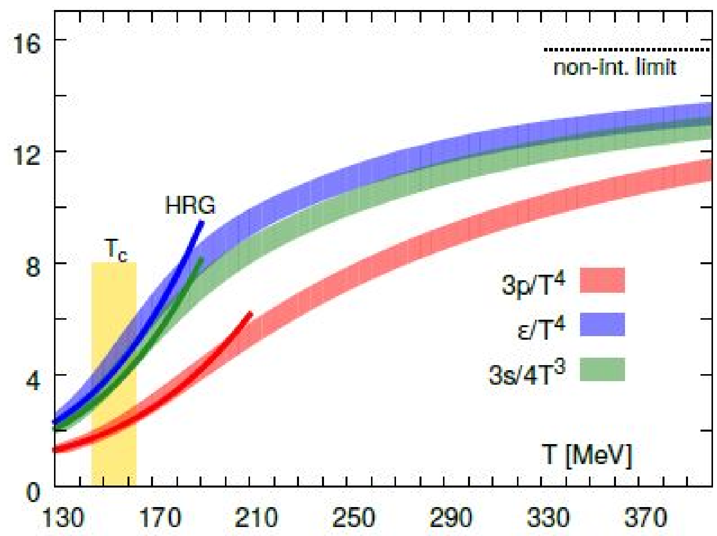

Figure 1.3: Equation of state for hot QCD matter at zero baryon chemical potential. Calculation on the lattice performed by the HotQCD collaboration [18]. Shown are the pressure p, energy density ϵ and entropy density s scaled with temperature to give dimensionless variables. The yellow band is the crossover region. The figure includes a comparison with hadronic resonance gas (HRG) calculations, see e.g. [19].

which quarks and gluons are confined in weakly-interacting hadrons and chiral symmetry is broken. As the temperature of the hadronic gas is increased, more hadronic species at greater density are found. In the crossover region, the density becomes so great that quarks and gluons become natural degrees of freedom. This gives way to the high-temperature phase of the quark-gluon plasma in which quarks and gluons are deconfined and chiral symmetry is restored. Both deconfinement and chiral symmetry restoration are continuous when the temperature increases at $\mu_B = 0$ in QCD. Thus there is no phase transition in the sense that all derivatives of thermodynamic quantities are non-divergent and continuous, and the transition between the phases is a crossover. Nevertheless, the quark-gluon plasma and the hadronic gas are two distinct phases with very different properties.

Despite the power of lattice simulations, they are limited in many ways. Firstly, lattice simulations cannot describe dynamical quantities from first principles. Such quantities are inherently time-dependent but in lattice simulations there is no time variable as time has been Wick rotated as in Eq. (1.8) in order to capture the effect of temperature. Examples of dynamical quantities include transport coefficients like shear viscosity and electric conductivity that describe how fast the plasma returns to thermal equilibrium after being perturbed and which are defined through Kubo formulas using linear response theory. Dynamical quantities also include probes of the quark-gluon plasma such as the rate of photon radiation. [4] An additional limitation of lattice QCD is that the Lagrangian in Eq. (1.8) becomes imaginary at finite baryon chemical potential. This makes the path integral oscillatory and makes numerical evaluation difficult, meaning that even thermodynamic quantities are difficult to measure at finite μ_B. Thus we must turn to experiments to learn about the dynamical properties of QGP, its interaction with probes such as jets and photons, as well as its thermodynamics at finite μ_B.

1.3 HYDRODYNAMICS IN HEAVY-ION COLLISIONS

Heavy-ion collisions offer a wealth of information on the quark-gluon plasma at high temperature. In particular, final stage hadrons in the collisions can be used to study collectivity in the quark-gluon plasma. A simple example is elliptic flow in the plane transverse to the beam axis of the initial nuclei, see Fig. 1.2. This is essentially defined as

$$v_2 = \frac{\frac{1}{4\pi} \int d\phi \ \int dp_T p_T \ \frac{d^3N}{d^3\mathbf{p}} \cos 2\phi}{\int d\phi \ \int dp_T p_T \ \frac{d^3N}{d^3\mathbf{p}}} \tag{1.9}$$

where ϕ is the angle in the transverse plane and $d^3N/d^3\mathbf{p} = d^3N/p_T dp_T d\phi d\eta$ is the differential yield of hadrons with p_T being transverse momentum and η being rapidity. A more rigorous discussion of elliptic flow is given in [22]. The coefficient v_2 describes how the flow of final-stage hadrons is elliptical in the transverse plane, with more hadrons flowing in one direction than the orthogonal direction. More generally, one can define flow coefficients v_n as the Fourier coefficients for yield in the transverse plane, i.e.

$$E\frac{d^3N}{d^3\mathbf{p}} = \frac{1}{2\pi}\frac{d^2N}{p_T dp_T d\eta}\left(1 + 2\sum_{n=1}^{\infty} v_n \cos n(\phi - \Psi_n)\right) \tag{1.10}$$

4 There are some workarounds to evaluate all of these quantities on the lattice, see e.g. [20, 21] Basically, one can try to analytically continue quantities evaluated at imaginary time to real time. This is not a well defined procedure numerically, and requires an ansatz which can be constrained by known physics.

where Ψ_n are event plane angles [22]. As an example, v_3 describes triangularity in the flow of final-stage hadrons. Fig. 1.4 shows experimental results for elliptic flow v_2 as the number of nucleons participating in a collision is varied. Elliptic flow is sizable, suggesting that the QGP formed in experiments behaves collectively, like a relativistic fluid, and is not simply a gas of very weakly interacting quarks and gluons which flow with equal probability in all directions. To quantify how the QGP behaves as a fluid, one must model heavy-ion collisions with relativistic hydrodynamics and compare predictions with experimental results.

Relativistic hydrodynamics uses fully covariant equations to describe the propagation in time of macroscopic excitations like energy, pressure and baryon currents, see [23, 24] for reviews. The central equation is the conservation of energy and momentum

$$\partial_\mu T^{\mu\nu} = 0 \tag{1.11}$$

where $T^{\mu\nu}$ is the stress-energy tensor. Additionally, any charge will have a corresponding conservation equation,

$$\partial_\mu J^\mu = 0 \tag{1.12}$$

with J^μ the current. At high enough energies, heavy-ion collisions have small baryon currents and all currents can be put to zero.

To give meaning to Eq. 1.11, one needs an expression for the stress-energy tensor. In the simplest possible setup, one assumes that the quark-gluon plasma is in local thermal equilibrium so that each macroscopic patch of the plasma has a well-defined temperature. This temperature can vary slowly throughout the system. Then

$$T^{\mu\nu} = (\epsilon + p)u^\mu u^\nu - g^{\mu\nu} p \tag{1.13}$$

where ϵ is the energy density, p is the pressure, u^μ is the four-velocity of the fluid with $u^2 = 1$ and $g^{\mu\nu} = (1, -1, -1, -1)$ is the metric. Conservation of energy, Eq. (1.11), gives that

$$\frac{d\epsilon}{d\tau} + (\epsilon + p)\theta = 0 \tag{1.14}$$

and

$$(\epsilon + p)\frac{du^\mu}{d\tau} - \nabla^\mu p = 0 \tag{1.15}$$

where $d/d\tau := u^\mu \partial_\mu$ is a time-like derivative and $\nabla_\mu := \partial_\mu - u_\mu d/d\tau$ is a space-like derivative in the fluid's rest frame. Furthermore, $\theta = \partial_\mu u^\mu$ is the expansion rate of the fluid. Eqs. 1.14 and 1.15 have a simple interpretation. The first equation is a simple conservation law: When $\theta > 0$, fluid flows out of a cell and the energy density must decrease. The second equation is essentially Newton's second law where gradients in pressure cause acceleration $du^\mu/d\tau$ where the inertia is $\epsilon + p$. This is a relativistic Navier-Stokes equation without viscosity.

A careful analysis shows that there are five dynamical variables in Eqs. 1.14 and 1.15 but only four equations in total. The fifth equation needed is the equation of state $\epsilon = \epsilon(p)$ which is taken from lattice simulations. Eq. (1.15) suffices to explain qualitatively the sizable elliptic flow v_2 found in experiments. When two nuclei collide, their overlap has an almond shape in the transverse plane, see Fig. 1.2. This gives a steeper pressure gradient in one direction, so according to Eq. (1.15) there will be more rapid flow in that direction and the QGP flows elliptically.

Despite giving a qualitative understanding of elliptic flow, ideal hydrodynamics is a poor approximation in heavy-ion collisions. This can for instance be seen in Fig. 1.4 where the prediction of ideal hydrodynamics overshoots the elliptic flow found in experiments. This shows that there are sizable deviations from local thermal equilibrium in experiments. To remedy this we must add more terms to the stress-energy tensor in Eq. (1.13). This is typically done by expanding in spatial gradients $\mathcal{O}(\partial)$ which are small if hydrodynamics truly describes long-wavelength excitations. Adding all possible first-order corrections[5] gives

$$T^{\mu\nu} = (\epsilon + p)u^\mu u^\nu - g^{\mu\nu}p + \zeta\theta\Delta^{\mu\nu} + 2\eta\sigma^{\mu\nu}. \tag{1.16}$$

In Eq. (1.16), the term with

$$\Delta^{\mu\nu} = g^{\mu\nu} - u^\mu u^\nu \tag{1.17}$$

5 We have defined the fluid velocity to be $(1,0,0,0)$ in the frame where there is no energy flow meaning that terms with $du^\mu/d\tau$ can be ignored at this order. This furthermore means that the energy density ϵ can only appear in the ideal part of the stress-energy tensor, as well as the pressure $p = p(\epsilon)$ which is fixed by the equation of state. This convention for the fluid's rest frame is known as the Landau frame [25]. Then $T^{\mu\nu}$ can be expressed solely in terms spatial derivatives $\partial_i u^\mu$ in the fluid's rest frame. They are conveniently decomposed into the two terms given. We furthermore assume that entropy increases locally.

is solely on the spatial diagonal of the stress-energy tensor in the fluid's rest frame. It describes resistance to uniform spatial expansion θ because of the bulk viscosity ζ. The second term has

$$\sigma^{\mu\nu} = \frac{1}{2}\left(\nabla^{\mu}u^{\nu} + \nabla^{\nu}u^{\mu}\right) - \frac{1}{3}\Delta^{\mu\nu}\theta. \tag{1.18}$$

where $\sigma^{\mu\nu}$ is traceless. It describes resistance to shear flow, i.e. flow where the velocity gradient is transverse to the velocity, due to the shear viscosity η. Larger transport coefficients η and ζ lead to faster decay of the fluid to equilibrium and faster entropy production. Using expansion to first order in spatial gradients as in Eq. (1.16) gives more complicated equations of motion in Eq. 1.11. In practice, hydrodynamic simulations of heavy-ion collisions, such as with MUSIC [26, 27], go all the way to second order because the first order contains unphysical faster-than-light propagation [23].[6]

Hydrodynamic simulations of heavy-ion collisions correctly describe a wide range of hadronic observables such as the yield of hadrons, their average transverse momentum, and correlations in the transverse plane such as elliptic flow. By varying the values of transport coefficients in hydrodynamic simulations, one can see which values best describe experiments. This allows for extracting the transport coefficients of QCD, see Fig. 1.4. This gives very low values of η/s where η is the shear viscosity and s is the entropy density of QGP, suggesting that the QGP is nearly a perfect fluid with minimal internal friction. In fact a calculation using the AdS/CFT correspondence in an infinitely strongly coupled supersymmetric theory found a lower limit of $\eta/s = 1/4\pi \approx 0.08$ in that theory [29] while for QGP η/s seems to be around $0.08 - 0.16$.[7]

1.4 STAGES OF HEAVY-ION COLLISIONS

Heavy-ion collisions cannot be described by hydrodynamics alone. Firstly, the QGP medium expands and cools and finally becomes a hadronic gas that is too dilute to be described by hydrodynamics. The evolution of these last stages is given by a kinetic

6 We note that recent work has shown that first-order hydrodynamics can be stable if one uses different dynamical variables [28].

7 Of course η/s is a temperature dependent quantity. Recent analyses using Bayesian techniques suggest the window we quote for η/s around the crossover temperature [30].

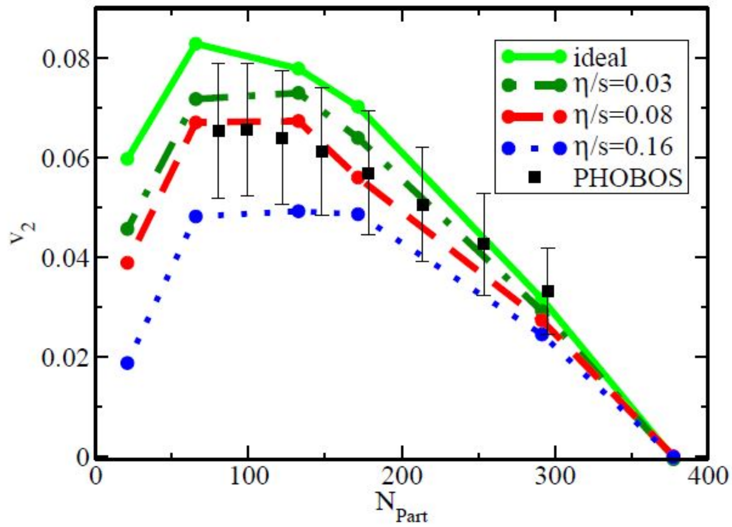

Figure 1.4: Early work on elliptic flow v_2 in Au+Au collision, comparing hydrodynamic simulations using different values of shear viscosity with experimental results [31].

theory of hadrons which can be simulated by numerical approaches such as URQMD [32] and SMASH [33]. To transition from hydrodynamics to hadronic kinetic theory requires a model of hadronization in which the continuous fluid is sampled and converted into particles [34].

The second reason for why hydrodynamics does not suffice, is that it requires physical initial conditions. This requires understanding how the violent initial collision of two nuclei gives rise to a hydrodynamical medium. This is a difficult problem. Early work used simple models, such as MC Glauber, where the initial energy density in the transverse plane comes from sampling nucleons in each nucleus, as well as sampling their binary collisions [35]. A more physical description of the creation of a hydrodynamic medium comes from the physics of the colour-glass condensate (CGC), see reviews in [36, 37].

The CGC framework describes small x gluons in a nucleon, where x is the momentum fraction carried by parton in a fast-moving nucleon. These low-energy gluon modes are highly occupied and can therefore be described classically. Their energy is below the saturation scale Q_s at which gluon creation is matched by gluon recombination. These low x gluons are sourced by large x partons in the nucleus which we picture as a current

$$j^{\mu,a}(x) = \delta^{\mu+}\sqrt{2}\,\delta(t-z)\,\rho^a(\mathbf{x}_\perp). \tag{1.19}$$

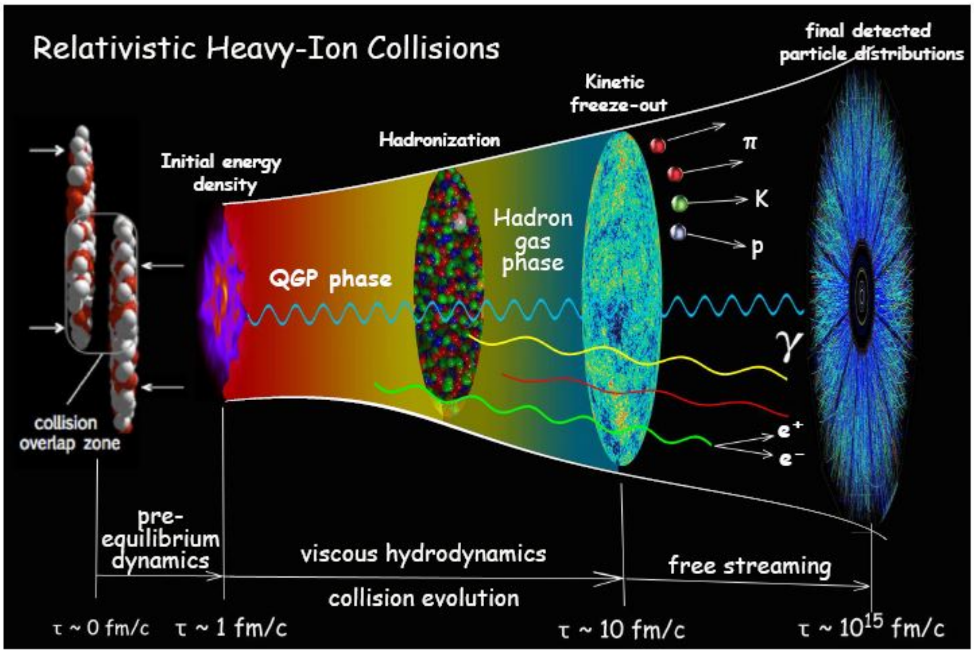

Figure 1.5: Different stages of heavy-ion collisions. Figure created by Chun Shen [38]. The pre-equilibrium dynamics is e.g. given by IP-Glasma followed by kinetic theory.

This current is squeezed into a thin pancake at $z = t$ by Lorentz contraction and has transverse density ρ which depends on position in the transverse plane $\mathbf{x}_\perp$. Assuming a light-cone gauge $A^0 + A^z = 0$, the current sources low x gluons

$$\mathbf{A}_\perp(x) = \frac{1}{g}\theta(t-z)\nabla_\perp\Lambda \tag{1.20}$$

in its wake [39, 40]. Here Λ solves the two-dimensional Poisson equation $\nabla_\perp^2\Lambda(\mathbf{x}_\perp) = -g\rho(\mathbf{x}_\perp)$. A model is needed for the transverse density ρ in Eq. (1.19). This is for example provided by the IP-Sat model (Impact-Parameter dependent Saturation model) [41, 42] which assumes that

$$\langle\rho^a(\mathbf{x}_\perp)\rho^b(\mathbf{y}_\perp)\rangle \propto \delta^{ab}\delta^{(2)}(\mathbf{x}_\perp - \mathbf{y}_\perp)Q_s^2(\mathbf{x}_\perp). \tag{1.21}$$

Roughly speaking, the saturation scale Q_s^2 is determined as the inverse size of a quark-antiquark dipole which interacts with the gluons in a proton with probability $\mathcal{O}(1)$. It is constrained by experimental data on deep inelastic scattering.

When two nuclei collide in heavy-ion collisions, there are classical fields as in Eq. (1.20) in the wake of each nucleus. These classical fields form the QCD medium which during its earliest CGC stages is known as the glasma. To find initial conditions for the glasma, one must match the solutions in Eq. (1.20) to the forward light cone at $\tau = 0$ with a suitable gauge transformation where $\tau = \sqrt{t^2 - z^2}$ is the proper time [43–45]. The non-Abelian fields are then evolved numerically on a lattice [46, 47] using the classical equations of motion, which reduce to the dynamics of the QCD Lagrangian in Eq. (1.1) in the continuum limit. For large enough nuclei the saturation scale is high enough to assume weak coupling $g \ll 1$ but due to high occupancy the evolution is non-perturbative.

The whole framework of the IP-Sat model and classical evolution of the glasma is known as IP-Glasma [48]. Hydrodynamic simulations of heavy-ion collisions using initial conditions from IP-Glasma are successful in explaining a range of hadronic observables. In particular, the fluctuating initial conditions from IP-Glasma explain higher order flow coeffcients, such as triangular flow, well [48, 49]. More recently, more sophisticated modelling of the glasma with dynamics in the rapidity direction stemming from quantum fluctuations has been developed [50, 51].

Despite the success of IP-Glasma and hydrodynamics in explaining hadronic observables in heavy-ion collisions, it is not necessarily theoretically consistent to pass between the two. This is because IP-Glasma, if evolved long enough, does not give rise to a hydrodynamic medium. To bridge the gap between these two theories, some recent calculations have started using QCD kinetic theory in between the glasma phase and the hydrodynamic phase [52, 53]. QCD kinetic theory describes quark and gluon quasiparticles that occasionally interact through two-to-two scattering and collinear bremsstrahlung, see below. It is valid for a weakly coupled medium in which collisions are infrequent. Kinetic theory is equivalent to the last stages of a glasma evolution where the occupation density is $1 \ll f \ll 1/g^2$. It is furthermore the microscopic equivalent of hydrodynamics, assuming weak coupling. Kinetic theory is particularly suited for the earliest stages of the hydrodynamic evolution where the medium can be so far from local thermal equilibrium that the gradient expansion described in Sec. 1.3 breaks down. Thus, kinetic theory is well suited to bridge between glasma and hydrodynamic calculations.

We have described a coherent model for heavy-ion collisions, see Fig. 1.5. The initial collision and the first instances in the evolution are described by models such as IP-Glasma. Then, one can have a short-lived kinetic theory evolution or pass directly to relativistic hydrodynamics which is the main bulk of the evolution. Finally, the hydrodynamic medium hadronizes and the hadrons interact until being measured in detectors. Ultimately, all these different models are different manifestations of non-equilibrium QCD.

1.5 JETS AND PHOTONS

Hadrons produced as the medium cools down are only sensitive to the final stages of a hydrodynamic evolution in heavy-ion collisions. Furthermore, they only probe the microscopic properties of the QGP through a handful of transport coefficients and the equation of state. Because of this, other experimental probes are essential to understand heavy-ion collisons. Ideally, they give access to the whole evolution of the QGP and are sensitive to its microscopic properties.

Photons are one such experimental probe. They are emitted by electrically charged quarks in the plasma. There are a number of other sources of photons in heavy-ion collisions such as the decay of final-stage hadrons, which can be subtracted by experimentalists, photons coming from the initial hard scattering of nucleons, and photons coming from the hadronic gas phase, see e.g. [54, 55] for reviews.[8] The challenge is therefore to accurately describe all these different photon sources, in order to get to the most interesting QGP photons. The most important results is that the contribution of QGP photons is needed to explain experimental result on total photon yield in heavy-ion collisions, meaning that photons confirm the presence of the QGP in experiments. On a more quantitative level, there is however tension between experimental results and theoretical predictions, with theory tending to underestimate the yield of photons as well as the elliptic flow of photons in the transverse plane [57].

Jets, which are largely collinear showers of highly energetic particles, are an even more important probe in heavy-ion collisions. In proton-proton collisions in vacuum, an initial hard scattering of two partons creates two, nearly back-to-back jets. The initial jet particles are highly virtual, i.e. highly off-shell, and rapidly decay into two partons with

8 Additional sources of photons, such as photons coming from the kinetic theory phase, have also been suggested [56].

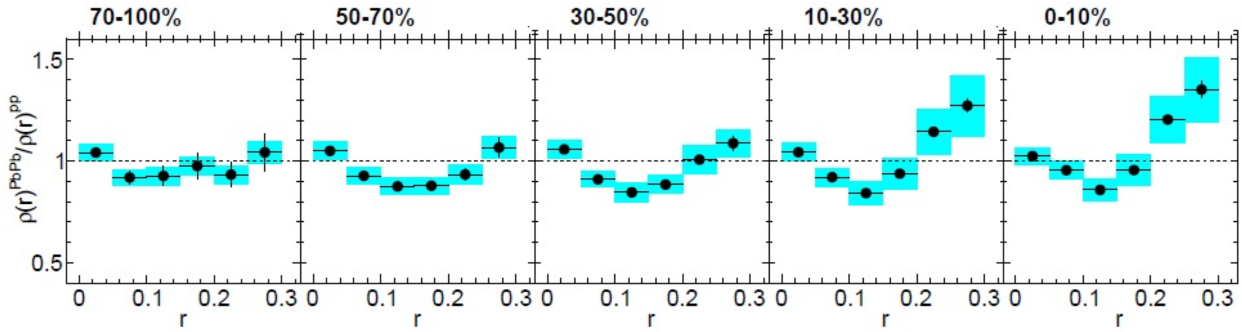

Figure 1.6: Jet shape ratio as measured by the CMS collaboration for PbPb collisions at $\sqrt{s_{NN}} = 2.76\,GeV$ [59]. This measures how the jet is distributed in a radial cone, for heavy-ion collisions in which a medium is formed and pp collisions in vacuum. At larger radius r there are more jet partons in heavy-ion collisions, suggesting that the medium broadens the jet. This is especially pronounced for central collisions, shown to the right, where the overlap of the two initial nuclei is larger and medium effects are greater.

less virtuality. These partons decay in turn, and a shower of partons at decreasing energy and virtuality is formed. Due to collinear divergences in QCD, collinear emission is strongly preferred in QCD and the whole jet moves more or less in the same direction. This process of jet branching, which is described at leading logarithmic order by a DGLAP evolution, continues until the partons hadronize [58].

In heavy-ion collisions, jets are formed in the same way as in proton-proton collisions during the initial collision of nucleons. The two jets are created inside the quark-gluon plasma and propagate through it. Interaction between the jet and the QGP medium changes the jet evolution, allowing us to gain detailed information about QGP through jet observables. In particular, at weak coupling, jet partons get random kicks from the medium which impart momentum transverse to the jet direction. This deflects jet partons and results in broader jets. The rate of transverse momentum broadening is given by the transport coefficient

$$\hat{q} = \frac{d\langle \mathbf{p}_\perp^2 \rangle}{dt} \tag{1.22}$$

where $\mathbf{p}_\perp$ is a transverse kick,t is time and $\langle \mathbf{p}_\perp^2 \rangle$ refers to medium averaging.

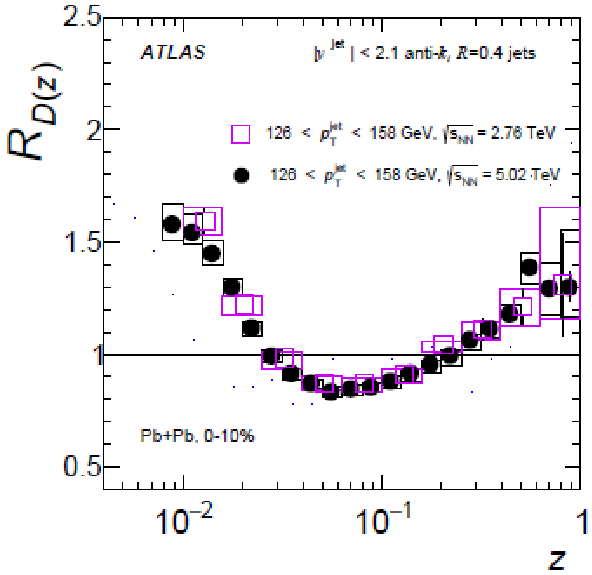

Figure 1.7: Ratio of fragmentation function in PbPb collisions with $\sqrt{s_{NN}} = 5.02$ TeV and in pp collisions, as measured by the ATLAS collaboration [60]. Here $z = p_T^{\text{hadron}} / P_T^{\text{jet}}$ is the the ratio of a jet hadron transverse momentum and the total jet transverse momentum. The medium causes an increased number of particles at lower energy.

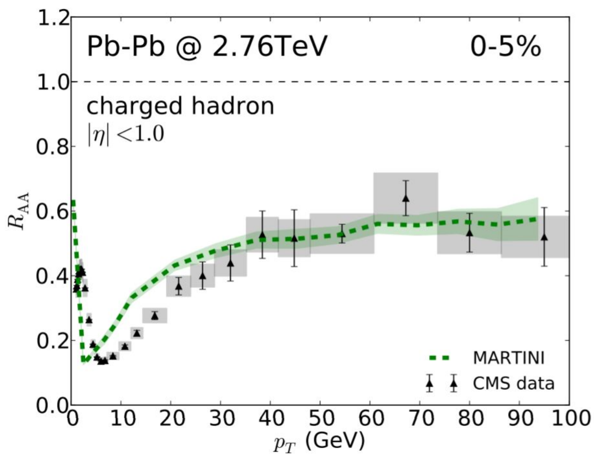

Figure 1.8: Experimental results on R_{AA} which is the ratio of jet yield in AA and pp collisions [61]. The quantity is below unity because of jet energy loss. For comparison we show a theoretical calculation with MARTINI [62].

Transverse momentum broadening can be measured in experiments. For example one can define the jet shape ratio $\rho(r)$ as

$$\rho(r) = \frac{1}{\Delta r}\frac{1}{N_{\text{jets}}}\sum_{\text{jets}}\frac{1}{\sum p_T}\sum_{\tilde{r}\in[r-\Delta r/2,r+\Delta r/2]} p_T. \tag{1.23}$$

which is essentially the distribution of jet parton p_T with distance r from the jet axis [59]. Here $\sum p_T$ sums over the transverse momenta of all hadrons in a jet, while $\sum_{\tilde{r}\in[r-\Delta r/2,r+\Delta r/2]} p_T$ only sums over hadrons at a distance r from the jet axis in an interval of size Δr. Here $r = \sqrt{(\eta-\eta_{\text{jet}})^2+(\phi-\phi_{\text{jet}})^2}$ where η is rapidity and ϕ is angle in the transverse plane. In Fig. 1.6 we show the ratio of $\rho(r)$ for heavy-ion collisions and for pp collisions, suitably normalized to account for the greated number of jets in heavy-ion collisions. The jet shape ratio is clearly broader in heavy-ion collisions. This is because of momentum broadening but also because of recoil particles, i.e. medium particles that gain energy from the jet through scattering and become part of the jet at large angle from the jet axis.[9]

The medium also stimulates additional splitting of jet partons. In vacuum, on-shell partons cannot split into two other partons. In a QGP medium this is made possible by transverse medium kicks that impart a small virtuality to the parton, allowing it to decay, see Fig. 1.14 and discussion below. This effect can be seen in the jet fragmentation function, where jets in heavy-ion collisions have a greater number of low-energy partons compared with jets in pp collisions, see Fig. 1.7.

The final effect of the medium is that it absorbs low-energy jet partons with energy of the order of the medium temperature. This results in jet energy which decreases the total yield of jets and high-energy hadrons. Experimentally, the decrease is quantified by the nuclear modification factor

$$R_{AA} := \frac{dN^{AA}/dp_T}{\langle N_{\text{coll}}\rangle dN^{pp}/dp_T} \tag{1.24}$$

where dN^{AA}/dp_T and dN^{pp}/dp_T are the differential yield in heavy-ion collisions and pp collisions respectively. Here $\langle N_{\text{coll}}\rangle$, the number of nucleon collisions, corrects for the

9 Of course, the detailed physics behind jet observables is complicated. In particular, when comparing jets in AA collisions and pp collisions with the same total final transverse momentum, one needs to take into account that the initial momentum of the two jets was different. This is because the hard parton seeding the jet in the AA collision was more energetic but has since lost energy to the medium. This complicates interpretation of experimental observables.

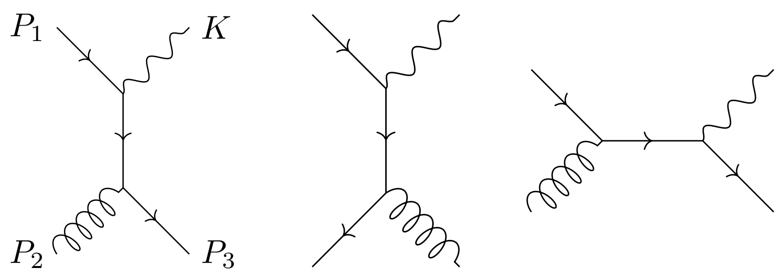

Figure 1.9: Two-to-two scattering channels with a photon in the final stage. As an example, in the first diagram P_1 is an initial quark, P_2 is an initial gluon, P_3 is a final quark and K is the final photon that is produced.

greater number of jets in heavy-ion collisions. The nuclear modification factor is below unity, see Fig. 1.8, showing that jets lose energy in heavy-ion collisions when compared with pp collisions.

1.6 PROCESSES IN A WEAKLY-COUPLED PLASMA

A detailed theoretical description is needed to predict experimental results on jets and photons in heavy-ion collisions. The framework of a weakly-coupled plasma enables one to calculate quantities such as medium-induced gluon radiation in jets, and the rate of photon production order by order in the strong coupling g.

For simplicity, we first consider the radiation of photons from a weakly-coupled QGP. There are two main channels at leading order $\mathcal{O}(e^2g^2)$ where e is the electromagnetic coupling. Firstly, there are two-to-two processes with a photon in the final stage, see Fig. 1.9. The quark mediator can have energy of the order of the medium temperature T in which case the rate R can be expressed using kinetic theory

$$E_k\frac{dR}{d^3k} = \frac{\mathcal{N}}{2(2\pi)^3}\int_{P_1}\int_{P_2}\int_{P_3}|\mathcal{M}|^2 f(E_1)f(E_2)\,(1\pm f(E_3))\,\delta^{(4)}(P_1+P_2-P_3-K). \quad (1.25)$$

Here $\mathcal{M}$ is the amplitude, calculated as in vacuum, K is the photon momentum, f are Bose-Einstein or Fermi-Dirac distribution for the density of gluons and quarks and $\int_P := \int \frac{d^3p}{2p(2\pi)^3}$. $\mathcal{N}$ includes colour factors and the sum over quark flavour. At leading order, the quark mediatior can also have softer energy gT in which case one needs a

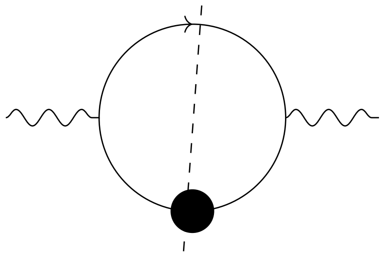

Figure 1.10: A diagram for the rate of photon production. The soft quark propagator is HTL resummed. After applying a cut one gets diagrams similar to those in Fig. 1.9

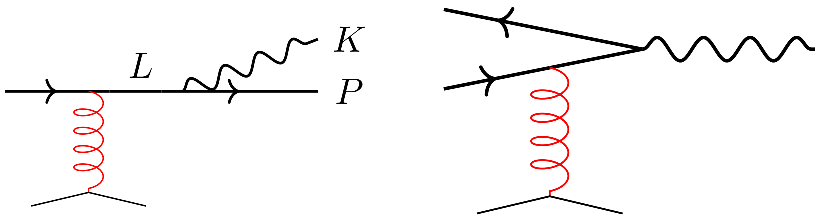

Figure 1.11: Photon emission through bremsstrahlung by a quark and through quark-antiquark pair annihilation. In both cases, emission is made possible because of a small medium kick, coloured in red. As an example, in the first diagram K is the produced photon, P is the quark after emission and L is the quark after one medium kick.

resummed quark propagator which takes into account medium effects in quark propagation, see Fig. 1.10. This is achieved by Hard Thermal Loops (HTL) effective theory discussed below [63–65]. Without this resummation one gets a divergent rate for photon production. Photon production through two-to-two channels was first evaluated for a medium in thermal equilibrium in [66, 67].

At leading order, there are equally important channels in which a photon is radiated collinearly through bremsstrahlung or through pair-annihilation, see Fig. 1.11. These diagrams might superficially seem to be subleading at order $\mathcal{O}(e^2g^4)$. However, because of collinear enhancement they are alsoleading order. This was first noted in [68]; see also [69, 70] for earlier discussions of photon production through bremsstrahlung in the quark-gluon plasma. The first full leading-order calculations of these channels was given by Arnold, Moore and Yaffe (AMY) in [71–73]. They have been implemented in the phenomenology of photons in heavy-ion collisions, see e.g. [57].

Collinear emission of a photon is kinematically allowed in a plasma because an on-shell quark can get a small transverse kick of momentum gT from the medium. This brings the quark slightly off-shell with virtuality $L^2 \sim g^2T^2$, see Fig. 1.11, allowing it to emit a photon. The small kick happens through gluon exchange where all medium effect given by HTL effective theory must be included. The opening angle between the quark and the photon is small because of the quark's small virtuality. More precisely we have that

$$L^2 = (P+K)^2 = 2pk(1-\cos^2\theta) \sim pk\,\theta^2 \tag{1.26}$$

where K is the photon momentum and P is the momentum of the quark after emission, showing that the opening angle is $\theta \sim gT$.

The small opening angle between the quark and photon means that their wavepackets overlap for a long time until the particles are sufficiently separated from one another. The time τ until separation can be estimated by noting that the opening angle is

$$\theta \sim \frac{\Delta p_\perp}{p} \sim \frac{\Delta x_\perp}{\tau} \tag{1.27}$$

where $\Delta p_\perp \sim gT$ is the transverse momentum of one of the partons and $\Delta x_\perp$ is the transverse separation of the two partons. By the uncertainty principle, $\Delta p_\perp \Delta x_\perp \sim 1$, we get that

$$\tau \sim \frac{p}{(\Delta p_\perp)^2} \sim \frac{1}{g^2T} \gg \frac{1}{T}. \tag{1.28}$$

since $g \ll 1$, which shows that the wavepackets are coherent for a long time. Crucially, the typical time between two transverse kicks of energy gT is also $1/g^2T$. Therefore, while the quark and the photon wavepackets overlap, the quark can get additional kicks from the medium. This effect is known as the Landau-Pomeranchuk-Migdal (LPM) effect. It leads to suppression in the rate of photon emission as coherence between the partons is reduced by additional kicks. The LPM effect was first discussed in the context of photon radiation off an electron in dense matter like in detectors in collider experiments [74–77].

Fig. 1.12 shows a leading-order diagram for photon emission through bremsstrahlung. Because of the LPM effect, the quark can get arbitrarily many transverse kicks while radiating the photon. It might seem surprising that despite the many vertices, the diagram is at leading order $\mathcal{O}(e^2g^2)$. This is borne out by a detailed quantum-field theoretical

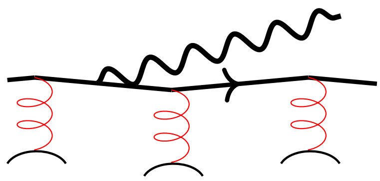

Figure 1.12: Leading order photon emission through bremsstrahlung, including the LPM effect. The quark can receive arbitrarily many medium kicks during emission.

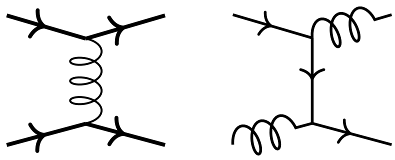

Figure 1.13: Examples of two-to-two scattering diagrams for quarks and gluons. These diagrams describe both quasiparticle interaction and jet-medium interaction in which case e.g. the upper particle is from the jet and the lower particle is from the medium.

calculation [73], see also our work [78] which applies to a non-equilibrium medium. In essence, each new kick gives an additional factor of g^2 through vertices but this is cancelled by a factor $1/g^2$ coming from pinching poles. These pinching poles describe the phase difference

$$\int_0^\infty dt\, e^{i(l^0-p^0-k^0)t} = \frac{i}{l^0-p^0-k^0} \tag{1.29}$$

between the quark before a kick l^0 and the quark and photon after a kick, p^0 and k^0. Due to the small transverse kicks, the phase difference is

$$\begin{aligned} l^0-p^0-k^0 &= \sqrt{l_z^2+l_\perp^2+m_\infty^2} - \sqrt{p_z^2+p_\perp^2+m_\infty^2} - k \\ &\approx \frac{l_\perp^2+m_\infty^2}{2l_z} - \frac{p_\perp^2+m_\infty^2}{2p_z} \sim g^2T \end{aligned} \tag{1.30}$$

where $l_z = p_z + k$ is the momentum in the direction of emission, $l_\perp \sim p_\perp \sim gT$ are transvere momenta and $m_\infty \sim gT$ is the thermal mass of quarks. We will discuss the evaluation of the diagram in Fig. 1.12 in detail in Sec. 5.1.

The physics of jet-medium interaction is similar to the physics of photon emission. At leading order there are two-to-two interaction channels, see Fig. 1.13, where soft mediators require HTL resummation. Furthermore, there are bremsstrahlung channels

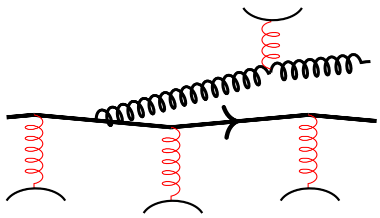

Figure 1.14: Gluon emission by a quark including the LPM effect. Both the quark and the gluon can receive arbitrarily many medium kicks during emission, coloured in red. This diagram can describe both an energetic jet parton radiating an energetic gluon and a medium quasiparticle emitting a gluon quasiparticle.

for medium-induced gluon emission, see Fig. 1.14. This process is at the heart of jet physics in a medium as it determines how the jet energy is distributed among the jet partons. The physics is similar to that of photon emission. An on-shell jet parton can emit a gluon collinearly as medium kicks bring it slightly off-shell. During the time that wavepackets separate, both the quark and the emitted gluon can receive medium kicks. For higher energy jet partons, the separation time is longer and the average medium kick is more energetic, see [79] for a discussion in the formalism of Arnold, Moore and Yaffe (AMY). This makes the LPM effect more pronounced and gives a large suppression in the rate of gluon emission through bremsstrahlung. Gluon emission in the AMY formalism was first derived in [71], and evaluated numerically in [80]. We discuss the detailed evaluation of gluon emission through bremsstrahlung in Sec. 5.1.

The processes we have described are not only relevant for the physics of jets and photons, but also for quasiparticle interaction in kinetic theory. Quark and gluon quasiparticles can interact through two-to-two scattering as in Fig. 1.13, as well as in one-to-two processes where a gluon is emitted collinearly, see Fig. 1.14 [81], and the inverse two-to-one process. In the latter case, the LPM effect needs to be taken into account.

In order to evaluate all processes with collinear bremsstrahlung, both photon emission and gluon emission by a jet parton or a quasiparticle, detailed information on momentum broadening is needed. This is given by the collision kernel $\mathcal{C}(\mathbf{p}_\perp)$, the rate at which a quark or a gluon receives transverse kicks $\mathbf{p}_\perp$. Evaluating this kernel also gives the transport coefficient $\hat{q}$ from Eq. (1.22) since

$$\hat{q} = \int \frac{d^2 p_\perp}{(2\pi)^2} p_\perp^2 \mathcal{C}(\mathbf{p}_\perp). \tag{1.31}$$

when broadening is dominated by soft gT kicks. There exist microscopic evaluations of the collision kernel $\mathcal{C}$ in a weakly-coupled plasma in thermal equilibrium, see [82, 83].

The AMY equations for jet splitting in a medium have been implemented numerically in an event generator called MARTINI [84], see also [85–87] for earlier phenomenological work on jets using AMY rates. In MARTINI, jets are created in the initial hard collision of nucleons as given by PYTHIA [88]. Jet partons then propagate in a hydrodynamic background describing the plasma and radiate gluons or interact with the medium elastically through two-to-two scattering. The partons are assumed to shed virtuality quickly so that the AMY rates for on-shell partons are applicable. Once jet partons have exited the medium, they are made to hadronize using PYTHIA. More recent versions have in addition included the recoil of medium particles in two-to-two scattering [62], as well as running strong coupling and the finite time needed for radiative processes [89]. MARTINI has been successful in explaining a range of experimental jet observables in heavy-ion collisions, such as the nuclear modification factor R_{AA} [62], see Fig. 1.8, dijet asymmetry [90] and jet shape function [62].

1.7 THIS THESIS

Jet-medium interaction in MARTINI and other numerical codes requires a microscopic description of the QGP medium. This is given by the momentum distribution $f(\mathbf{p})$ of medium quarks and gluons. Usually, an equilibrium distribution is assumed which only depends on the temperature of the hydrodynamic background. This is inconsistent with the hydrodynamic background being out of equilibrium, as shown by the need to use second order hydrodynamics. Thus it is important to evaluate jet-medium interaction for a non-equilibrium momentum distributions $f(\mathbf{p})$. Similarly, non-equilibrium effects should be taken into account when calculating the rate of photon production.

More generally, two things stand out in our discussion of heavy-ion collisions. Firstly, the medium created in experiments is out of thermal equilibrium at all times and the deviations can be big. This is especially true during the early glasma and kinetic theory stages of a collision, but even in the hydrodynamic phase there are substantial deviations from local thermal equilibrium. Secondly, jets and photons are sensitive probes of the medium created in heavy-ion collisions and require detailed modelling, taking into account all aspects of the medium. It is therefore important to have a theoretical understanding of jets and photons in a quark-gluon plasma out of thermal equilibrium. This could e.g. allow for extracting detailed information on the non-equilibrium properties of QGP from experiments, such as equilibration of the QGP and its transport coefficients.

Earlier work has evaluated photon emission in a non-equilibrium plasma through two-to-two scattering, see Fig. 1.9. This work assumed a non-equilibrium distribution of quarks and gluons, see [91–93], as well as our work in [94] which considered bulk viscous corrections. However, the equally important bremsstrahlung channel has not been evaluated out of equilibrium. It is especially important to evaluate gluon bremsstrahlung in a non-equilibrium medium since this is the basis of jet evolution in medium and the backbone of QCD kinetic theory. To date there are no consistent calculations of collinear emission out of equilibrium.

A number of challenges arise when evaluating photon and gluon emission through bremsstrahlung in a non-equilibrium plasma. In particular the collision kernel $\mathcal{C}(\mathbf{p}_\perp)$ for momentum broadening, the central ingredient for evaluating collinear emission, is seemingly divergent in a non-equilibrium plasma. Furthermore, the equations for the rate of collinear radiation are much more difficult to solve numerically in a non-equilibrium, anisotropic medium.

In this thesis, we discuss all aspects of parton momentum broadening and the collinear emission of photons and gluons in a non-equilibrium medium. In Sec. 2, we discuss HTL effective theory and momentum broadening and evaluate the collision kernel $\mathcal{C}(\mathbf{p}_\perp)$ in a non-equilibrium plasma. In Sec. 3, we explain why the kernel diverges due to instabilities and how this should be cured. In our discussion we derive time-dependent two-point correlators for gluons in an unstable plasma. We furthermore discuss a phenomenological prescription for the collisions kernel. In Sec. 4, we evaluate the kernel, showing that there is less momentum broadening out of equilibrium due to increased screening. Finally, in Sec. 5, we develop a numerical scheme for evaluating non-equilibrium collinear emission and show that photon emission is reduced in a non-equilibrium plasma. Some technical details and a discussion of the real-time formalism are relegated to appendices.

Part II

NON-EQUILIBRIUM QGP PLASMA AT WEAK COUPLING

2

NON-EQUILIBRIUM QGP PLASMA AT WEAK COUPLING

2.1 HTL EFFECTIVE THEORY

We want to use jets and photons to probe the non-equilibrium physics of QCD. This requires calculating the rate of collinear gluon and photon emission in a non-equilibrium QGP medium, which in turn depends on the rate of transverse momentum broadening. Transverse momentum broadening in a non-equilibrium medium can only be calculated with a thorough understanding of weakly coupled quark-gluon plasma, $g \ll 1$, such as is given by hard thermal loops (HTL) effective theory, see [95] for a review.

HTL effective theory relies on a separation of scales. Most of the energy in a weakly-coupled plasma is carried by quark and gluon quasiparticles at hard energy scale Λ, where Λ is analogous to temperature in thermal equilibrium. The quasiparticles are localized with size $1/\Lambda$ and interact only occasionally as the average time between interaction is $\sim 1/g^4\Lambda$.[1] Therefore, the hard quasiparticles are described by kinetic theory, by specifying a distribution $f(\mathbf{p}; x^\mu)$ in momentum space which varies throughout space-time. The evolution of the distribution is given by a Boltzmann equation

$$v^\mu \frac{\partial f}{\partial x^\mu} + \mathbf{F} \cdot \frac{\partial f}{\partial \mathbf{p}} = \overline{C}[f, A]. \tag{2.1}$$

Here, the first term has $v^\mu = P^\mu/p = (1, \mathbf{v})$ and gives propagation at velocity $\mathbf{v}$. The second term describes deflection due to an external force $\mathbf{F}$ in the plasma. Finally, $\overline{C}[f, A]$ quantifies how the quasiparticles' momentum or species is changed in the collisional processes listed in Sec. 1.6 [81].

1 The rate of two-to-two scattering channels is $\Gamma \sim g^4\Lambda$ as the diagram and its conjugate each have two vertices. Thus the typical time between interaction is $1/\Gamma \sim 1/g^4\Lambda$.

The quark and gluon quasiparticles have colour charge and radiate gluon fields. The radiated fields are at energy scale $E \sim g\Lambda$ and have wavelength $1/g\Lambda$. In thermal equilibrium, their occupation density is given by the Bose-Einstein distribution

$$\frac{1}{e^{E/\Lambda}-1} \sim \frac{1}{g} \gg 1. \tag{2.2}$$

Due to high occupation density, the gluon fields are classical and can be described by the classical equations of motions of QCD. In particular

$$\mathcal{D}_\mu \mathcal{F}^{\mu\nu} = j^\nu, \tag{2.3}$$

where $\mathcal{D}_\mu$ is a covariant derivative in the adjoint representation and $\mathcal{F}^{\mu\nu}$ is the gluon field-strength tensor, defined in Eq. (1.5). These long-wavelength or soft gluons are sourced by a quasiparticle current

$$j^\nu = \int \frac{d^3p}{(2\pi)^3} \frac{p^\mu}{p} \left[2N_f f_q(\mathbf{p}) + 2N_c f_g(\mathbf{p})\right] \tag{2.4}$$

where f_q is the distribution of quarks and f_g is the distribution of gluons with N_f the number of quark flavours and $N_c = 3$ the number of colours.

Together, Eqs. (2.1) and (2.3) form coupled equations for the evolution of the quasiparticle density f and the field strength tensor $F^{\mu\nu}$ of soft gluons. Physically, soft gluons are radiated by quasiparticles, and in turn the quasiparticles are deflected in the force field created by soft gluons

$$F^i = g\left(\mathcal{F}^{i0} - \frac{1}{2}\epsilon^{ijk}\mathcal{F}^{jk}\right). \tag{2.5}$$

Here ϵ^{ijk} is the Levi-Civita tensor in three dimensions. By solving Eqs. (2.1) and (2.3) together, one can eliminate the hard quasiparticles, giving an effective theory only in terms of soft gluons. This effective theory is known as hard thermal loops (HTL).

We briefly reproduce the well-known kinetic theory derivation of the retarded self-energy in HTL effective theory. This includes all leading-order interaction with hard quasiparticles. For simplicity, we consider photons in a QED plasma, instead of gluons in a QCD plasma, so that we need not worry about colour indices and non-Abelian interaction. The original calculation in thermal equilibrium for an electromagnetic plasma was performed in [96], and for a QCD plasma in [97]. For a review see [95].

We write the quasiparticle momentum distribution in a QED plasma as

$$f(\mathbf{p}) = f_0(\mathbf{p}) + \delta f_\pm(x^\mu; \mathbf{p}) \tag{2.6}$$

where $f_0(\mathbf{p})$ is the distribution of hard particles and $\delta f_\pm \ll f_0$ are small fluctuations for positrons and electrons. These small fluctuations are generated as hard particles are deflected in the soft background field, which in turn is radiated by the hard particles $f_0(\mathbf{p})$. Dropping the subleading collision term in Eq. (2.1) we get that

$$v^\mu \frac{\partial \delta f_\pm}{\partial x^\mu} = -\mathbf{F}_\pm \cdot \frac{\partial f_0}{\partial \mathbf{p}} \tag{2.7}$$

since f_0 is independent of spacetime. Here, the sign of the force $\mathbf{F}_\pm$ depends on the particle charge. Eq. (2.7) has solution

$$\delta f_\pm(x^\mu; \mathbf{p}) = -\frac{d f_0}{d\mathbf{p}} \cdot \int_{-\infty}^{t} dt' \; \mathbf{F}_\pm(t', \mathbf{x} - \mathbf{v}(t - t')) \tag{2.8}$$

which can be seen checked explicitly. The corresponding current is

$$\begin{aligned} j^\mu(x) &= e \int \frac{d^3p}{(2\pi)^3} v^\mu \left[\delta f_+ - \delta f_-\right] \\ &= 2e^2 \int \frac{d^3p}{(2\pi)^3} v^\mu \frac{\partial f_0}{\partial \mathbf{p}} \cdot \int_{-\infty}^{t} dt' \; \left(\mathbf{E}(t', \mathbf{x} - \mathbf{v}(t - t')) + \mathbf{v} \times \mathbf{B}(t', \mathbf{x} - \mathbf{v}(t - t'))\right). \end{aligned} \tag{2.9}$$

where $\mathbf{E}$ is the electric field and $\mathbf{B}$ is the magnetic field. Going to Fourier space this gives

$$j^\mu(K) = (-i)\, e^2 \int \frac{d^3p}{(2\pi)^3} v^\mu \frac{\partial f_0}{\partial \mathbf{p}} \cdot \frac{\mathbf{E}(K) + \mathbf{v} \times \mathbf{B}(K)}{k^0 - \mathbf{v} \cdot \mathbf{k} + i\epsilon}. \tag{2.10}$$

Assuming that $f_0(\mathbf{p}) = f_0(-\mathbf{p})$, and using the relation between $\mathbf{E}$, $\mathbf{B}$ and A^μ, a straightforward calculation gives that [95]

$$j^\mu(K) = \Pi^{\mu\nu}(K) A_\nu(K) \tag{2.11}$$

where

$$\Pi^{\mu\nu}_{\text{ret}}(Q) = -2e^2 \int \frac{d^3p}{(2\pi)^3} \frac{\partial f_0}{\partial P^\omega} \left[-v^\mu g^{\omega\nu} + \frac{Q^\omega v^\mu v^\nu}{v \cdot Q + i\epsilon} \right] \Bigg|_{v=(1,\hat{\mathbf{p}})} \tag{2.12}$$

Here $\hat{\mathbf{p}} = \mathbf{p}/p$. From linear response theory we identify $\Pi^{\mu\nu}$ as the retarded self-energy for soft photons.

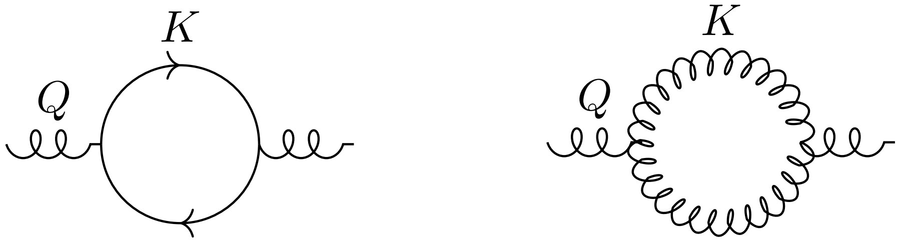

(a) (b)

Figure 2.1: Diagrams needed for self-energy in HTL effective theory. Here $Q \sim g\Lambda$ is the energy scale of soft gluons described by HTL effective theory and $K \sim \Lambda$ is the scale of hard quasiparticles that are integrated out.

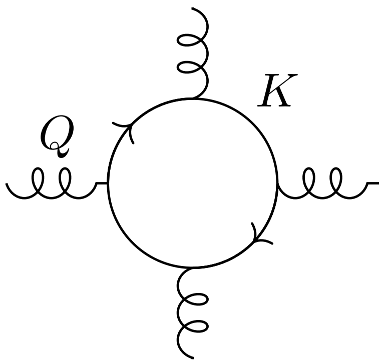

Figure 2.2: An example of a diagram needed for n-point functions in HTL effective theory. We show a four-point vertex with a hard quark loop. $Q \sim g\Lambda$ are the soft gluons described by the theory and $K \sim \Lambda$ are integrated out.

The corresponding expression in QCD is nearly identical. The non-equilibrium HTL retarded self-energy can be shown by an analogous kinetic theory argument [98] to be

$$\Pi^{\mu\nu}_{\text{ret}}(Q) = -g^2 \int \frac{d^3p}{(2\pi)^3} \frac{\partial f_{\text{tot}}}{\partial P^\omega} \left[-v^\mu g^{\omega\nu} + \frac{Q^\omega v^\mu v^\nu}{v \cdot Q + i\epsilon} \right] \bigg|_{v=(1,\hat{\mathbf{p}})}, \tag{2.13}$$

Here $f_{\text{tot}}(\mathbf{p}) = 2N_f f_q(\mathbf{p}) + 2N_c f_g(\mathbf{p})$ where f_q is the distribution of quarks andf_g is the distribution of gluons.

Hard thermal loop effective theory was originally derived diagrammatically using quantum-field theory. The theory was first developed in [63–65] using the imaginary-time formalism but has also been extended to the real-time formalism in thermal equilibrium [99]. Furthermore, the HTL effective Lagrangian was found for non-equilibrium systems [100] where it is specified by the momentum distribution $f(\mathbf{p})$ of the hard particles that are integrated out. The diagrammatic and kinetic theory approach have been shown to be equivalent [95, 100]. Partial resummation of higher order corrections has been done to establish the running of the coupling in HTL effective theory [101].

The vertices in the HTL effective theory Lagrangian can be seen in Figs. 2.1 and 2.2. All relevant diagrams have a hard quark or gluon running in the loop as these are the excitations that are integrated out. For soft gluons with momentum $P \sim g\Lambda$ the inverse bare propagator is $\sim P^2 \sim g^2\Lambda^2$ while the HTL self-energy is also $\sim g^2\Lambda^2$. Therefore, one must use HTL resummed propagators for soft gluons. The diagrammatic evaluation of the retarded self-energy in Fig. 2.1 gives identical results to Eq. (2.13). Similarly, interaction vertices with a hard loop are at the same order as the usual interaction vertices. In this thesis, we will only need the soft gluon self-energy and not higher order vertices.

The focus in this thesis is on HTL effective theory in a non-equilibrium plasma. In this case, the distribution of hard particles is given by a non-equilibrium distribution $f_0(\mathbf{p})$. As before all dynamical information about the hard quasiparticles is integrated out, leaving e.g. Eq. 2.13 for the retarded self-energy of soft gluons. In order for HTL effective theory to be applicable in a non-equilibrium setting, some conditions need to be met [81]. For instance, soft gluon modes cannot be so heavily populated that the diagrams in Fig. 2.1 are of the same order or smaller than corresponding diagrams with a soft gluon running in the loop. Furthermore, one needs to assume a plasma with zero net quasiparticle current $\langle j^\mu \rangle = 0$ and therefore zero net soft gluon field strength $\mathcal{F}^{\mu\nu} = 0$.

2.2 MOMENTUM BROADENING AND ENERGY LOSS

The rate of transverse momentum broadening is a central quantity in a quark-gluon plasma. It is furthermore needed to calculate the rate of collinear gluon production in jets and in kinetic theory, as well as the rate of collinear photon production. In order to calculate the rate of transverse momentum broadening in a non-equilibrium medium one needs a detailed microscopic description of transverse kicks by soft gluons at energy $g\Lambda$. This is given by non-equilibrium HTL effective theory and has not been evaluated

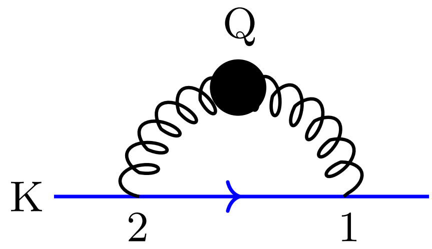

Figure 2.3: A self-energy diagram for a quark interacting ction with a soft gluon. The gluon propagator is resummed.

consistently before.[2] Transverse momentum broadening can also happen through hard kicks with energy $\sim \Lambda$. However, such hard kicks are much less frequent and their probability is parametrically suppressed during the formation time in gluon or photon emission.[3]

For concreteness, we will focus on transverse momentum broadening of a quark in our calculation. Our derivation uses non-equilibrium quantum field theory and clarifies some points from earlier work in the literature. The quark can either be a jet parton or a medium quark. Our discussion can easily be generalized for a gluon by introducing different colour factors. Furthermore, it can be generalized to apply to heavy quarks by giving the quark a mass, see below.

The decay rate for a quark interacting with soft gluons is given by

$$\Gamma = \frac{1}{4k} \mathrm{Tr}\left[\not{K} \Sigma_{21}\right], \tag{2.14}$$

see [106]. Here Σ_{21} is the quark self-energy. The indices 12 refer to time ordering in the self-energy, for further details see App. A. The quark-self energy is

$$\begin{aligned} \Sigma_{21}(K) = g^2 C_F \int \frac{d^4Q}{(2\pi)^4}\, D_{21}^{\mu\nu}(Q) \\ \times \gamma_\mu \left(\not{K} - \not{Q}\right) \gamma_\nu \left[1 - f_q(\mathbf{k} - \mathbf{q})\right] 2\pi\delta((K-Q)^2). \end{aligned} \tag{2.15}$$

2 Momentum broadening using HTL effective theory out of equilibrium was considered independently in [102] and in [103]. However, as pointed out in [104], the analysis in these papers was not correct. Ref. [102] assumed a KMS relation for the rr propagator (see Eq. 5 in the reference), which is incorrect in a non-equilibrium plasma and ignores the details of how non-equilibrium hard particles radiate soft gluons. Similarly, [103] used a classical argument that implicitly assumed a KMS condition. Furthermore, these papers did not evaluate the results numerically due to divergences coming from instability poles.

3 For a parametrically large jet parton energy $E \gtrsim T/g^4$, the formation time becomes long enough to allow for hard kicks during emission, see [105].

see Fig. 2.3. Here

$$D_{21}^{\mu\nu}(Q) = \int d^4(x-y)\, e^{iQ\cdot(x-y)} \langle A^\mu(x) A^\nu(y) \rangle \tag{2.16}$$

is one component of the HTL soft gluon correlator, see App. A for further information. We are interested in soft momentum kicks, $Q \sim g\Lambda$, while the quark momentum is $K \gtrsim \Lambda$. Using that $Q \ll K$ and $K^2 = 0$, the decay rate is

$$\frac{d\Gamma}{d^4Q} = \frac{g^2 C_F}{(2\pi)^4} D_{21}^{\mu\nu}(Q) v_\mu v_\nu \, \delta(v \cdot Q) \tag{2.17}$$

where $v^\mu = K^\mu/k = (1, \widehat{\mathbf{k}})$ is scaled momentum for the on-shell parton. For a heavy quark with mass M, the delta function in Eq. (2.15) is replaced by $\delta((K-Q)^2 - M^2)$ with $K^2 = M^2$. Then Eq. (2.17) applies for heavy quarks except that $v^\mu = K^\mu/k = (\sqrt{k^2 + M^2}/k, \widehat{\mathbf{k}})$.

To get more physically transparent results we can write the gluon correlator in a different basis of two-point correlators. We write

$$D_{21}^{\mu\nu} = \frac{1}{2}\left[D_{\text{ret}}^{\mu\nu} - D_{\text{adv}}^{\mu\nu}\right] + D_{rr} \tag{2.18}$$

Here we have defined a retarded correlator

$$D_{\text{ret}}^{\mu\nu}(x,y) = \theta(t_x - t_y)\langle [A^\mu(x), A^\nu(y)] \rangle, \tag{2.19}$$

an advanced correlator

$$D_{\text{adv}}^{\mu\nu}(x,y) = -\theta(t_y - t_x)\langle [A^\mu(x), A^\nu(y)] \rangle \tag{2.20}$$

and a statistical correlator

$$D_{rr}^{\mu\nu}(x,y) = \frac{1}{2}\langle \{A^\mu(x), A^\nu(y)\} \rangle \tag{2.21}$$

which we will also call the rr correlator. The reason for this name and further information on these propagators can be found in App. A.

The physical interpretation of these correlators is straightforward. The retarded correlator describes propagation forward in time with $t_x > t_y$. Because the commutator $[A^\mu(x), A^\nu(y)] = A^\mu(x)A^\nu(y) - A^\nu(y)A^\mu(x)$ vanishes at spacelike distances, propagation is only in the forward lightcone and therefore causal. The advanced correlator describes propagation backwards in time. It is easy to see that $D^{\mu\nu}_{\text{adv}}(x,y) = D^{\nu\mu}_{\text{ret}}(y,x)$ and in momentum space $D^{\mu\nu}_{\text{ret}}(Q) = D^{\nu\mu}_{\text{adv}}(Q)^*$, showing that these two functions are not independent. The statistical rr correlator is non-vanishing even for classical commuting fields and is defined in terms of an anticommutator $\{A^\mu(x), A^\nu(y)\} = A^\mu(x)A^\nu(y) + A^\nu(y)^\mu(x)$. It gives the occupation density of different modes in the plasma.

The rate of momentum broadening of a parton is

$$\hat{q} := \frac{d\left\langle q_\perp^2\right\rangle}{dt} \tag{2.22}$$

where $\langle q_\perp^2 \rangle$ is the average transverse momentum squared imparted on the jet parton in time t. Eqs. (2.17) and (2.18) give that

$$\begin{aligned} \hat{q} &= \int d^4Q\, q_\perp^2 \frac{d\Gamma}{d^4Q} \\ &= \int \frac{d^2q_\perp}{(2\pi)^2}\, q_\perp^2\, \mathcal{C}(\mathbf{q}_\perp) \end{aligned} \tag{2.23}$$

where the collision kernel for transverse momentum broadening is

$$\mathcal{C}(\mathbf{q}_\perp) = g^2 C_F \int \frac{dq^0 dq^z}{(2\pi)^2}\, D^{\mu\nu}_{rr}(Q) v_\mu v_\nu\, 2\pi\delta(v\cdot Q) \tag{2.24}$$

at leading order. Here we have used that in the HTL regime, $D_{rr} \sim 1/g^3$ while $D_{\text{ret}} \sim 1/g^2$ so that $D_{21} \approx D_{rr}$. Essentially, this is because the rr correlator depends on the occupation density of soft gluons which is $\sim 1/g$ in this regime. We will show this explicitly below. Eq. (2.24) shows that at leading order, transverse momentum broadening is due to soft gluons present in the medium and depends on their occupation density. We note that the rate of longitudinal momentum broadening, i.e. broadening in the jet parton direction,

$$\hat{q}_L := \frac{d\langle(\Delta p_z)^2\rangle}{dt} = \int d^4Q\, q_z^2 \frac{d\Gamma}{d^4Q} \tag{2.25}$$

can similarly be shown to be

$$\hat{q}_L \approx g^2 C_F \int \frac{d^4Q}{(2\pi)^4}\, q_z^2\, D^{\mu\nu}_{rr}(Q) v_\mu v_\nu\, 2\pi\delta(v\cdot Q). \tag{2.26}$$

Our derivation can also be used to evaluate the rate of energy loss of a jet parton or a quasiparticle in the medium. Energy loss takes place through three processes: Collinear emission of a hard gluon, hard two-to-two scattering and interaction with soft gluons [107]. Here we focus on energy loss through soft gluons, the rate of which is given by

$$\widehat{e} = \int d^4Q\, q^0 \frac{d\Gamma}{d^4Q} \tag{2.27}$$

where q^0 is the energy lost by the jet parton and $\frac{d\Gamma}{d^4Q}$ comes from Eq. (2.17). It is helpful to use the decomposition in Eq. (2.18). As $D_{rr}^{\mu\nu}(x,y) = D_{rr}^{\nu\mu}(y,x)$, it can be shown that

$$D_{rr}^{\mu\nu}(Q)v_\mu v_\nu = D_{rr}^{\mu\nu}(-Q)v_\mu v_\nu. \tag{2.28}$$

Substituting this in Eq. (2.27) we see that the rr correlator does not contribute to energy loss due to soft gluons. This means that the jet parton is equally likely to gain momentum q^0 and to lose momentum q^0 when interacting with soft gluons present in the medium. Therefore,

$$\widehat{e} = g^2C_F \int \frac{d^4Q}{(2\pi)^4}\, q^0 \frac{1}{2}\left(D^{\mu\nu}_{\text{ret}} - D^{\mu\nu}_{\text{adv}}\right)(Q)v_\mu v_\nu\, 2\pi\delta(v\cdot Q). \tag{2.29}$$

The retarded and advanced correlators denote soft gluons emitted by the jet parton itself. Therefore, energy loss is not due to soft gluons present in the medium but rather due to the quark's own radiation field.

That energy loss because of soft gluons is due to the jet parton's own radiation field, can also be seen from a classical argument, see e.g. [108, 109]. The rate of energy lost due to a current passing through an electromagnetic field is

$$\widehat{e} = \text{Re} \int d^3x\, \mathbf{J}_{\text{ext}}(x)\cdot \mathbf{E}_{\text{ind}}(x). \tag{2.30}$$

Here the current comes from the jet parton itself $\mathbf{J}_{\text{ext}} = g\mathbf{v}\delta^{(3)}(\mathbf{x}-\mathbf{v}t)$ which travels at the speed of light with velocity $\mathbf{v}$ and the electric field $\mathbf{E}_{\text{ind}}$ is induced by the jet parton. From linear response theory we know that the induced electric field is

$$E^i_{\text{ind}}(Q) = iq^0 D^{ij}_{\text{ret}}(Q) J^j_{\text{ext}}(Q). \tag{2.31}$$

if one assumes the temporal-axial gauge $A^0 = 0$. Using that the current in momentum space is $2\pi g\mathbf{v}\delta(q^0 - \mathbf{v}\cdot\mathbf{q})$ we get a rate of energy loss that reproduces Eq. (2.29) in the temporal-axial gauge. This classical derivation can also reproduce Eq. (2.29) when working in another gauge but then current conservation needs to be assumed explicitly [110]. Colour factors can easily be derived by including the relevant colour matrices.

We have shown generally that momentum broadening is due soft gluons present in the medium, while energy loss is due to dissipation in the jet parton's own radiation field and not due to soft gluons in the medium. In thermal equilibrium, there is the same qualitative difference between transverse momentum broadening and energy loss through soft gluons. However, momentum broadening and energy loss are linked through the fluctuation-dissipation relation in thermal equilibrium. Specifically, in equilibrium, the rr correlator is related to the retarded and advanced correlators through the Kubo-Martin-Schwinger relation [111, 112]

$$D_{rr}(Q) = \left(\frac{1}{2} + f_{\mathrm{B}}(q^0)\right) \left[D_{\mathrm{ret}}(Q) - D_{\mathrm{adv}}(Q)\right], \tag{2.32}$$

see a derivation in App. A. This formula says that each gluon mode has an occupation density $\frac{1}{2} + f_{\mathrm{B}}(q^0)$ where $1/2$ is the occupation density of fluctuations in vacuum and

$$f_{\mathrm{B}}(q^0) = \frac{1}{e^{q^0/T} - 1} \tag{2.33}$$

is the equilibrium Bose-Einstein distribution. Therefore, Eq. (2.32) just says that in thermal equilibrium, the soft gluons in a medium are thermalized. Using Eq. (2.32) and that $f_B(q^0) \approx T/q^0$ for soft gluons, one can show that

$$\widehat{q}_L = T\widehat{e}. \tag{2.34}$$

This is a fluctuation-dissipation relation which links longitudinal momentum broadening which happens through fluctuating soft gluons in the medium, and energy loss which is a dissipative process happening through the parton's radiation field.

Additional simplification takes place in thermal equilibrium where sum rules give simple formulas for the collision kernel [82, 83]. The result is that the collision kernel from Eq. (2.24) is

$$\mathcal{C}_{\mathrm{eq}}(\mathbf{q}_\perp) = g^2 C_F T \left(\frac{1}{\mathbf{q}_\perp^2} - \frac{1}{\mathbf{q}_\perp^2 + m_D^2}\right). \tag{2.35}$$

The term $1/(q_\perp^2 + m_D^2)$ describes transverse kicks from chromoelectric modes which are screened by the Debye mass m_D^2. The term $1/q_\perp^2$ describes kicks from chromomagnetic modes which are not screened in thermal equilibrium. The derivation of Eq. (2.35) assumed the KMS condition or the imaginary time formalism for static modes, both of which are not valid out of equilibrium. More recently, the equilibrium collision kernel has been evaluated at next-to-leading order in g [83]. That paper also suggested that the kernel could be evaluted on the lattice in an effective theory called EQCD which is equivalent to HTL for static observable. This gives non-perturbative information about the equilibrium collision kernel after being matched to full QCD. Such lattice studies have been performed, see [113], [114] and references therein.

Our goal is to evaluate momentum broadening in a non-equilibrium plasma. Then Eqs. (2.32), (2.34) and (2.35) are not valid and one needs to evaluate the rr correlator for soft gluons analytically in full detail. This will be the task in the remainder of this section.

2.3 SOFT GLUON CORRELATORS IN AN ANISOTROPIC PLASMA

Tranverse momentum broadening of a parton by soft gluons kicks is described by the gluon rr correlator, see Eq. (2.23), which characterizes the density of gluons in a medium. These soft gluons are sourced by hard quasiparticles. To fix ideas we choose a momentum distributions for hard quarks and gluons at energy Λ. A standard choice in the literature is the anisotropic distribution

$$f(\mathbf{p}) = \sqrt{1+\xi}\, f_{\text{eq}}\left(\sqrt{p^2+\xi(\mathbf{n}\cdot\mathbf{p})^2}\right), \tag{2.36}$$

which was first proposed in [115]. We call $f(\mathbf{p})$ anisotropic because it depends explicitly on the direction of $\mathbf{p}$. Here f_{eq} is the distribution of quarks and gluons in thermal equilibrium with the temperature replaced by a hard scale Λ. More specifically, for quarks we have the Fermi-Dirac distribution $f(p) = 1/(e^{p/\Lambda}+1)$ and for gluons we have the Bose-Einstein distribution $f(p) = 1/(e^{p/\Lambda}-1)$. In Eq. (2.36), the equilibrium distribution is elongated or contracted along the axis $\mathbf{n}$ as quantified by the anisotropy parameter ξ. For $\xi > 0$ the distribution is oblate and for $\xi < 0$ it is prolate. The distribution is well defined for ξ between -1 and $+\infty$. The prefactor $\sqrt{1+\xi}$ guarantees that the total number density of hard particles is the same as in thermal equilibrium, giving a consistent comparison between non-equilibrium and equilibrium results. This is in line with most work in the literature which fixes the number density. One could equally imagine fixing the energy density. Independent of whether one fixes number or energy density, our main results all remain nearly the same.

Earlier work on correlators in an anisotropic plasma has mostly focused on the retarded correlator. It describes propagation and dispersion relations of soft gluon modes, screening, as well as parton energy loss, see Eq. (2.29). However, it is insufficient for momentum broadening. In [115, 116], the retarded gluon correlator was derived for the momentum distribution in Eq. (2.36) and dispersion relations analyzed, see also [117] for an intuitive discussion. The retarded gluon correlator was analyzed in more detail in [118], and in [119] it was evaluated for more complicated anisotropic distributions. Furthermore, the quark retarded propagator was found in [120, 121]. There has been much less work on the *rr* correlator which we evaluate fully for the first time, however see [122] for the static component D^{00}_{rr}.

In the time domain, the *rr* propagator defined in Eq. (2.21) is given by

$$D^{\mu\nu}_{rr}(x,y) = \int d^4w \int d^4z \, D^{\mu\omega}_{\text{ret}}(x,w)\Pi^{\omega\chi}_{aa}(w,z)D^{\chi\nu}_{\text{adv}}(z,y), \tag{2.37}$$

see App. A for a derivation.[4] We omit writing colour indices explicitly in our discussion. Eq. (2.37) has a simple interpretation. The self-energy component

$$\Pi^{\mu\nu}_{aa}(w,z) := \frac{1}{2}\langle\{j^\mu(w), j^\nu(z)\}\rangle, \tag{2.38}$$

where $j^\mu A^\mu$ is the interaction-term in the QCD Lagrangian, describes the rate of creating a pair of soft gluon excitations at points w and z. Here the index aa refers to the time-ordering of the current operators j^μ in Eq. (2.38), see App. A. After being created, the soft gluons then propagate forward in time until points x and y where we measure their density. The propagation is described by the retarded and advanced correlators, see Eqs. (2.19) and (2.20). Going to momentum space we get that

$$D^{\mu\nu}_{rr}(Q) = D^{\mu\omega}_{\text{ret}}(Q)\,\Pi^{\omega\chi}_{aa}(Q)\,D^{\chi\nu}_{\text{adv}}(Q). \tag{2.39}$$

We will discuss assumptions made in the derivation of Eq. (2.39) in Sec. 3.1.

4 We use modern summation notation where $A^\omega B^\omega = A_\omega B^\omega = g_{\mu\nu}A^\mu B^\nu$.

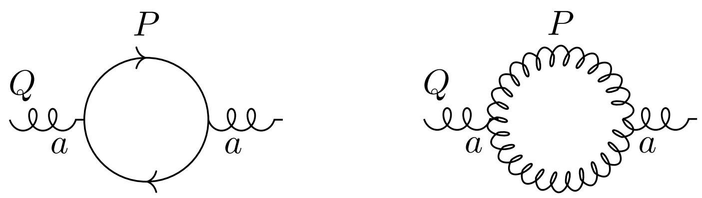

Figure 2.4: Diagrams needed to evaluate Π_{aa}. Here $P \sim \Lambda$ and $Q \sim g\Lambda$.

Throughout our discussion we assume the Hard Thermal Loops (HTL) regime. This means that soft gluon self-interaction is suppressed relative to interaction between soft gluons and hard quasiparticles [81]. Then the rate of production is

$$\Pi^{\mu\nu}_{aa}(Q) = g^2 \int \frac{d^3p}{(2\pi)^3} v^\mu v^\nu 2\pi\delta(v \cdot Q)\Big|_{v=(1,\hat{\mathbf{p}})} \times \left[2N_f f_q(\mathbf{p})\left(1 - f_q(\mathbf{p})\right) + 2N_c f_g(\mathbf{p})\left(1 + f_g(\mathbf{p})\right)\right] \tag{2.40}$$

This can be seen by evaluating the diagrams in Fig. 2.4, see [81]. Here, hard particles with momentum $\mathbf{p} \sim \Lambda$ radiate soft gluons with momentum $\mathbf{Q} \sim g\Lambda$, so the rate includes hard particle momentum distribution with Bose enhancement and Pauli blocking in the final state. In our specific case, teh momentum distribution is given by Eq. (2.36). The delta function comes from demanding that the quasiparticles are on shell both before and after emission, $P^2 = (P+Q)^2$.

The retarded correlator is

$$D^{\mu\nu}_{\text{ret}}(x,y) = D^{0\,\mu\nu}_{\text{ret}}(x,y) + \int d^4z \int d^4w\, D^{0\,\mu\omega}_{\text{ret}}(x,z)\Pi^{\omega\chi}_{\text{ret}}(z,w)D^{\chi\nu}_{\text{ret}}(w,y) \tag{2.41}$$

see App. A. Here D^0_{ret} is the bare retarded correlator and Π_{ret} is the retarded self-energy. Going to momentum space in Feynman gauge gives that

$$D^{\mu\nu}_{\text{ret}}(Q) = i\left(\left[Q^2 - \Pi_{\text{ret}}\right]^{-1}\right)^{\mu\nu} \tag{2.42}$$

where the retarded HTL self-energy is

$$\Pi^{\mu\nu}_{\text{ret}}(Q) = -g^2 \int \frac{d^3p}{(2\pi)^3} \frac{\partial f_{\text{tot}}}{\partial P^\omega}\left[-v^\mu g^{\omega\nu} + \frac{Q^\omega v^\mu v^\nu}{v \cdot Q + i\epsilon}\right]\Bigg|_{v=(1,\hat{\mathbf{p}})} \tag{2.43}$$

with $f_{\text{tot}}(\mathbf{p}) = 2N_f f_q(\mathbf{p}) + 2N_c f_g(\mathbf{p})$, as was argued in Sec. 2.1. One should interpret $\partial f_{\text{tot}}/\partial P^0 = 0$. In our case the momentum distribution comes from Eq. (2.36).

We begin by analyzing the tensorial structure of the self-energies in Eqs. (2.40) and (2.43) which are symmetric, rank-two tensors.[5] The only tensors in the problem are the metric $g^{\mu\nu}$, the fluid velocity u^μ which is $u^\mu = (1, 0, 0, 0)$ in the fluid's rest frame, the gluon momentum $Q^\mu = (q^0, \mathbf{q})$ and the vector defining the anisotropy direction $\mathbf{n}^\mu$. This gives a total of seven symmetric, rank-two tensors. We furthermore see that $Q^\mu \Pi^{\mu\nu}_{aa}(Q) = Q^\mu \Pi^{\mu\nu}_{\mathrm{ret}}(Q) = 0$ which is a consequence of gauge invariance in the HTL approximation [64]. This gives three constraints on the self-energies, one for each vector in the problem, reducing to four the number of tensors that Π_{ret} and Π_{aa} depend on.

There is some flexibility in how the polarization tensors are chosen. Working in the rest frame of the fluid, we choose the first two tensors to be

$$P_T^{ij} = \delta^{ij} - \frac{q^i q^j}{\mathbf{q}^2} \tag{2.44}$$

with all other components zero and

$$P_L^{\mu\nu} = \frac{Q^\mu Q^\nu}{Q^2} - g^{\mu\nu} - P_T^{\mu\nu}. \tag{2.45}$$

Both of these tensors are present in thermal equilibrium [17]. Here P_T is transverse to $\mathbf{q}$ and describes transverse propagation like in vacuum while P_L describes longitudinal polarization. For the latter two tensors it is convenient to define

$$\tilde{n}^\mu = (0, \frac{\hat{\mathbf{n}}^i}{\sqrt{\hat{n}^2}}) \tag{2.46}$$

where

$$\hat{\mathbf{n}} = \mathbf{n} - \frac{\mathbf{q}\cdot\mathbf{n}}{\mathbf{q}^2}\mathbf{q}. \tag{2.47}$$

so that $\tilde{n}^\mu$ is orthogonal both to the fluid's velocity u^μ and to the gluon momentum Q^μ. We then define

$$C^{\mu\nu} = \tilde{n}^\mu \tilde{n}^\nu. \tag{2.48}$$

which describes propagation along the anisotropy vector. Finally we define the tensor D by

$$\begin{aligned} D^{00} &= 0, \\ D^{0i} = D^{i0} &= \frac{\mathbf{q}^2}{\omega^0}\tilde{n}^i, \\ D^{ij} &= q^i \tilde{n}^j + q^j \tilde{n}^i \end{aligned} \tag{2.49}$$

5 The first term in Eq. (2.43) can be shown to be symmetric in μ and ν by an integration by parts.

which mixes the gluon three-momentum and the anisotropy vector. Here $\omega = q^0$. All four tensors P_T, P_L, C, D satisfy $P_T^{\mu\nu} Q^\nu = 0$ etc. Our choice of the four tensors differs from that of [115] and [118] which only needed the spatial components and from that of [122] which used a different, and from our point of view, more complicated basis of tensors.

It is easy to see that these four tensors form a closed set under anticommutation defined as

$$\{X, Y\}^{\mu\nu} = X^{\mu\omega}\, Y^{\omega\nu} + Y^{\mu\omega}\, X^{\omega\nu}. \tag{2.50}$$

Defining $E = P_T - C$ gives simpler anticommutation relations so we will use the set E, P_L, C and D from now on. A straightforward calculation gives that

$$\begin{aligned}
P_L^2 &= -P_L \\
E^2 &= -E \\
C^2 &= -C \\
D^2 &= -\frac{Q^2 \mathbf{q}^2}{\omega^2}\,(C + P_L) \\
\{E, P_L\} = \{E, C\} &= \{E, D\} = \{P_L, C\} = 0 \\
\{P_L, D\} &= \{C, D\} = -D.
\end{aligned} \tag{2.51}$$

We see that some of the tensors are not orthogonal to each other. Commutators within our set of four tensors would give new tensors but fortunately we will not need those.

Assuming the momentum distribution in Eq. (2.36), we can express the self-energies Π_{aa} and Π_{ret} in terms of these four tensors. Writing

$$-i\Pi_{aa}^{\mu\nu} = \alpha P_L^{\mu\nu} + \beta E^{\mu\nu} + \gamma C^{\mu\nu} + \delta D^{\mu\nu}, \tag{2.52}$$

one can show that

$$\begin{aligned}
\alpha &= \frac{Q^2}{\mathbf{q}^2}\Pi^{00} \\
\gamma &= \Pi^{ij}\tilde{n}^i\tilde{n}^j \\
\delta &= \frac{\omega}{\mathbf{q}^2}\Pi^{0i}\tilde{n}^i \\
\beta &= -\alpha - \gamma - \Pi^{\mu}{}_{\mu}.
\end{aligned} \tag{2.53}$$

where these functions quantify the rate of producing gluons with a specific polarizations. These functions can be expressed in terms of the gluon frequency ω, the three-momentum component parallel to the anisotropy vector $q_{\parallel} = \mathbf{n}\cdot\mathbf{q}$ and the three-momentum component orthogonal to the anisotropy vector $q_{\perp} = |\mathbf{q} - (\mathbf{n}\cdot\mathbf{q})\,\mathbf{n}|$. After a change of variables $\tilde{p} = p\sqrt{1+\xi\,(\mathbf{v}\cdot\mathbf{n})^2}$, we see that Eq. (2.40) can be written as

$$\Pi^{\mu\nu}_{aa} = 2\pi m_0^2\,\Lambda\,\Xi^{\mu\nu} \tag{2.54}$$

where the mass parameter is

$$m_0^2 = \frac{g^2}{2\pi^2}\int_0^\infty d\tilde{p}\;\tilde{p}^2\left[2N_f f_q^0(1-f_q^0) + 2N_c f_g^0(1+f_g^0)\right], \tag{2.55}$$

with f_q^0 the Fermi-Dirac distribution and f_g^0 the Bose-Einstein distribution, both at temperature Λ. The scale m_0^2 happens to be the Debye mass in thermal equilibrium but that is simply because we elongated and contracted equilibrium distributions to get the anisotropic distribution in Eq. (2.36). Furthermore, the angular function in Eq. (2.54) is

$$\Xi^{\mu\nu} = \int\frac{d\Omega}{4\pi}\,v^\mu v^\nu\frac{\delta(\omega-\mathbf{v}\cdot\mathbf{q})}{\left(1+\xi\,(\mathbf{v}\cdot\mathbf{n})^2\right)^{3/2}}\Bigg|_{v^0=v}. \tag{2.56}$$

Eq. (2.53) for the components in Π_{aa} then can be written more explicitly as

$$i\alpha = 2\pi\Lambda\,m_0^2\,\frac{\omega^2-q^2}{q^2}\,P^{00}, \tag{2.57}$$

$$\begin{aligned} i\delta &= 2\pi\Lambda\,m_0^2\,\frac{\omega/q}{\sqrt{q^2-(\mathbf{q}\cdot\mathbf{n})}} \\ &\quad\times\left(P^{0i}n^i - \frac{\mathbf{q}\cdot\mathbf{n}\,\omega}{q^2}P^{00}\right), \end{aligned} \tag{2.58}$$

$$\begin{aligned} i\gamma &= 2\pi\Lambda\,m_0^2\,\frac{1}{1-(\mathbf{q}\cdot\mathbf{n})^2/q^2} \\ &\quad\times\left(P^{ij}n^in^j - \frac{2\mathbf{q}\cdot\mathbf{n}\,\omega}{q^2}P^{0i}n^i + \frac{(\mathbf{q}\cdot\mathbf{n})^2\omega^2}{q^4}P^{00}\right) \end{aligned} \tag{2.59}$$

$$i\beta = -i\alpha - i\gamma. \tag{2.60}$$

We have used that $\Xi^{\mu\nu}Q_\mu = 0$ so that the only non-trivial components of the angular function are

$$\Xi^{00} = \frac{1}{4\pi q}\int_0^{2\pi}d\phi\;\frac{1}{\left[1+\xi\left(\tilde{q}_{\parallel}\tilde{\omega} - \tilde{q}_{\perp}\sqrt{1-\tilde{\omega}^2}\cos\phi\right)^2\right]^{3/2}}, \tag{2.61}$$

$$\Xi^{0i}n^i = \frac{1}{4\pi q}\int_0^{2\pi} d\phi \, \frac{\tilde{q}_{\parallel}\tilde{\omega} - \tilde{q}_{\perp}\sqrt{1-\tilde{\omega}^2}\cos\phi}{\left[1+\xi\left(\tilde{q}_{\parallel}\tilde{\omega} - \tilde{q}_{\perp}\sqrt{1-\tilde{\omega}^2}\cos\phi\right)^2\right]^{3/2}}, \tag{2.62}$$

and

$$\Xi^{ij}n^i n^j = \frac{1}{4\pi q}\int_0^{2\pi} d\phi \, \frac{\left(\tilde{q}_{\parallel}\tilde{\omega} - \tilde{q}_{\perp}\sqrt{1-\tilde{\omega}^2}\cos\phi\right)^2}{\left[1+\xi\left(\tilde{q}_{\parallel}\tilde{\omega} - \tilde{q}_{\perp}\sqrt{1-\tilde{\omega}^2}\cos\phi\right)^2\right]^{3/2}}, \tag{2.63}$$

where we have used the delta function to eliminate the angle θ between $\mathbf{v}$ and $\mathbf{q}$. Here $\tilde{\omega} = \omega/q$, $\tilde{q}_{\parallel} = q_{\parallel}/q$ and $\tilde{q}_{\perp} = q_{\perp}/q$ are normalized components of the gluon four-momentum. The remaining integrals in ϕ can be done numerically.

In a similar fashion the retarded self-energy can be written as

$$-i\Pi^{\mu\nu}_{\text{ret}} = \Pi_L P_L^{\mu\nu} + \Pi_e E^{\mu\nu} + \Pi_c C^{\mu\nu} + \Pi_d D^{\mu\nu}. \tag{2.64}$$

We will reproduce the different components for completeness, but they were already derived in [115]. They are

$$i\Pi_L = \frac{1}{2}m_0^2 \frac{\omega^2 - q^2}{q^2}\Sigma^{00}, \tag{2.65}$$

$$i\Pi_d = \frac{1}{2}m_0^2 \frac{\omega/q}{\sqrt{q^2 - (\mathbf{q}\cdot\mathbf{n})}} \times \left(\Sigma^{0i}n^i - \frac{\mathbf{q}\cdot\mathbf{n}\,\omega}{q^2}\Sigma^{00}\right), \tag{2.66}$$

$$i\Pi_c = \frac{1}{2}m_0^2 \frac{1}{1-(\mathbf{q}\cdot\mathbf{n})^2/q^2} \times \left(\Sigma^{ij}n^i n^j - \frac{2\mathbf{q}\cdot\mathbf{n}\,\omega}{q^2}\Sigma^{0i}n^i + \frac{(\mathbf{q}\cdot\mathbf{n})^2\omega^2}{q^4}\Sigma^{00}\right) \tag{2.67}$$

$$\Pi_e = -\Pi_L - \Pi_c + \frac{\arctan\sqrt{\xi}}{\sqrt{\xi}}m_0^2 \tag{2.68}$$

where the angular components are

$$\Sigma^{00} = \int_{-1}^{1} dz \, \frac{1}{(1+\xi z^2)^2} \times \Big[-1 + \Big(\omega + \xi q_\parallel z\Big) \, R(\omega - q_\parallel z, q_\perp \sqrt{1-z^2}) \Big], \tag{2.69}$$

$$\Sigma^{0i} n^i = \int_{-1}^{1} dz \, \frac{z}{(1+\xi z^2)^2} \times \Big[-1 + \Big(\omega + \xi q_\parallel z\Big) \, R(\omega - q_\parallel z, q_\perp \sqrt{1-z^2}) \Big], \tag{2.70}$$

$$\Sigma^{ij} n^i n^j = \frac{1+\xi}{\xi^{3/2}} \left(\arctan \sqrt{\xi} - \frac{\sqrt{\xi}}{1+\xi} \right) + \int_{-1}^{1} dz \, \frac{z^2}{(1+\xi z^2)^2} \times \Big[-1 + \Big(\omega + \xi q_\parallel z\Big) \, R(\omega - q_\parallel z, q_\perp \sqrt{1-z^2}) \Big] \tag{2.71}$$

and

$$\begin{aligned} R(a,b) &= \int_0^{2\pi} \frac{d\phi}{2\pi} \frac{1}{a - b\cos\phi + i\epsilon} \\ &= \theta(a^2 - b^2) \frac{\operatorname{sgn}(a)}{\sqrt{a^2 - b^2}} - \theta(b^2 - a^2) \frac{i}{\sqrt{b^2 - a^2}} \end{aligned} \tag{2.72}$$

for real values of a and b. The remaining integrals can be done analytically but the resulting expressions are very complicated. Therefore, we prefer to evaluate them numerically. See [123] for an alternative numerical evaluation.

Using the retarded self-energy in Eq. (2.64) we get that the retarded correlator is

$$D_{\text{ret}} = \frac{i}{Q^2 - \Pi_L P_L - \Pi_e E - \Pi_c C - \Pi_d D}. \tag{2.73}$$

Expanding in the self-energy components Π shows that

$$D_{\text{ret}} = \frac{i g^{\mu\nu}}{Q^2} + \frac{i}{Q^2} \sum_{n=1}^{\infty} \left(\frac{\Pi_L}{Q^2} P_L + \frac{\Pi_e}{Q^2} E + \frac{\Pi_c}{Q^2} C + \frac{\Pi_d}{Q^2} D \right)^n. \tag{2.74}$$

Each term on in the sum can be expressed with anticommutators, showing that the retarded correlator only depends on the four tensors in our basis as well as the metric $g^{\mu\nu}$. A detailed calculation gives

$$\begin{aligned} D^{\mu\nu}_{\text{ret}} &= \frac{-iQ^\mu Q^\nu}{(Q^2)^2} + iE^{\mu\nu} \tilde{D}^B_{\text{ret}} \\ &+ i \left[(Q^2 - \Pi_c) P_L^{\mu\nu} + (Q^2 - \Pi_L) C^{\mu\nu} + \Pi_d D^{\mu\nu} \right] \tilde{D}^A_{\text{ret}} \end{aligned} \tag{2.75}$$

where

$$\tilde{D}^{A}_{\text{ret}} = \frac{1}{\left(Q^2 - \Pi_L\right)\left(Q^2 - \Pi_c\right) - R\,\Pi_d^2} \tag{2.76}$$

and

$$\tilde{D}^{B}_{\text{ret}} = \frac{1}{Q^2 - \Pi_e} \tag{2.77}$$

with $R = Q^2\mathbf{q}^2/\omega^2$. The poles of Eqs. (2.76) and (2.77) give the dispersion relations of soft gluons in an anisotropic system. The excitations mostly represent the same physics as the excitations in an equilibrium system but with different detailed dispersion relations. However, anisotropic plasmas also contain novel physics, namely unstable modes which will be discussed in Sec. 3.1.

We can finally evaluate the rr correlator in Eq. (2.39) in an anisotropic plasma. Momentum broadening is given by $D^{\mu\nu}_{rr}\hat{K}_\mu\hat{K}_\nu$ so we only need the symmetric component of the correlator, namely

$$\begin{aligned} D^{(\mu\nu)}_{rr} &:= \frac{1}{2}\left[D_{rr} + D^{\dagger}_{rr}\right]^{\mu\nu} \\ &= \frac{1}{2}\left[D_{\text{ret}}\left(-i\Pi_{aa}\right)D_{\text{adv}} + D_{\text{adv}}\left(-i\Pi_{aa}\right)D_{\text{ret}}\right]^{\mu\nu} \end{aligned} \tag{2.78}$$

This formula can be evaluated by using that for any rank-two tensors X, Y and Z, we have

$$XYZ + ZYX = \frac{1}{2}\left(\{X,\{Y,Z\}\} - \{Y,\{Z,X\}\} + \{Z,\{X,Y\}\}\right) \tag{2.79}$$

The right-hand side in Eq. (2.79) is solely in terms of anticommutators. Using our expressions for the retarded correlator in Eq. (2.75), the self-energy Π_{aa} in Eq. (2.52), as well as the anticommutation relations in Eq. (2.51) we get that

$$\begin{aligned} D^{(\mu\nu)}_{rr} =& -\tilde{D}^{A}_{\text{ret}}\left(\tilde{D}^{A}_{\text{ret}}\right)^{*} \\ &\times\Bigg[\left\{\alpha\,|X|^2 - 2\delta R\,\mathrm{Re}(XW^*) + \gamma R\,|W|^2\right\}P_L^{\mu\nu} \\ &+\left\{\gamma\,|Z|^2 - 2\delta R\,\mathrm{Re}(ZW^*) + \alpha R\,|W|^2\right\}C^{\mu\nu} \\ &+\Big\{-\alpha\,\mathrm{Re}(XW^*) - \gamma\,\mathrm{Re}(ZW^*) \\ &+\delta\,\mathrm{Re}(XZ^*) + \delta R\,|W|^2\Big\}D^{\mu\nu}\Bigg] \\ &\quad -\tilde{D}^{B}_{\text{ret}}\left(\tilde{D}^{B}_{\text{ret}}\right)^{*}\beta E^{\mu\nu}. \end{aligned} \tag{2.80}$$

This is the central result of this chapter. Here

$$X = Q^2 - \Pi_c, \tag{2.81}$$

$$Z = Q^2 - \Pi_L, \tag{2.82}$$

and

$$W = -\Pi_d. \tag{2.83}$$

and $\tilde{D}^A_{\rm ret}$ and $\tilde{D}^B_{\rm ret}$ are defined in Eqs. (2.76) and (2.77). The self-energy components are given in Eqs. (2.57) to (2.60) and in Eqs. (2.65) to (2.68).

Part III

PLASMA INSTABILITIES AND HARD PROBES

3

PLASMA INSTABILITIES AND HARD PROBES

3.1 INSTABILITIES IN A QUARK-GLUON PLASMA

So far, we have derived the collision kernel $\mathcal{C}(\mathbf{p}_\perp)$ in an anisotropic plasma. The collision kernel gives the rate of transverse momentum broadening of a parton as it interacts with soft gluons in the medium, see Eqs. (2.24) and (2.80). The collision kernel is an essential quantity in a plasma. It allows one to evaluate the transport coefficient $\hat{q}$, see Eq. (2.23). It also gives the rate of collinear emission of photons and gluons. This rate is central to the physics of jet-medium interaction, photon radiation from the plasma, as well as a kinetic theory description of the plasma.

A numerical evaluation of the collision kernel $\mathcal{C}(\mathbf{p}_\perp)$ and $\hat{q}$ shows that the expressions we have derived are divergent. This suggests that some assumptions in our calculation are not correct. It is clearly vital to understand the physical reason for this divergence and to derive an anisotropic collision kernel which is free from divergences. This will be the task of this chapter.

The divergence in $\hat{q}$ can be shown to be logarithmic. For simplicity, we consider the case when both the jet parton momentum and the anisotropy vector $\mathbf{n}$ are in the z direction. We furthermore assume a small anisotropy $\xi \ll 1$. We focus on the term that goes like $E^{\mu\nu}$ in the rr correlator in Eq. (2.80) but the other terms can similarly be shown to give a logarithmic divergence. Expanding Eq. (2.68) for Π_e at small anisotropy $\xi \ll 1$ gives [115, 118]

$$\begin{aligned}\Pi_e = m_0^2 \left(\frac{\omega}{q}\right)^2 - \frac{i\pi}{4} m_0^2 \frac{\omega}{q} + \mathcal{O}\left(\left(\frac{\omega}{q}\right)^3\right) \\ + \xi \left[-\frac{1}{6}(1+\cos 2\theta) m_0^2 + \mathcal{O}\left(\frac{\omega}{q}\right)\right].\end{aligned} \tag{3.1}$$

where the assumption of $\omega \ll q$ will be justified below. Here θ is the angle between the soft gluon momentum $\mathbf{q}$ and the anisotropy vector $\mathbf{n}$. The retarded propagator has poles at

$$\omega^2 = q^2 + \Pi_e \approx q^2 - \xi \frac{1}{6}(1 + \cos 2\theta) m_0^2 \tag{3.2}$$

in this regime. We immediately see the presence of poles $\omega = i\gamma$ with $\gamma > 0$ when $\mathbf{q}$ is sufficiently small. These poles are called instability poles and turn out to be the culprit behind the divergence in $\hat{q}$.

To evaluate the divergence in $\hat{q}$ due to instability poles schematically, we drop all dependence on the angle θ and replace the function β in Eq. (2.80) by the parametric estimate $g\Lambda^2$. Since

$$\widehat{q} \approx g^2 C_F \int \frac{d^2 q_\perp}{(2\pi)^2}\, q_\perp^2 \int \frac{d\omega dq^z}{(2\pi)^2}\, \delta(\omega - q^z)\, v_\mu v_\nu\, D_{rr}^{\mu\nu}(Q). \tag{3.3}$$

we get that the contribution of the term that goes like $E^{\mu\nu}$ in Eq. (2.80) is schematically

$$\begin{aligned} \widehat{q} &\sim g^3 \Lambda^2 \int d^2 q_\perp\, q_\perp^2 \int d\omega dq^z \, \frac{\delta(\omega - q^z)}{|\omega^2 - q^2 - \Pi_e|^2} \\ &\sim g^3 \Lambda^2 \int d^2 q_\perp\, q_\perp^2 \int d\omega dq^z \, \frac{\delta(\omega - q^z)}{(q_\perp^2 + m_0^2 \left(\frac{\omega}{q}\right)^2 - \xi m_0^2)^2 + \left(m_0^2 \frac{\omega}{q}\right)^2} \end{aligned} \tag{3.4}$$

It is easy to see that the divergence happens when $\mathbf{q}_\perp \sim \sqrt{\xi} m_0$ and $\omega \sim q_\perp^3 / m_0^2 \sim \xi^{3/2} m_0$ in which case the denominator goes like $\sim \xi^2 m_0^4$. The scaling of ω and $\mathbf{q}_\perp$ justifies our assumption that $\omega/q \ll 1$ for ξ small. We furthermore see that the divergence is only present because of the instability poles which leads to the term $-\xi m_0^2$. Using a change of variable Eq. (3.4) can be rewritten as

$$\begin{aligned} \widehat{q} &\sim g^3 \Lambda^2 \int dq^z \int dq_\perp \frac{q_\perp^3}{(\frac{m_0 q^z}{\sqrt{\xi}})^2 + (q_\perp^2 - \xi m_0^2)^2} \\ &\sim g^4 \Lambda^3 \int du \int_{\sqrt{\xi}+\delta} dv \, \frac{v^3}{u^2/\xi + (v^2 - \xi)^2} \end{aligned} \tag{3.5}$$

where $u = q^z/m_0$ and $v = q_\perp/m_0$. We have introduced a cutoff δ around the divergent region, defined by $q_\perp > \sqrt{\xi} m_0 + \delta m_0$. With this cutoff our expression for momentum broadening can be evaluated by going to radial coordinates. We get

$$\widehat{q} \sim g^4 \Lambda^3 \xi^{3/2} \log\left(\sqrt{\xi}\delta\right). \tag{3.6}$$

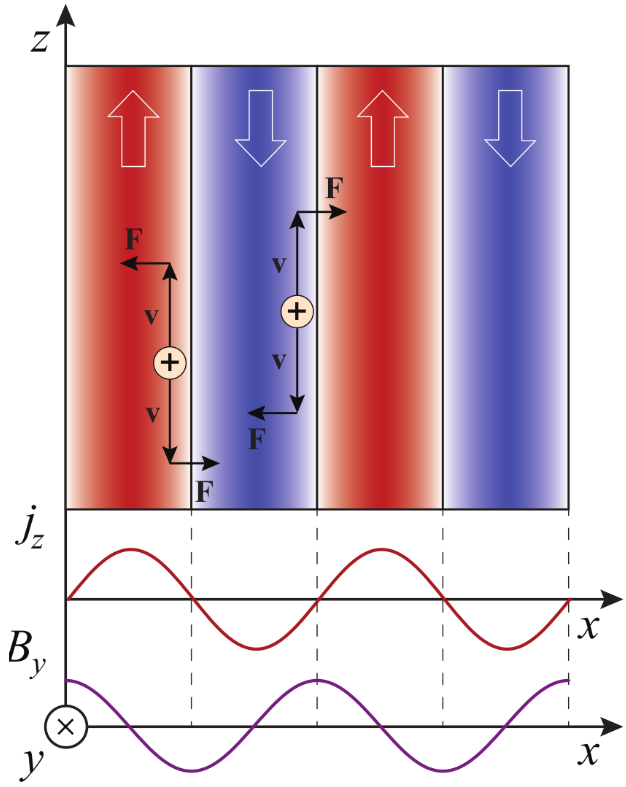

Figure 3.1: A cartoon to explain the physics of instability modes. From [124].

This is a logarithmic divergence when $\delta \to 0$. In the limit of $\xi \to 0$ where we tend towards isotropy, the divergence goes away.

The logarithmic divergence due to instabilities when calculating $\hat{q}$ in an anisotropic plasma was noted earlier in [102] and [103] but the detailed calculation of $\hat{q}$ incorrectly assumed a KMS condition which is only true in equilibrium. Ref. [103] suggested that this divergence should be cured by a next-to-leading order calculation of the retarded gluon self-energy with diagrams that describe soft gluon self-interaction. However, the analysis in that paper was done in the imaginary-time formalism which only applies to a thermally equilibrated plasma. The NLO diagrams proposed to cure the divergence should be analyzed in the real-time formalism, where they can be shown to be divergent themselves and therefore unable to cure the leading-order part. Ref. [102] also mentions the possibility that the divergences should be cured by including time dependence, which we believe to be the correct solution. We note that the divergence in the collision kernel was also mentioned in [81] without a detailed calculation.

We have seen that the divergence in $\hat{q}$ is due to instability poles $\omega = i\gamma$. The physics of these instabilities in a QCD plasma has been widely studied. Early works including [125, 126] showed the presence of these instabilities and suggested that they might be important for the early stages of heavy-ion collisions. Further qualitative discussions of the physics of QCD instabilities have been given in [117, 127, 128] see also [124] for a review. In essence, all plasmas have spontaneous thermal fluctuations in the current of quasiparticles. Consider a current fluctuation of particles travelling in the z direction with a fixed wavelength given by momentum q_x, see Fig. 3.1. This current fluctuation will source a chromomagnetic field B_y, also shown in Fig. 3.1. Analyzing charged quasiparticles travelling nearly in the z direction, one sees that they are deflected in the field and make the current fluctuation stronger. In return this generates an even stronger chromomagnetic field, and so on, leading to exponential growth, both in the current and in the density of soft gluons in chromomagnetic modes. This makes the plasma unstable.

The physics of instabilities is more complicated than suggested by Fig. 3.1. Quasiparticles that do not travel in the z direction are also deflected by the chromomagnetic field fluctuation but a detailed analysis shows that they tend to decrease the current fluctuation slightly [117]. This effect wins out in equilibrium, explaining why instabilities are not seen in an equilibrated plasma. In an anisotropic plasma, when more particles travel in the z direction than in other directions, the net effect of quasiparticles can be to increase the current fluctuation, leading to exponential growth. This happens even at low values of anisotropy.

The presence of instabilities depends on the wavelength of the current fluctuation. When the wavelength of the current fluctuation decreases and q_x increases, particles travelling in the z direction fly through multiple current filaments and do not contribute to the current. Thus there is no exponential growth. This explains why instabilities are only found for small momenta, $\mathbf{q} \sim \sqrt{\xi} g\Lambda$.

A detailed analysis of instabilities in a QCD plasma requires finding all instability poles $\omega = i\gamma$ of the retarded propagator in Eq. (2.75) [115]. In general, a mode with dispersion relation $\omega = E - i\Gamma$ gives contribution

$$D_{\text{ret}}(t_x, t_y) \sim \int \frac{dp^0}{2\pi} \frac{e^{-ip^0(t_x-t_y)}}{p^0 - E + i\Gamma} \sim \theta(t_x - t_y) e^{-iE(t_x-t_y)} e^{-\Gamma(t_x-t_y)} \tag{3.7}$$

to the retarded propagator in the time domain, as can be seen by continuing the integration contour to the lower half complex plane and using the residue theorem. Since instability poles have dispersion relation $\omega = i\gamma$ with $\gamma > 0$ we expect them to give a contribution $e^{\gamma(t_x - t_y)}$ in the time domain.[1] This signals exponential growth in the density of soft gluons. We note that it is highly unusual for a retarded propagator to have poles in the upper half plane. Using the contour along the real line as usually when going the time domain, then gives a contribution $D_{\text{ret}}(t_x, t_y) \neq 0$ for $t_x < t_y$ in contradiction of the definition of the retarded propagator in Eq. (2.19). We discuss this further below.

To understand the divergence in $\hat{q}$, we must analyze the assumptions made in Sec. 2. We made a number of assumptions when calculating $\hat{q}$ in an anisotropic plasma in Sec. 2. Firstly, we assumed that the medium changes slowly compared to the time between soft gluon kicks. This allowed us to specify a momentum distribution $f(\mathbf{p})$ of hard particles which we assumed did not change between medium kicks. Secondly, we used non-equilibrium propagators which are derived with the momentum distribution $f(\mathbf{p})$ specified in the distant past at initial time $t_0 \to -\infty$, see App. A. This is justified if momentum broadening happens quickly compared to changes in $f(\mathbf{p})$.

For a plasma with instability modes these assumptions break down. If we specify an initial condition at time $t_0 = -\infty$ in the HTL regime, instability modes will have infinite time to grow until a medium kick takes place. Thus the density of instability modes will be infinite when the jet parton finally receives a medium kick leading to a divergent rate of momentum broadening due to kicks from instability modes. This problem is not unique to momentum broadening. It arises for any probe that depends on the density of gluons in a anisotropic medium, such as the imaginary part of the heavy-quark potential [122].

From a theoretical point of view, the solution to divergences in $\hat{q}$ is to specify initial conditions at a finite initial time, $t_0 = 0$. Then instability modes only grow to a finite strength, leading to well-behaved results for $\hat{q}$. Such a calculation requires HTL resummed propagators in an unstable plasma with initial conditions at time $t_0 = 0$. We will derive such propagators in the next few sections. This is not only important for the calculation of non-equilibrium transverse momentum broadening, but also to under-

1 We give a more rigorous derivation of this result below.

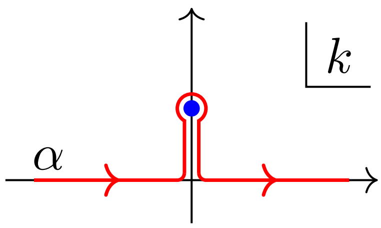

Figure 3.2: The contour α needed to evaluate the retarded correlator in the time domain.

stand more fully instabilities in a non-equilbrium quark-gluon plasma from the point of view of quantum field theory.

3.2 RETARDED GLUON CORRELATOR IN AN UNSTABLE PLASMA

We want to find the HTL correlator of soft gluons in a non-equilibrium system with instabilities. In our calculation, we specify initial conditions at time $t_0 = 0$ through the momentum distribution of hard quarks and gluons $f(\mathbf{p})$. We furthermore assume that there are initially no soft gluons. As we assume the HTL approximation, all self-interaction of soft gluons is ignored, meaning that our calculation is valid up until times when the gluon density has grown so much that gluon self-interaction is comparable to interaction with hard particles. Furthermore, we assume that the momentum distribution of hard particles does not change appreciably during our calculation; this is well justified as the time scale for change in momentum distributions is $\sim 1/g^4\Lambda$ [81].

We start by analyzing the HTL resummed retarded propagator D_{ret} which is defined by

$$\begin{aligned} D_{\text{ret}}(x,y) &= D^0_{\text{ret}}(x,y) \\ &+ \int d^4z \int d^4w\, D^0_{\text{ret}}(x,z)\Pi_{\text{ret}}(z,w)D_{\text{ret}}(w,y) \end{aligned} \tag{3.8}$$

where D^0_{ret} is the free retarded propagator and Π_{ret} is the HTL resummed propagator. For easier notation we omit tensor and colour indices. In thermal equilibrium, and more generally in any system with initial condition at $t_0 = -\infty$, one can Fourier transform to momentum space to get

$$D_{\text{ret}}(P) = D^0_{\text{ret}}(P) + D^0_{\text{ret}}(P)\Pi_{\text{ret}}(P)D_{\text{ret}}(P) \tag{3.9}$$

This was our procedure in Eqs. (2.42) and (2.75). However, when specifying initial conditions at time $t_0 = 0$, there is no momentum space and we must take a different route.

Using the properties of retarded functions we write Eq. (3.8) as

$$\begin{aligned} D_{\text{ret}}(t_x, t_y; \mathbf{p}) &= D^0_{\text{ret}}(t_x - t_y; \mathbf{p}) \\ &+ \int_{t_y}^{t_x} dt_z \int_{t_y}^{t_z} dt_w \, D^0_{\text{ret}}(t_x - t_z; \mathbf{p}) \, \Pi_{\text{ret}}(t_z - t_w; \mathbf{p}) \, D_{\text{ret}}(t_w, t_y; \mathbf{p}). \end{aligned} \tag{3.10}$$

We have Fourier transformed to three-momentum space, as we assume a system with infinite spatial extent. In the HTL approximation, the self-energy is $\Pi_{\text{ret}}(t_z, t_w; \mathbf{p}) = \Pi_{\text{ret}}(t_z - t_w; \mathbf{p})$ which only depends on bare propagators for hard particles which have no knowledge of the initial time, see App. A. To avoid cluttered notation, we will omit writing dependence on three-momentum $\mathbf{p}$ in what follows and denote time variables by $x := t_x$, $y := t_y$ etc.

In Eq. (3.10) the retarded function obeys $D_{\text{ret}}(x + \tau, y + \tau) = D_{\text{ret}}(x, y)$, suggesting that it is independent of the initial time. We therefore will try writing

$$D_{\text{ret}}(x, y) = \int_\alpha \frac{dk}{2\pi} \, e^{-ik(x-y)} D_{\text{ret}}(k) \tag{3.11}$$

where $D_{\text{ret}}(k)$ is an unknown function of the frequency variable which we call k. Importantly, this is not a Fourier transform since we choose an integration contour α that goes above all poles of $D_{\text{ret}}(k)$, including those that might be in the upper half complex plane, see Fig. 3.2. This ensures that $D_{\text{ret}}(x, y) = 0$ for $x < y$, as can be seen by continuing the contour to the upper half complex plane and using the residue theorem.

We must find the function $D_{\text{ret}}(k)$ in Eq. (3.11) and show that this is indeed the solution of Eq. (3.10). The challenge is to evaluate the last term in Eq. (3.10) which we can write as

$$\begin{aligned} &\int_y^x dz \int_y^z dw \int \frac{dk_1}{2\pi} \int \frac{dk_2}{2\pi} \int_\alpha \frac{dk_3}{2\pi} \\ &e^{-ik_1(x-z)} e^{-ik_2(z-w)} e^{-ik_3(w-y)} \, D^0_{\text{ret}}(k_1) \, \Pi_{\text{ret}}(k_2) \, D_{\text{ret}}(k_3). \end{aligned} \tag{3.12}$$

using that D^0_{ret} and Π_{ret} can be Fourier transformed like usually. We can perform the time integrals explicitly because of the finite limits. If the upper limit of the w integral were still $+\infty$, the integral would not be obviously convergent since k_3 can be in the upper half complex plane, giving exponential growth in the factor $e^{-ik_3(w-y)}$. Using the finite limits, we get

$$\int \frac{dk_1}{2\pi} \int \frac{dk_2}{2\pi} \int_\alpha \frac{dk_3}{2\pi}\, D^0_{\rm ret}(k_1)\, \Pi_{\rm ret}(k_2)\, D_{\rm ret}(k_3)\, f(k_1,k_2,k_3) \tag{3.13}$$

with

$$\begin{aligned} f(k_1,k_2,k_3) = &-\frac{e^{-ik_1(x-y)}}{(k_1-k_2)(k_1-k_3)} \\ &-\frac{e^{-ik_2(x-y)}}{(k_2-k_1)(k_2-k_3)} - \frac{e^{-ik_3(x-y)}}{(k_3-k_1)(k_3-k_2)}. \end{aligned} \tag{3.14}$$

We will evaluate the remaining frequency integrals in Eq. (3.13) using some tricks. It can be easily verified that despite individual terms in Eq. (3.14) having poles in k_1, k_2 and k_3, the function $f(k_1,k_2,k_3)$ as a whole has no poles. Thus we can introduce principal values in all the variables, namely the substitution

$$\begin{aligned} &f(k_1,k_2,k_3) \longrightarrow \\ &\frac{1}{8} \sum_{\substack{\{k_1\to k_1+i\epsilon_1\} \\ \{k_1\to k_1-i\epsilon_1\}}} \sum_{\substack{\{k_2\to k_2+i\epsilon_2\} \\ \{k_2\to k_2-i\epsilon_2\}}} \sum_{\substack{\{k_3\to k_3+i\epsilon_3\} \\ \{k_3\to k_3-i\epsilon_3\}}} f(k_1,k_2,k_3). \end{aligned} \tag{3.15}$$

where ϵ_1, ϵ_2 and ϵ_3 are infinitesimal and positive and will be set to zero in the end. An important check on the calculation is that the order in which the infinitesimal quantities are set to zero does not matter. Using the residue theorem, Eq. (3.13) can then be evaluated in detail, since the infinitesimal quantities have removed the poles of each term off the real axis, see App. B. In this involved calculation, particular care is needed for integration on the contour α. The final result is that Eq. (3.13) is identical to

$$\int_\alpha \frac{dk}{2\pi}\, e^{-ik(x-y)}\, D^0_{\rm ret}(k)\, \Pi_{\rm ret}(k)\, D_{\rm ret}(k) \tag{3.16}$$

Having evaluated the challenging term in Eq. (3.10), we can finally find the retarded correlator for soft gluons in an unstable plasma. We see that Eq. (3.10) is equivalent to

$$\begin{aligned} &\int_\alpha \frac{dk}{2\pi}\, e^{-ik(x-y)} \left[D_{\rm ret}(k) - D^0_{\rm ret}(k) - D^0_{\rm ret}(k) \Pi_{\rm ret}(k) D_{\rm ret}(k) \right] \\ &\quad = 0. \end{aligned} \tag{3.17}$$

This gives an explicit solution for $D_{\rm ret}(k)$ and shows that

$$\begin{aligned} D_{\rm ret}(t_x,t_y;\mathbf{p}) &= \int_\alpha \frac{dp^0}{2\pi}\, e^{-ip^0(t_x-t_y)} D_{\rm ret}(p^0,\mathbf{p}) \\ &= \int_\alpha \frac{dp^0}{2\pi}\, e^{-ip^0(t_x-t_y)} \left[(D^0_{\rm ret}(P))^{-1} - \Pi_{\rm ret}(P) \right]^{-1} \end{aligned} \tag{3.18}$$

Our result for the retarded correlator in an unstable plasma Eq. (3.18) is intuitive. Even though there is strictly speaking no frequency domain in a system with initial time $t_0 = 0$, Eq. (3.18) is nearly a Fourier transform, except that the contour α goes above instability poles in the upper half complex plane. [2]

This guarantees causality since $D_{\text{ret}}(t_x, t_y) = 0$ for $t_x < t_y$. It furthermore shows that instability poles $p^0 = i\gamma$ gives time dependence

$$D_{\text{ret}} \sim \theta(t_x - t_y) e^{\gamma(t_x - t_y)} \tag{3.19}$$

which signals exponential growth. Finally, our calculation confirms that the evaluation of the retarded propagator in momentum space using Eq. (2.42), see e.g. [115, 118, 119], is correct, given that one uses the contour α to transform to the time domain. Our result is general and applies to any momentum distribution of hard quasiparticles.

We note that the advanced correlator can similarly be shown to be

$$D_{\text{adv}}(x,y) = \int_{\tilde{\alpha}} \frac{dk}{2\pi}\, e^{-ik(x-y)} D_{\text{adv}}(k). \tag{3.20}$$

where $D_{\text{adv}}(k) = D_{\text{ret}}(k)^*$ and the integration contour is $\tilde{\alpha} = \alpha^*$ which goes below all poles of $D_{\text{adv}}(k)$.

3.3 ENERGY LOSS IN AN UNSTABLE PLASMA

Energy loss due to soft gluons of a single heavy quark or a jet parton in plasma depends on the retarded correlator, see Sec. 2.2. Having found the correct retarded correlator in an unstable non-equilibrium plasma, it is important to see how it affects energy loss.

The first complete evaluation of heavy-quark energy loss in a thermally equilibrated quark-gluon plasma was given in [129, 130]. This calculation included both the contribution of hard collisional processes and the contribution of soft gluons. The soft gluon

2 We could understand Eq. (3.18) as an inverse Laplace transform from the time domain to the frequency domain, see a discussion in [110] employing a classical treatment. However, the actual Laplace transform from the frequency domain to the time domain would be of the form $\int_0^\infty d(t_x - t_y) e^{ip^0(t_x - t_y)} e^{\gamma(t_x - t_y)}$ which is an ill-defined integral. Therefore, we prefer not use the language of Laplace transforms and simply see $D_{\text{ret}}(k)$ as a function that gives the correct retarded function in the time domain when using Eq. (3.18). In the end, only the time domain is physical in a non-equilibrium system.

contribution was given by Eq. (2.29), expressed using the imaginary-time formalism and evaluated in temporal-axial gauge, $A^0 = 0$. However, the derivation was entirely different and used solely classical arguments, see e.g. [108, 109].

We reproduce the classical argument for energy loss of a jet parton due to soft gluons, which was briefly explained in Sec. 2.2. The rate of energy loss is

$$\hat{e} = \mathrm{Re} \int d^3x \, \mathbf{J}_{\mathrm{ext}}(x) \cdot \mathbf{E}_{\mathrm{ind}}(x). \tag{3.21}$$

where $\mathbf{J}_{\mathrm{ext}} = g\mathbf{v}\delta^{(3)}(\mathbf{x} - \mathbf{v}t)$ is the current of a jet parton and $\mathbf{E}_{\mathrm{ind}}(x)$ is the electric field induced by the current. Linear response theory tells us that in temporal-axial gauge where $A^0 = 0$, the induced electric field, $E^i_{\mathrm{ind}}(x) = -\partial_{x^0} A^i(x)$, is

$$E^i_{\mathrm{ind}}(x) = -\partial_{x^0} \int d^4y \, D^{ij}_{\mathrm{ret}}(x-y) J^j_{\mathrm{ext}}(y) \tag{3.22}$$

This can easily be taken to momentum space, giving that

$$\begin{aligned} E^i_{\mathrm{ind}}(x) &= -\partial_{x^0} \int d^4y \int \frac{d^4Q}{(2\pi)^4} e^{-i(x-y)\cdot Q} D^{ij}_{\mathrm{ret}}(Q) \int \frac{d^4K}{(2\pi)^4} e^{-iK\cdot y} J^j_{\mathrm{ext}}(K) \\ &= \int \frac{d^4Q}{(2\pi)^4} e^{-ix\cdot Q} \, iq^0 \, D^{ij}_{\mathrm{ret}}(Q) \, J^j_{\mathrm{ext}}(Q) \end{aligned} \tag{3.23}$$

which is the usual linear response theory relation in momentum space. Substituting the current of the jet parton in Eq. (3.21) then gives that

$$\hat{e} = gv^i \mathrm{Re} \int \frac{d^4Q}{(2\pi)^4} e^{-ix\cdot Q} \, iq^0 \, D^{ij}_{\mathrm{ret}}(Q) \, J^j_{\mathrm{ext}}(Q) \Big|_{\mathbf{x}=\mathbf{v}t} \tag{3.24}$$

which is equivalent to

$$\hat{e} = g^2 \, \mathrm{Re} \int \frac{d^4Q}{(2\pi)^4} \, iq^0 \, v^i v^j \, D^{ij}_{\mathrm{ret}}(Q) \, 2\pi\delta(q^0 - \mathbf{v}\cdot\mathbf{k}). \tag{3.25}$$

This reproduces Eq. (2.29) which we derived using the real-time formalism, assuming temporal-axial gauge, up to colour factors.

Eq. (2.29) was used to evaluate energy loss of a heavy-quark in an anisotropic and unstable plasma in [131, 132]. However, it is not correct in this case as was pointed out in [110]. Specifically, the linear response relation in Eq. (3.22) becomes

$$E^i_{\mathrm{ind}}(x) = -\partial_{x^0} \int d^4Y \int_\alpha \frac{d^4Q}{(2\pi)^4} e^{-i(X-Y)\cdot Q} D_{\mathrm{ret}}(Q) \int \frac{d^4K}{(2\pi)^4} e^{-iK\cdot Y} J_{\mathrm{ext}}(K). \tag{3.26}$$

Because of the contour α, there is no easy way to perform the Y integral and Eq. (3.23) is not correct. In fact, assuming that equation gives acausal evolution. This is because Eq.

(3.23) assumes that the integration contour to go to the time domain is along the real line. Given an instability pole $p^0 = i\gamma$, the retarded correlator in the time domain is then

$$D_{\text{ret}}(t_x, t_y) \sim \theta(t_y - t_x) e^{\gamma(t_x - t_y)} \tag{3.27}$$

which is unphysical as $D_{\text{ret}} \neq 0$ for $t_x < t_y$. We emphasize that the calculation in [131, 132] of the contribution of other modes to energy loss, including soft fluctuating modes and hard scattering, is correct.

A correct calculation considers the energy loss of a jet parton traversing the plasma from time $t_0 = 0$ up until a time T. The total energy loss is then

$$\Delta E = \text{Re} \int_0^T dt \int d^3x\, \mathbf{J}_{\text{ext}}(x) \cdot \mathbf{E}_{\text{ind}}(x). \tag{3.28}$$

Using the retarded propagator from Eq. (3.18), then gives that

$$\Delta E = \int_0^T dt \int_\alpha \frac{d^4Q}{(2\pi)^4} (-iq^0) v_i v_j D^{ij}_{\text{ret}}(Q)\, \frac{e^{i(\mathbf{v}\cdot\mathbf{q} - q^0)t} - 1}{i(q^0 - \mathbf{v}\cdot\mathbf{q})} \tag{3.29}$$

where the frequency integral over q^0 has contour α and the factor $\frac{e^{i(\mathbf{v}\cdot\mathbf{q}-q^0)t}-1}{i(q^0-\mathbf{v}\cdot\mathbf{q})}$ replaces the delta function in Eq. (3.25). As a similar result was derived in [110] using classical arguments, we only discuss this result briefly. For a system without instabilities, Eq. (3.29) can be shown to be equivalent to

$$\hat{e} = \frac{\Delta E}{dt} = \int \frac{d^3q}{(2\pi)^3} iq^0 v_i v_j D^{ij}_{\text{ret}}(Q) \Big|_{q^0 = \mathbf{v}\cdot\mathbf{q}}, \tag{3.30}$$

reproducing our earlier result.[3] However, for an instability mode $\frac{A}{q^0 - i\gamma}$ in the retarded correlator, one gets an extra contribution

$$\hat{e} = \frac{\Delta E}{dt} \approx e^{\gamma T}\, \text{Re} \int \frac{d^3q}{(2\pi)^3} \gamma\, A^{ij} v_i v_j \frac{e^{i\mathbf{v}\cdot\mathbf{q}T}}{\mathbf{v}\cdot\mathbf{q} - i\gamma} \tag{3.31}$$

where $\gamma = \gamma(\mathbf{q})$ is the growth rate of instability modes. Importantly, the rate of energy loss grows exponentially because the density of instability modes sourced by the jet parton grows with time T.

3 To go from Eq. (3.29) to Eq. (3.30), one can write $\frac{1}{q^0 - \mathbf{v}\cdot\mathbf{q}} = \frac{1}{2}\left(\frac{1}{q^0 - \mathbf{v}\cdot\mathbf{q} + i\epsilon} + \frac{1}{q^0 - \mathbf{v}\cdot\mathbf{q} - i\epsilon}\right)$ where ϵ is an infinitesimal quantity and then apply the residue theorem. One needs to assume that factors e^{-ibt} where b is a pole of the retarded propagator with Im$b < 0$, are small. Physically, this means that one allows sufficient time to pass so that correlations with the initial modes decays away.

3.4 rr CORRELATOR AND INSTABILITIES

A correct calculation of the retarded propagator for soft gluons in an unstable plasma shows that parton energy loss grows exponentially. This is due to the exponential growth in the density of instability modes. We will now do a corresponding analysis for the rr propagator and see which implications it has for transverse momentum broadening in an unstable plasma.

The rr correlator for soft gluons in a non-equilibrium plasma with initial conditions specified at time $t_0 = 0$ is given by

$$D_{rr}(x, y) = \int_0^x dz \int_0^y dw\, D_{\text{ret}}(x - z)\, \Pi_{aa}(z - w)\, D_{\text{adv}}(w - y), \tag{3.32}$$

see App. A. As we assume that there are no initial gluons in our theoretical setup, an extra term describing correlations to initial gluon density drops out. We have used the properties of the retarded and advanced correlator to rewrite the integration limits. Assuming the HTL approximation gives $\Pi_{aa}(z, w) = \Pi_{aa}(z - w)$ when the soft gluon density has not grown to be too high. Substituting Eqs. (3.18) and (3.20) into Eq. (3.32) and performing the time integrals, the rr correlator can then be rewritten as

$$\begin{aligned} D_{rr}(x, y) = &\int_\alpha \frac{dk_1}{2\pi} \int \frac{dk_2}{2\pi} \int_{\tilde{\alpha}} \frac{dk_3}{2\pi} \\ &\left[-e^{-ik_2x}e^{ik_2y} + e^{-ik_1x}e^{ik_2y} + e^{-ik_2x}e^{ik_3y} - e^{-ik_1x}e^{ik_3y}\right] \\ &\times \frac{1}{(k_1 - k_2)(k_2 - k_3)}\, D_{\text{ret}}(k_1)\, \Pi_{aa}(k_2)\, D_{\text{adv}}(k_3) \end{aligned} \tag{3.33}$$

where the k_1 and k_2 integrals use the contour from Fig. 3.2 and its conjugate.

We will use a separation of scales to evaluate Eq. (3.33). Our discussion is general, as we can have any momentum distribution of hard quasiparticles as long as the momentum anisotropy

$$\xi = \frac{\langle |p_1| \rangle - \langle |p_2| \rangle}{\langle |p_1| \rangle} \tag{3.34}$$

is small, $\xi \ll 1$. Here $\langle |p_1| \rangle$ and $\langle |p_2| \rangle$ are the typical momentum of quasiparticles in two directions. We write

$$D_{\text{ret}}(k) = \widehat{D}_{\text{ret}}(k) + \sum_i \frac{A_i}{k - i\gamma_i} \tag{3.35}$$

where γ are all poles with $|\gamma| \ll g\Lambda$. These can be the instability poles that lead to exponential growth in soft gluon density and have $|\gamma| \sim \xi^{3/2} g\Lambda$ [128], as well as slowly decaying modes with decay rate $\ll g\Lambda$. The density of the instability modes depends on the detailed history of the medium as their density grows exponentially until their non-linear interaction caps the growth. The rest of the propagator is captured by $\widehat{D}_{\text{ret}}$ which only has poles of order $g\Lambda$. These are fluctuating modes which are constantly sourced by hard particles in the medium. As they decay on time scales $\sim 1/g\Lambda$, they have no information about the history of the medium. Similarly, we write the advanced function as

$$D_{\text{adv}}(k) = \widehat{D}_{\text{adv}}(k) + \sum_j \frac{A_j^*}{k + i\gamma_j} \tag{3.36}$$

where the fluctuating part is $\widehat{D}_{\text{adv}} = \widehat{D}^*_{\text{ret}}$.

One must be careful when separating the retarded propagator at two scales like in Eq. (3.35). There is a branch cut from $\omega = -|\mathbf{k}| - i\epsilon$ to $\omega = |\mathbf{k}| - i\epsilon$ which corresponds to Landau damping. This branch cut is normally chosen to lie slightly below the real axis, see Fig. 3.3a, but then a part of it is at scale $\ll g\Lambda$ and the separation of scale is spoiled. Instead we choose a branch cut that avoids that region like in Fig. 3.3b. In this case, decaying modes corresponding to Landau damping appear on the second Riemann sheet [116]. Ultimately, retarded correlators only exist in the time domain where they are independent of the branch cut chosen in the frequency domain [133]. Therefore, the choice of branch cut is immaterial for final results.

Unlike for the retarded correlator, which we could evaluate exactly, controlled approximations are needed to evaluate the remaining integrals in Eq. (3.33). Firstly, starting a system at initial time $t_0 = 0$ introduces oscillations e^{-iax} where $\operatorname{Re} a \sim g\Lambda$. These oscillations are also present in a thermally equilibrated system with an initial time and have nothing to do with non-equilibrium physics. Averaging momentum broadening over a time $x - y \gg 1/g\Lambda$ allows us to drop such term, whose oscillation cancels out during the time interval $x - y$ we are interested in. Another way to see this is to note that photon or gluon emission takes time $x - y \sim 1/g^2\Lambda \gg 1/g\Lambda$ and the rate of momentum broadening should be averaged over that time interval. See [134] for a detailed discussion of the oscillating modes. Secondly, we only consider times $x, y \gg 1/g\Lambda$, i.e. we ignore times just after the system is started. This allows us to drop terms of the form e^{-iax} with

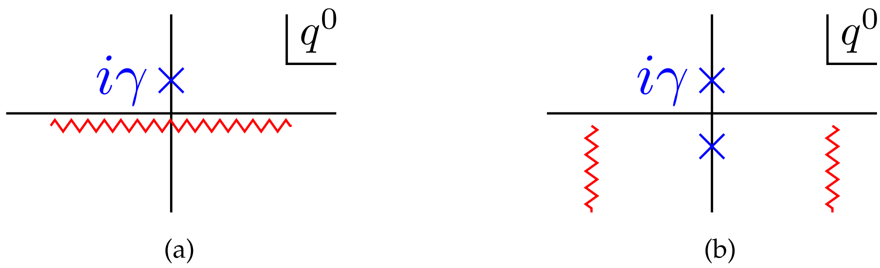

Figure 3.3: Branch cuts in a retarded propagator. Fig. 3.3a is the conventional choice for the branch cut while Fig. 3.3b is our choice to enforce a separation of scales. With our choice poles on the the second Riemann sheet appear, see the lower half plane in Fig. 3.3b.

$\mathrm{Im}\, a < 0$, $\mathrm{Re}\, a \sim g\Lambda$. This means that modes present in the initial conditions have had time to decay and we are only left with instability modes and fluctuating modes sourced by the hard particles.

The use of these controlled approximations allows us to evaluate Eq.(3.33). The detailed calculation can be found in Appendix B. It relies on inserting principal values, just like in Eq. (3.15), and evaluating the integrals term by term using the residue theorem. The result is that

$$
\begin{aligned}
D_{rr}(x,y) \approx & \int \frac{dk}{2\pi}\, \widehat{D}_{\rm ret}(k)\, \Pi_{aa}(k)\, \widehat{D}_{\rm adv}(k) \;\; e^{-ik(x-y)} \\
& + \sum_i \int \frac{dk}{2\pi}\, \frac{A_i}{k - i\gamma_i}\, \Pi_{aa}(k)\, \widehat{D}_{\rm adv}(k) \; \left(e^{-ikx} - e^{\gamma_i x}\right) e^{iky} \\
& + \sum_j \int \frac{dk}{2\pi}\, \widehat{D}_{\rm ret}(k)\, \Pi_{aa}(k)\, \frac{A_j^*}{k + i\gamma_j}\; e^{-ikx} \left(e^{iky} - e^{\gamma_j y}\right) \\
& + \sum_{i,j} \int \frac{dk}{2\pi}\, \frac{A_i}{k - i\gamma_i}\, \Pi_{aa}(k)\, \frac{A_j^*}{k + i\gamma_j} \\
& \qquad\qquad \times \left(e^{-ikx} - e^{\gamma_i x}\right) \left(e^{iky} - e^{\gamma_j y}\right).
\end{aligned}
\tag{3.37}
$$

The first term comes from fluctuating modes which are sourced at each instant by hard quasiparticles. This term has no information about the initial time since it only depends on the time difference $x - y$. It has the same structure as the usual expression for the rr correlator in momentum space, see Eq. (2.39). The last term comes from the instability modes in Eq. (3.35) and has explicit dependence on the time x and y. It contains factors with explicit exponential growth $e^{\gamma_i x}$ and $e^{\gamma_j y}$. Finally, the two terms in the middle correspond to cross-terms between fluctuating and instability modes.

Eq. (3.37) can be understood in a simple way. We can write the rr propagator as

$$\begin{aligned} D_{rr}(x,y) &= \int dw \int dz\, D_{\text{ret}}(x,w)\Pi_{aa}(w,z)D_{\text{adv}}(z,y) \\ &= \int dw \int dz \int \frac{dk}{2\pi}\, D_{\text{ret}}(x,w)\, e^{-ik(w-z)}\, \Pi_{aa}(k)D_{\text{adv}}(z,y) \end{aligned} \tag{3.38}$$

where we have Fourier transformed Π_{aa} and omitted dependence on the three-momentum. A mode in the retarded propagator with energy E and decay rate Γ is

$$D_{\text{ret}}(x,w) \sim \theta(x-w)e^{-iE(x-w)-\Gamma(x-w)} \tag{3.39}$$

in the time domain. In thermal equilibrium, or more generally a system with initial time $t_0 = -\infty$, this mode contributes

$$\int_{-\infty}^{x} dw\, e^{-ikw} e^{-i(E-i\Gamma)(x-w)} = \frac{ie^{-ikx}}{k-E+i\Gamma} \tag{3.40}$$

to the rr propagator in Eq. (3.38). However, in a system with initial time $t_0 = 0$, it contributes

$$\begin{aligned} &\int_{0}^{x} dw\, e^{-ikw} e^{-i(E-i\Gamma)(x-w)} \\ &= \frac{i}{k-E+i\Gamma}\left[e^{-ikx} - e^{-i(E-i\Gamma)x}\right]. \end{aligned} \tag{3.41}$$

where the integration limits have changed. This expression does not have a pole at $k = E - i\Gamma$ since a pole can strictly speaking only form after an infinite time of propagation. More generally, a mode $k = b$ of the retarded propagator contributes

$$\frac{1}{k-b}\left(e^{-ikx} - e^{-ibx}\right) \tag{3.42}$$

to the rr propagator. For an instability pole $b = i\gamma$ this is

$$\frac{1}{k-i\gamma}\left(e^{-ikx} - e^{\gamma x}\right) \tag{3.43}$$

and the term $e^{\gamma x}$ must be included, as in Eq. (3.37). However, for a fluctuating mode with $b \sim g\Lambda$, our approximations have shown that the term e^{-ibx} can be dropped. Effectively, the fluctuating modes quickly forget about the initial conditions because they decay quickly and because we can ignore artificial oscillations that arise because of the finite initial time. Thus the contribution of a fluctuating mode to Eq. (3.37) is simply

$$\frac{1}{k-b}e^{-ikx}. \tag{3.44}$$

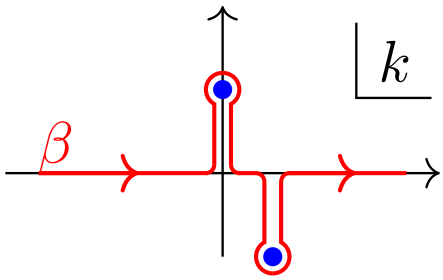

Figure 3.4: The contour β used to derive the rr propagator in Eq. (3.46). The pole in the upper half plane corresponds to γ_i and the pole in the lower half plane corresponds to γ_j.

Eq. (3.37) can be written in a different and illuminating way by using a few further approximations. The last term in Eq. (3.37) has no poles so the k integral can be written with an alternative contour β, see Fig. 3.4. This contour goes along the real line and above all instability poles of G_{ret} in the upper half plane and below all instability poles of G_{adv} in the lower half plane. A simple calculation with the residue theorem then gives

$$\begin{aligned}&\sum_{i,j}\int_\beta \frac{dk}{2\pi}\,\frac{A_i}{k-i\gamma_i}\,\Pi_{aa}(k)\,\frac{A_j^*}{k+i\gamma_j}\left(e^{-ikx}-e^{\gamma_i x}\right)\left(e^{iky}-e^{\gamma_j y}\right)\\ &=\frac{A_i\Pi_{aa}(0)A_j^*}{\gamma_i+\gamma_j}\left[e^{\gamma_i x}e^{\gamma_j y}-\theta(x-y)e^{\gamma_i(x-y)}-\theta(y-x)e^{\gamma_j(y-x)}\right].\end{aligned} \tag{3.45}$$

We can ignore all poles of Π_{aa}[4] and write $\Pi_{aa}(a_i)\approx\Pi_{aa}(a_j^*)\approx\Pi_{aa}(0)$ using branch cuts that avoid the region $k\ll g\Lambda$. Furthermore, in Eq. (3.37) cross-terms between fluc-

4 This is justified as follows: Let's write Π_{aa} as $A/(k-B)$ where $B\sim g\Lambda$ is a pole and A is the residue. After doing the contour integral, the pole B will give $A/(B-a_i)(B-a_j^*)\sim A/(g^2\Lambda)$ while an instability pole will give $A/(a_i-B)(a_i-a_j^*)\sim A/\xi g^2\Lambda$ which is much larger.

tuating and instability modes can be omitted as the oscillation in the fluctuating modes dominates over the growth in the instability modes.[5] The final result is that

$$\begin{aligned} D^{\mu\nu}_{rr}(t_x, t_y; \mathbf{k}) \approx & \int \frac{dk^0}{2\pi}\, e^{-ik^0(t_x - t_y)} \\ & \quad \times \left[\widehat{D}_{\rm ret}(k^0; \mathbf{k})\, \Pi_{aa}(k^0; \mathbf{k})\, \widehat{D}_{\rm adv}(k^0; \mathbf{k})\right]^{\mu\nu} \\ + \sum_{i,j} & \frac{\left[A_i \Pi_{aa}(0) A^*_j\right]^{\mu\nu}}{\gamma_i + \gamma_j} \left[e^{\gamma_i t_x} e^{\gamma_j t_y} - \theta(t_x - t_y) e^{\gamma_i (t_x - t_y)} - \theta(t_y - t_x) e^{\gamma_j (t_y - t_x)}\right]. \end{aligned} \tag{3.46}$$

which is a central result of this chapter. This is the first derivation of the rr propagator in an unstable plasma.

It is easy to understand the result in Eq. (3.46) for the occupation density of soft gluons in an unstable medium. The first term comes from fluctuating modes. It only depends on the time difference $t_x - t_y$ and has no information about the initial time. For the anisotropic momentum distribution in Eq. (2.36), the correlators $D_{\rm ret}$, $D_{\rm adv}$ are identical to our result in Eq. (3.18) except that instability poles have been subtracted. Furthermore, Π_{aa} comes from Eq. (2.52) and describes the rate of soft gluons emission by anisotropic hard particles. The contribution of these fluctuating modes to jet parton momentum broadening is

$$\mathcal{C}(\mathbf{q}_\perp) = g^2 C_F \int \frac{dq^0 dq^z}{(2\pi)^2}\, \widehat{D}^{\mu\nu}_{rr}(Q) v_\mu v_\nu\, 2\pi\delta(v \cdot Q) \tag{3.47}$$

where

$$\widehat{D}_{rr} = \widehat{D}_{\rm ret}(k^0; \mathbf{k})\, \Pi_{aa}(k^0; \mathbf{k})\, \widehat{D}_{\rm adv}(k^0; \mathbf{k}). \tag{3.48}$$

The second term in Eq. (3.46) describes instability modes with growth rates $\gamma_{i,j}$. It depends explicitly on the times t_x and t_y. In particular, the term $e^{\gamma_i x} e^{\gamma_j y}$ shows that the occupation density of the soft gluon field A^μ grows exponentially. As before Π_{aa} quantifies the rate at which instability modes are sourced and A and A^* describe the

5 This can be seen in a straight-forward fashion. We consider a term $e^{(id+c)t}$ in which $d \sim g\Lambda$ gives oscillations and $c \sim \xi g\Lambda$ gives exponential growth. Averaging over the time t can be done by introducing an initial time t_0 which we let vary over scale $\sigma \sim 1/g^2\Lambda$. This can be done easily by introducing a Gaussian width σ for t_0, i.e. integrating $e^{(id+c)(t-t_0)} e^{-t_0^2/2\sigma^2}$ over t_0. This gives a factor $e^{-\frac{1}{2}\sigma^2(d^2 - c^2 + 2icd)}$ which is heavily suppressed since $d \gg c$ and $\sigma d \gg 1$. A full field theoretical calculation would give the same result of exponential suppression.

polarization of instability modes as they traverse the plasma. This term vanishes at the initial time $t_x, t_y \to 0$ when instability modes are not occupied. It is furthermore finite for slow growth rate $\gamma \to 0$, the regime where $\widehat{q}$ in our naive calculation diverges, see Eq. (3.5). The instability part in Eq. (3.46) gives the effect of instability modes on jet parton momentum broadening. Most importantly, we see that the rate of momentum broadening goes like $e^{2\gamma T}$ where T is time. Therefore, the rate of momentum broadening grows exponentially in an unstable plasma. This was explored in more detail for the idealized case of infinite anisotropy in [104], as well as in numerical simulations in [135].

3.5 FATE OF INSTABILITIES IN HEAVY-ION COLLISIONS

We have derived correlators that describe soft gluons in an anisotropic system, see Eqs. (3.18) and (3.46). Special care was needed for instability modes for which a correct prescription is essential when calculating the rate of energy loss or momentum broadening. This theoretical analysis is valid in a regime where soft gluons do not have such a high occupation that their self-interaction becomes dominant.

Ultimately, we are interested in calculating anisotropic momentum broadening in heavy-ion collisions. Our analysis of fluctuating modes remains correct in that case: The fluctuating modes are radiated by hard quasiparticles and decay at each instant in the kinetic and hydrodynamic phases so the detailed history of the medium is not needed. However, instabilities are sourced right from the beginning of heavy-ion collisions. They have enough time to enter the non-linear regime where gluon self-interaction is dominant so that during the kinetic or hydrodynamic stages of collisions, the description of instabilities in Eq. (3.46) is no longer correct. Detailed numerical simulations of the history of the medium are needed to determine the occupation density and dispersion relations of the instability modes at these later stages.

There has been much numerical work on the evolution of QCD instabilities in heavy-ion collisions, as well as in more general setups. The goal with this work was to understand the dynamical evolution of instabilities, as well as to establish whether they can lead to sufficiently fast isotropization to allow for a hydrodynamic description, see [124, 136] for an overview. We will review this numerical work, aiming to explain what role instabilities play in the kinetic theory and hydrodynamic stages we are interested in.

In the simple case of QED plasmas, there are is no self-interaction of gauge fields. Weibel instabilities in a QED plasma therefore continue to grow exponentially until they become so strong that hard particles are substantially deflected in the instability photon field [137]. This isotropizes the hard particle distribution which caps the growth of instabilities.

In a QCD plasma, it is important to establish whether instability modes stop growing due to deflection of hard particles like in a QED plasma or due to self-interaction of the gauge field. Early calculations used a non-linear hard loop framework. This assumes a separation of scales into hard particles and soft classical fields with instabilities. The hard particles are described by a Boltzmann equation like in Eq. (2.1) where interaction of particles is ignored. Writing $f(X, \mathbf{p}) = f^0(\mathbf{p}) + \delta f(X, \mathbf{p})$ where f^0 is a fixed anisotropic distribution and $\delta f \ll f^0$ are fluctuations, leads to

$$v^\mu \frac{\partial \delta f}{\partial x^\mu} = -\mathbf{F} \cdot \frac{\partial f_0}{\partial \mathbf{p}} \tag{3.49}$$

The soft particles are described by classical Yang-Mills equations

$$\mathcal{D}_\mu \mathcal{F}^{\mu\nu} = j^\nu[\delta f], \tag{3.50}$$

where the hard current j^ν depends on the fluctuations δf. Solving Eqs. (3.49) and (3.50) together, one can eliminate dependence on the fluctuations δf. This leads to dynamical equations for the soft gluons where their non-linear interaction is taken into account, unlike in the usual HTL formalism. This allows for a much heavier occupation of soft gluons. These equations can be discretized and solved numerically. They depend on the momentum distribution f_0 of hard particles. Crucially, the distribution f_0 is assumed to be fixed, meaning that this framework does not allow for hard quasiparticles to be substantially deflected by the soft classical fields. This restricts the range of applicability of the non-linear hard loop framework.

Early non-linear hard loop calculations in $1+1\,D$ suggested that an unstable QCD plasma evolves similar to an unstable QED plasma, with isotropization of hard quasiparticles stopping the growth of instability fields [138, 139]. These calculation assumed homogeneity in the transverse plane so that variables only depended on the beam axis

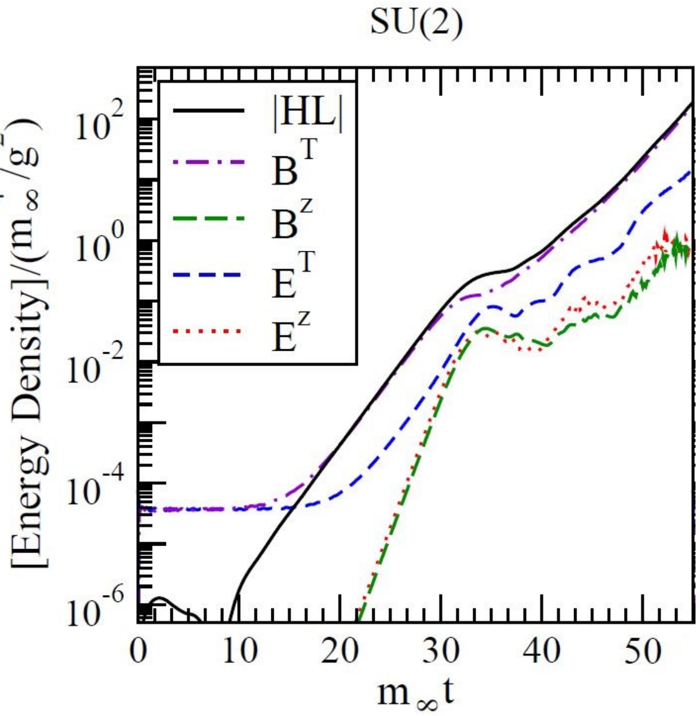

(a) Time evolution in a $1+1\,D$ simulation. The transverse magnetic field $B_\perp$ grows exponentially which triggers exponential growth in B_z and E_z due to non-linear effects. Around $m_\infty t \sim 40$ a different growth rate sets in as the fields Abelianize. The black curve is the total energy density in soft gluons.

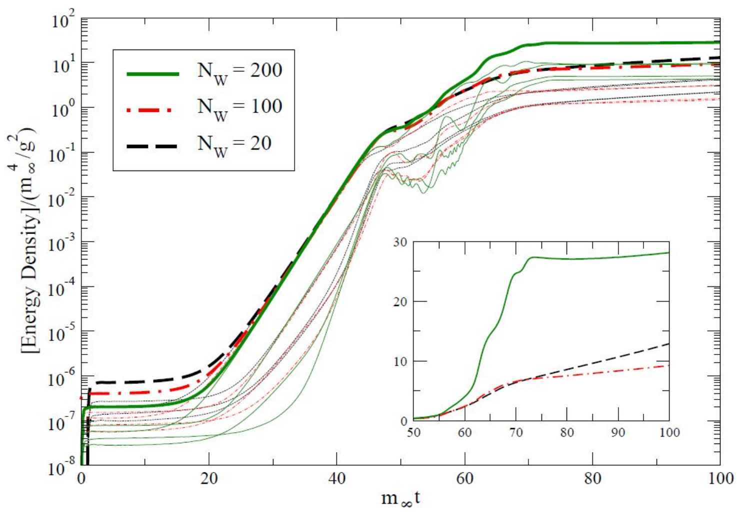

(b) Time evolution in a $3+1\,D$ simulation. The qualitative behaviour is similar to the $1+1\,D$ until exponential growth stops due to non-linear effects.

Figure 3.5: Time evolution of energy density of different chromoelectric and chromomagnatic modes in non-linear hard loop calculations [138].

z and time t.[6] The simulations found an initial exponential growth in the transverse chromomagnetic field $B_\perp$ at the rate γ predicted by linear HTL, see Fig. 3.5a. This is the regime described by our results in Eqs. (3.18) and (3.46). Other components, namely B^z and E^z, depend on $B_\perp$ due to the non-linear Yang-Mills equations and start to grow at twice the rate once $B_\perp$ is sufficiently occupied. Once these different components become comparable in strength, exponential growth resumes at a different rate. This last regime of exponential growth was explained qualitatively in [140] by showing that an $1+1\,D$ effective Lagrangian of the gluon field is minimized by Abelian configurations of the gluons, i.e. configurations where A^μ commutes with itself. Thus the gluons become effectively Abelian and the exponential growth continue like for photons in QED. This is supported by measuring the observable [141]

$$C = \frac{3}{\sqrt{2}} \frac{\left[\frac{1}{V}\int d^3x \ \left\{([j_x, j_y])^2 + ([j_y, j_z])^2 + ([j_z, j_x])^2\right\}\right]^{1/2}}{\frac{1}{V}\int d^3x \mathbf{j}^2} \tag{3.51}$$

which vanishes for an effective Abelian colour configuration and becomes 1 for a non-Abelian colour configuration where j_i are all randomly distributed in colour space. In $1+1\,D$ simulations, this observable drops nearly to zero during the last stage of exponential growth, see Fig. 3.6.

Later calculations in $3+1\,D$, in which dynamics in the transverse plane is included, gave a qualitatively different picture. In Fig. 3.5b different components of the chromomagnetic and chromoelectric fields are shown with time. Like in $1+1\,D$ there is initial exponential growth captured by the analytic growth rate, and a brief interval where the growth slows down as non-linear effects set in. However, after that exponential growth stops and one simply gets slow, linear growth due to non-linear effects [138, 141]. This linear growth has been explained by a cascade which transfers energy from the IR to the UV of soft modes, similar to turbulence in hydrodynamics [142, 143]. Therefore, abelianization does not take place in more realistic $3+1\,D$ simulations and instability modes nearly saturate. This conclusion is supported by measuring the observable C from Eq. (3.51), see Fig. 3.6. There is a brief window of abelianization but non-Abelian effects are important at later times and stop the exponential growth of soft modes.

6 This is justified if the initial density of soft fields is very low so that it takes a long time for instabilities to grow and occupation density is dominated by the most rapidly increasing mode which is in the z direction.

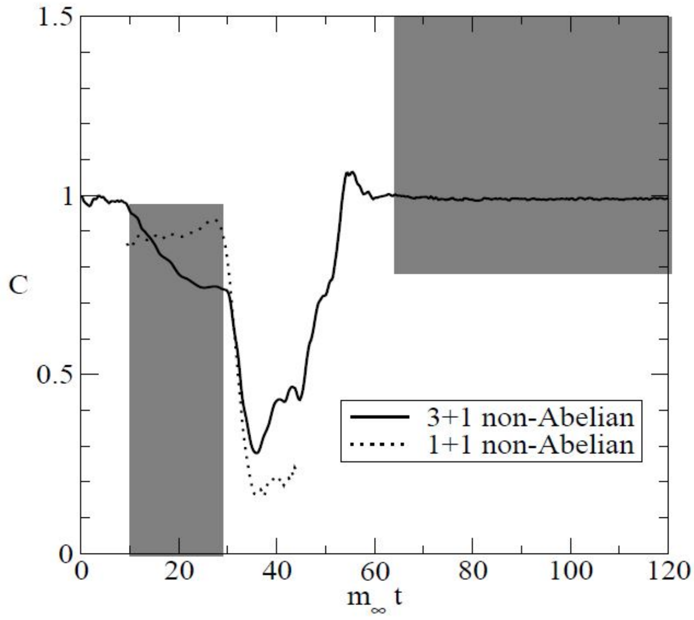

Figure 3.6: Measurement of C defined in Eq. (3.51) in non-linear hard loop calculations [141]. In $1+1\,D$ simulations, the gluons effectively Abelianize around $m_\infty t \sim 40$ while in $3+1\,D$ there is a brief period of Abelianization after which a non-Abelian colour configuration is reached.

A number of further works have explored growth of instabilities in the non-linear hard loop regime. In [144] it was found that the evolution of instabilities in the correct $SU(3)$ gauge theory is qualitatively similar to evolution in $SU(2)$ theory. Increasing the momentum space anisotropy, the authors of [145] did not find saturation in instability growth, but with more realistic initial conditions of strong fields, a linear growth regime seems to set in like at small anisotropy [146]. To make calculations even closer to heavy-ion collisions, simulations have been performed in a longitudinally expanding background [147, 148] where collisionless expansion of hard particles is assumed. Such work found continued exponential growth, both in $1+1\,D$ [149] and in $3+1\,D$ [150], similar to the case of a static system with a large momentum anisotropy.

Despite offering insight into the dynamics of QCD instabilities, work in the non-linear hard loop regime does not capture the physics of heavy-ion collisions. This is partially because the initial conditions in many of these works is not in accordance with the glasma initial conditions of heavy-ion collisions and also because they lack longitudinal expansion. More importantly, hard loop calculations ignore the backreaction of soft modes on hard modes and thus can only be trusted for a short time. This is partially remedied by Wong-Yang-Mills calculations which include the dynamics of hard, classical particles through the Wong equations [151], see [152] for details on numerical implementation. In [153, 154] Wong-Yang-Mills simulations for an anisotropic QCD plasma showed qualitatively similar results to hard loop calculations, namely initial exponential growth arrested by non-linear effects and followed by a cascade of energy to UV modes. These calculations furthermore saw isotropization due to backreaction on hard particles.

The most serious problem however with hard-loop calculations, as well as Wong-Yang-Mill simulations, is the assumptions that degrees of freedom can be neatly separated into long-wavelength fields and hard particles. For instance, in the UV cascade seen in hard-loop calculations, energy in the classical fields is transferred to modes with energy comparable to hard particles. However, there is no way of converting classical fields at that energy scale into particles [154]. This is remedied by classical-statistical calculations which provide the most up-to-date analysis of instabilities in heavy-ion collisions.

Classical-statistical calculations only include classical fields. This is justified in the early stages of heavy-ion collisions where energy density is dominated by soft gluons. The gluon fields are discretized on a lattice and obey the Yang-Mills equations of motion. Initial conditions are sampled from a statistical distribution coming from glasma physics. Early work considered classical-statistical field theory in a non-expanding box with anisotropic initial conditions [155, 156]. The results where strikingly similar to hard-loop calculation and Wong-Yang-Mills calculations with initial exponential growth in $B_\perp$, followed by faster growth in other components, and isotropization of instability modes. Building on this, [47, 157, 158] included longitudinal expansion in classical-statistical simulations to describe glasma evolution in heavy-ion collisions, see also [159, 160] for similar work. In these calculation boost invariance was broken by adding fluctuation in chromoelectric field that respect Gauss' law. This generates instabilities whose growth saturates due to non-linear interaction.

More recent classical-statistical calculations [161, 162] give the most up-to-date analysis of isntabilities in heavy-ion collisions. They evolve gluon fields for a longer time than all previous work, providing new information for behaviour at later times. They furthermore include all the physical aspects of heavy-ion collisions, such as realistic glasma initial conditions and longitudinal expansion. The early evolution is similar to previous calculations: primary instabilities in $B_\perp$ generate faster growing unstable modes in other field components due to non-linear interaction until a stage of a UV cascade is reached. This work was however able to provide a more detailed study of the UV cascade for a longer time. The cascade is captured by a self-similar evolution where the momentum distribution of classical excitations at proper time τ is

$$f(p_\perp, p_z, \tau) = (Q\tau)^\alpha f_S\left((Q\tau)^\beta p_\perp, (Q\tau)^\gamma p_z\right). \tag{3.52}$$

The numerically extracted exponents α, β, γ can be theoretically predicted assuming energy and number conservation as well as dominance of small-angle scattering [162]. Crucially, the cascade is a non-thermal fixed point, meaning that a wide range of different initial conditions with different details of instability growth, all converge towards the evolution in Eq. (3.52). [7] At late enough times, occupation density drops to ~ 1 and classical calculations can no longer be trusted. This is the regime where kinetic theory simulations become important.

3.6 PHENOMENOLOGICAL PRESCRIPTION FOR THE COLLISION KERNEL

Numerical work on instabilities provides a coherent picture of their role in heavy-ion collisions, assuming a medium with not too strong coupling. After the initial collision in which a glasma of highly occupied soft gluons is formed, the breaking of boost invariance generates instabilities. After a short period of exponential growth, followed by non-linear interaction, a cascade towards higher energy modes begins. The most recent work has shown that this cascade is a non-thermal fixed point which is reached by a wide variety of initial conditions. Therefore, detailed information about the instability modes is forgotten.

We are interested in describing the plasma produced in heavy-ion collision during the kinetic theory and hydrodynamic stages. Just as in Sec. 3.4, we can separate the soft

7 The same non-thermal fixed point dominates the dynamics of highly occupied, longitudinally expanding scalar field theory with initial instabilities [163, 164]. Further fixed points in other momentum regimes and at even later times have been identified [165], as well as in other theories [166, 167].

gluon modes into ultrasoft modes at energy $\ll g\Lambda$ and fluctuating modes at energy $g\Lambda$. Once the kinetic theory or hydrodynamic stages have been reached, ultrasoft modes have become saturated and there is no exponential growth from instability modes. The dispersion relations of ultrasoft modes are therefore completely different from the dispersion relation of the original instability modes and their occupation density must be determined in simulations.

In this work, we will focus on the physics of the fluctuating modes at energy $g\Lambda$ and their contribution to momentum broadening. These modes are sourced by hard quasiparticles in the system at each instant. Since they are sourced and decay rapidly, their density only depends on the instantaneous momentum distribution of hard quasiparticles $f(\mathbf{p})$, as we calculated in Sec. 2.3. We will subtract ultrasoft modes, including instability modes which dominate the first instances of heavy-ion collisions. Using this phenomenological prescription, we can get consistent, finite answers for momentum broadening due to fluctuating modes in the plasma.

This prescription relies on two assumptions. Firstly, we assume that fluctuating modes are well described by non-equilibrium HTL effective theory. This is a reasonable expectation as non-linear interaction of fluctuating modes is suppressed relative to interaction with hard modes. Furthermore, interaction between fluctuating modes and ultrasoft modes can be ignored if the occupation density of ultrasoft modes is not extremely high.[8] This expectation is furthermore supported by recent classical-statistical simulations. Intriguingly, they show that in the vicinity of non-thermal fixed points, isotropic systems reach a HTL-like separation of scales where correlators in the soft sector are well described by a HTL ansatz [168]. This provides clues that HTL becomes a good approximation early on in heavy-ion collisions and arises dynamically.

The second assumption we make is that occupations density of ultrasoft modes during the kinetic theory and hydrodynamic stages of heavy-ion collisions is not high enough to substantially alter momentum broadening. The extent to which this is correct is a question of details, as different setups in simulations give different occupation densities for ultrasoft modes. As mentioned, the non-thermal fixed point in isotropic classical-statistical simulations is well described by HTL effective theory [168]. Nevertheless, in that setup

8 The interaction between fluctuating and ultrasoft modes is suppressed by the small region of phase space occupied by ultrasoft modes, as well as the momentum dependent vertices.

there are certain probes, such as heavy-quark diffusion, that are extremely sensitive to the deep IR and for which HTL needs to be complemented by a description of ultrasoft modes [169]. Further studies are needed to establish whether non-HTL ultrasoft modes are important for the collision kernel for momentum broadening in heavy-ion collisions. In such a case, our calculation of the collision kernel $\mathcal{C}(\mathbf{p}_\perp)$ gives a correct description for transverse momenta $p_\perp \sim g\Lambda$ but must be complemented at lower momenta. In principle, the collision kernel at lower momenta could be measured in classical-statistical simulations, by using the definition of the kernel in terms of Wilson lines [170]. However, the applicability of such results for the kinetic theory and hydrodynamic stages is unclear as the occupation density of hard modes during those stages is not high enough to warrant the assumption of classical fields, central to classical-statistical simulations.

Part IV

MOMENTUM BROADENING IN AN ANISOTROPIC PLASMA

4

MOMENTUM BROADENING IN AN ANISOTROPIC PLASMA

4.1 DEPENDENCE ON ω_{cut}

The anisotropic collision kernel $\mathcal{C}(\mathbf{q}_\perp)$ is a complicated function. It depends on medium properties like the anisotropy of the medium defined in Eq. (2.36) and the hard scale Λ. It also depends on the momentum direction of the jet parton which is being broadened. We specify the jet parton direction through the angle θ between the anisotropy vector $\mathbf{n}$ and the parton momentum $\mathbf{k}$, see Fig. 4.1. Since the medium is symmetric under $\mathbf{n} \to -\mathbf{n}$, we only need to consider $0 \leq \theta \leq \pi/2$. The collision kernel furthermore depends on both the magnitude and the direction of the transverse kick $\mathbf{p}_\perp$. We specify the direction of the kick in the jet's transverse plane by an angle ϕ, defined to be 0 when it is in the plane spanned by $\mathbf{n}$ and $\mathbf{k}$. In what follows, we assume a QCD plasma with three flavours of massless quarks.

Before studying how the anisotropic collision kernel depends on medium properties and the jet direction, we must clarify our prescription for subtracting away ultrasoft

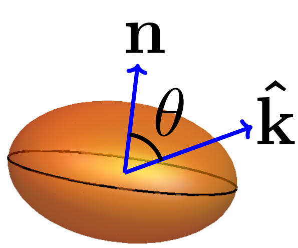

Figure 4.1: Definition of θ which specifies the jet parton direction. The vector $\mathbf{n}$ specifies the principal direction of the momentum distribution of hard quasiparticles while $\hat{\mathbf{k}}$ is the momentum direction of the jet parton.

modes. As explained in Sec. 3.6, we separate the gluon modes into ultrasoft instability modes with energy $\sim \xi^{3/2} g\Lambda$ whose density depends on the history of the medium, and fluctuating modes with energy $\sim g\Lambda$ which are continually sourced by hard particles in the medium. This is done by imposing a cut ω_{cut}, where

$$\xi^{3/2} g\Lambda \ll \omega_{\mathrm{cut}} \ll g\Lambda. \tag{4.1}$$

We focus on fluctuating modes and subtract ultrasoft modes. We do this by locating numerically all poles with frequency $|\omega| < \omega_{\mathrm{cut}}$ in the retarded propagator and subtract their contribution from the propagator. Specifically, in either Eq. (2.76) or Eq. (2.77) which we denote as $1/A(\omega)$, we find all poles $\omega = i\gamma$ below the cut ω_{cut}. Using

$$\begin{aligned}\frac{1}{A(\omega)} &= \frac{1}{\frac{A(\omega)}{(\omega-i\gamma)}(\omega - i\gamma)} \\ &= \frac{1}{A(\omega) - \left(\frac{A(\omega)}{\omega-i\gamma}\right)^2} - \frac{1}{(\omega - i\gamma) - \frac{A(\omega)}{\omega-i\gamma}} \frac{1}{\omega - i\gamma}\end{aligned} \tag{4.2}$$

we drop the second term in the last line which contains the instability pole and replace $1/A(\omega)$ by

$$\frac{1}{A(\omega) - \left(\frac{A(\omega)}{\omega-i\gamma}\right)^2}. \tag{4.3}$$

This term has no pole at $\omega = i\gamma$ because

$$A(\omega) - \left(\frac{A(\omega)}{\omega - i\gamma}\right)^2 = \frac{A(\omega)}{\omega - i\gamma}\left[\omega - i\gamma - \frac{A(\omega)}{\omega - i\gamma}\right] \tag{4.4}$$

where $\frac{A(\omega)}{\omega-i\gamma}$ is finite everywhere and non-zero at $\omega = i\gamma$.

As explained in Sec. 3.4, we must choose a branch cut in the retarded self-energy which avoids the ultrasoft region of $\omega \sim \xi^{3/2} g\Lambda$, see Fig. 3.3. Choosing such a branch cut reveals poles in the lower half complex plane on the second Riemann sheet. These poles are very slowly decaying modes corresponding to Landau damping at finite momentum.[1] Our prescription is to subtract all instability poles in the upper half complex plane which gives exponential growth, as well as all poles in the lower half plane on the

1 In thermal equilibrium, Landau damping modes with $\omega \approx 0$ only occur for $\mathbf{q} \approx 0$. In an anisotropic medium, some of these Landau damping modes move to the upper half complex plane and become instability poles. This creates damping modes with $\omega \approx 0$ at finite $\mathbf{q}$, see Fig. 4.2

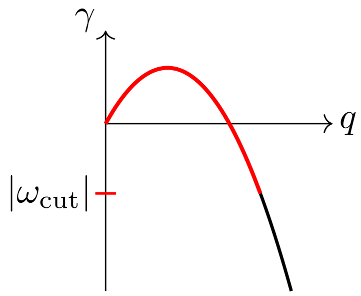

Figure 4.2: In our phenomenological prescription, all modes $\omega = i\gamma$ with $\gamma \geq 0$ and with $0 > \gamma > |\omega_{\text{cut}}|$ are subtracted. These modes are depicted as red in the figure.

second Riemann sheet which have $|\omega| < \omega_{\text{cut}}$, see Fig. 4.2. The subtracted poles in the lower half plane evolve slowly and are sensitive to soft gluon self-interaction, just like instability poles in the upper half plane. Their subtraction is furthermore necessary to respect the separation of scales between fluctuating modes and ultrasoft modes.

In order to find poles numerically on the second Riemann sheet we must have analytic expressions for Π_{ret} on that sheet, obtained by analytically continuing Π_{ret} from the upper half complex plane. For this purpose, the expressions in Eqs. (2.64) to (2.72) which have one remaining numerical integral are not sufficient.[2] For the purposes of this subsection where we explore the dependence on ω_{cut}, we will therefore use analytic expression for the Π_{ret}, derived in [115, 118] assuming that $\xi \ll 1$. For all other components of D_{rr} we use full expressions and in later subsections we will use full expressions for Π_{ret} as well, valid for all values of ξ.

It is important to check how sensitive the collision kernel is to the exact value of the momentum cut ω_{cut} we impose. The growth rate of instability modes scales as $\gamma \sim \xi^{3/2} g\Lambda$ [128] where the maximal growth rate of the modes in Eq. (2.76) is $\gamma_{max} \approx 0.15\,\xi^{3/2} g\Lambda$. Thus a reasonable value for the cut between modes in the lower half plane we subtract and fluctuating modes is

$$\omega_{\text{cut}} = a_{\text{cut}}\, \xi^{3/2} g\Lambda \tag{4.5}$$

2 To analytically continue a function $f(z) = \int_{\mathcal{C}} \frac{dw}{2\pi i} F(z,w)$ defined for certain z, it is incorrect to simply analytically continue the integrand $F(z,w)$. This is easily seen when $F(z,w) = 1/(w-z)$ and $\mathcal{C}$ is a circle around 0 with radius 1. For z inside the circle, we get $f(z) = 1$ which easily analytically continues to the whole complex plane. However, analytically continuing $F(z,w)$ and performing the w integral gives 0 when z it outside the circle.

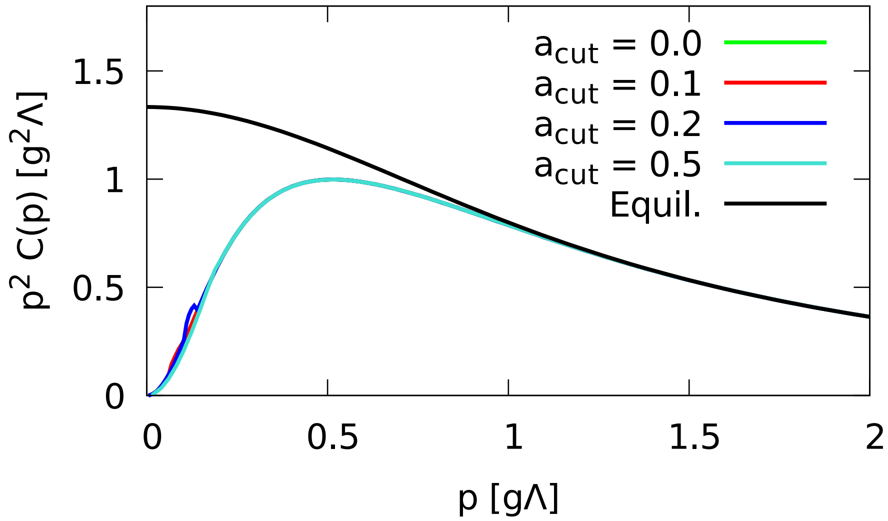

(a) Anisotropy $\xi = -0.1$, jet direction $\theta = \pi/2$

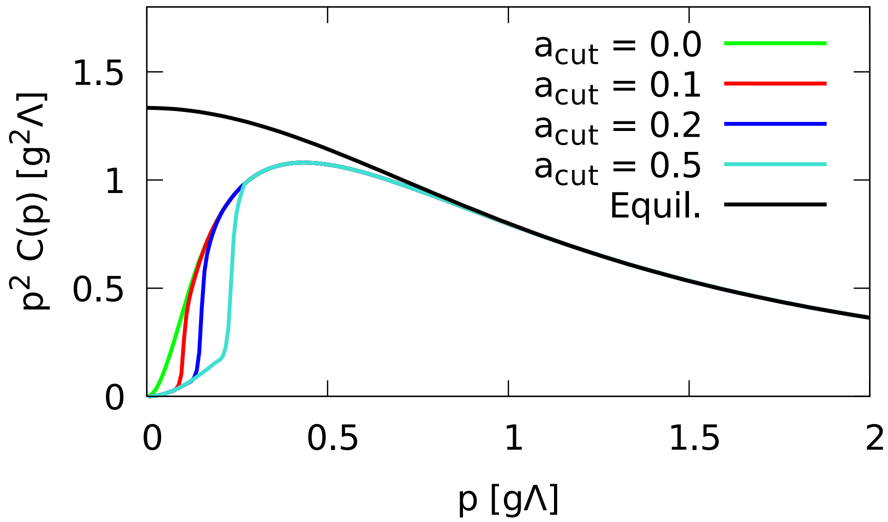

(b) $\xi = -0.1$, $\theta = \pi/3$

Figure 4.3: Dependence of transverse momentum broadening $\mathbf{p}_\perp^2 \mathcal{C}(\mathbf{p}_\perp)$ on momentum cutoff ω_{cut} for two different jet directions. Evaluated for $\xi = -0.1$. The black curve corresponds to the equilibrium result. For $\xi < 0$ at $\pi/4 < \theta \leq \pi/2$, and for $\xi > 0$ at $0 \leq \theta < \pi/4$, there is similarly little cutoff dependence. The quantity a_{cut} is defined in Eq. (4.5).

with the number $a_{\text{cut}} \sim 0.1 - 0.5$. We will always subtract instability poles in the upper half plane corresponding to exponential growth, see Fig. 4.2.

The dependence of the collision kernel on ω_{cut} is modest for a wide range of values of the anisotropy ξ and the jet direction θ. For instance, we show in Fig. 4.3 the amount of momentum broadening $\mathbf{p}_\perp^2 \mathcal{C}(\mathbf{p}_\perp)$ at small negative anisotropy of $\xi = -0.1$ and two values of θ. The dependence on ω_{cut} is mild and of course only existent for low values of $\mathbf{p}_\perp$ since instabilities are only present at low momenta. The dependence is similarly mild for jet direction $\frac{\pi}{4} < \theta \leq \frac{\pi}{2}$ when $\xi < 0$ and for jet direction $0 \leq \theta < \frac{\pi}{4}$ when $\xi > 0$.

For some other values of ξ and θ there is greater dependence on the value of the cut. This can be seen in Fig. 4.4. Similar qualitative behaviour can be seen for jet direction $0 \leq \theta < \frac{\pi}{4}$ when $\xi < 0$ and for jet direction $\frac{\pi}{4} < \theta \leq \frac{\pi}{2}$ when $\xi > 0$.

The physical difference between Figs. 4.3 and 4.4 comes from long-wavelength modes. Even though we cut away ultrasoft modes there remain slowly-decaying modes with dispersion relations $\omega = -i\gamma$ where $\gamma \gtrsim \omega_{\text{cut}}$. These poles are close to the instability regions and arise in the part of the retarded propagator given by Eq. (2.76). For some values of the jet momentum, these modes are transverse to the jet and can thus impart a great deal of momentum to a jet parton before they decay after a fairly long time. A detailed analysis of the location of these poles, see [118], shows that such poles appear for values of ξ and θ described in Fig. 4.4.

Using our earlier calculation, we can easily get an analytic estimate for the dependence on ω_{cut} in the presence of slowly-decaying modes with momentum transverse to the jet parton, like in Fig. 4.4. In Eq. (3.6) we showed that

$$\widehat{q} \sim g^4 \Lambda^3 \xi^{3/2} \log\left(\sqrt{\xi}\delta\right) \tag{4.6}$$

where we introduced a cutoff around the region of instabilities $\mathbf{q}_\perp \gtrsim \sqrt{\xi} m_0 + \delta m_0$ after a suitable redefinition of variables. As there is a liner relation between δ and our cutoff ω_{cut} we get that

$$\widehat{q} \sim g^4 \Lambda^3 \xi^{3/2} \log \omega_{\text{cut}} \tag{4.7}$$

This shows that the dependence on the cut ω_{cut} is logarithmic and thus fairly mild. Furthermore, the coefficient in front is $\xi^{3/2}$ which is smaller than the typical correction

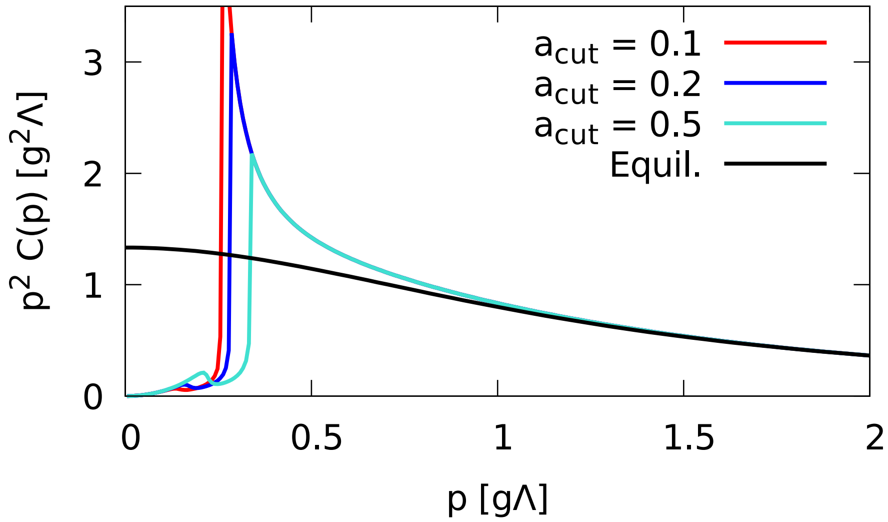

(a) Anisotropy $\xi = -0.1$, jet direction $\theta = 0$

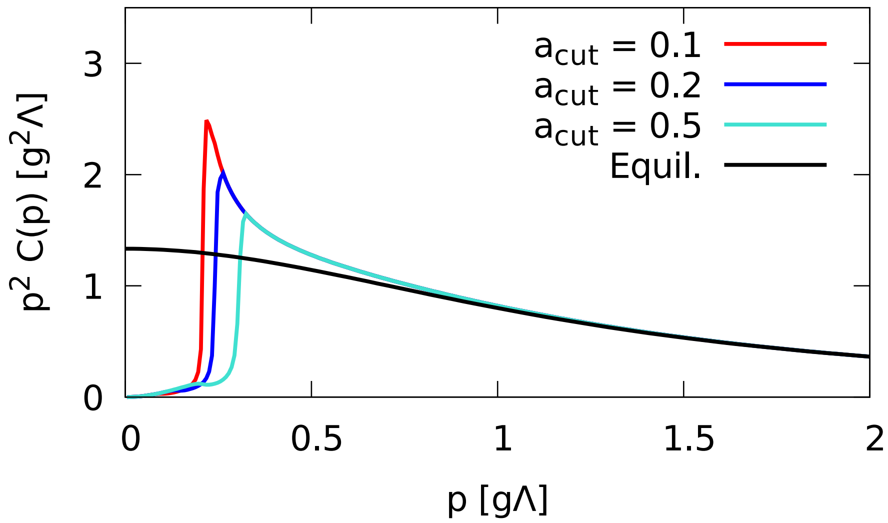

(b) $\xi = -0.1$, $\theta = \pi/6$

Figure 4.4: Dependence of transverse momentum broadening on momentum cutoff for two other values of jet direction. For $\xi < 0$ at $0 \leq \theta < \pi/4$ and for $\xi > 0$ at $\pi/4 \leq \theta \leq \pi/2$, the cutoff dependence is similar to these figures with more dependence than in Fig. 4.3.

$\mathcal{O}(\xi)$ due to anisotropy. This small overall coeffcient is due to the small region of phase space in which instabilities are found.

A full calculation of the collision kernel requires information not only on the fluctuating modes which we evaluate, but also the occupation density and dispersion relation of ultrasoft modes below ω_{cut} at certain time in the evolution of the quark-gluon plasma. Having such information on ultrasoft modes would cancel all dependence on ω_{cut}. This can for example be seen in Eq. (4.7) where the logarithmic dependence on ω_{cut} would drop out as the physical description is continuous. Including ultrasoft modes is clearly relevant for values of ξ and θ which are highly sensitive to ultrasoft modes like in Fig. 4.4. However, for values of ξ and θ where there is less sensitivity to ω_{cut}, as in Fig. 4.3, we believe that our calculation is consistent and that dependence on ultrasoft modes will be more limited given the small region of phase space they occupy. We will focus on such values of ξ and θ in the rest of this section and choose $\omega_{\text{cut}} = 0.0$ for simplicity.

4.2 DEPENDENCE ON ANISOTROPY AND JET DIRECTION

Momentum broadening is qualitatively different in an anisotropic medium, compared with an equilibrium medium. In Fig. 4.5 we show momentum broadening for a jet travelling in the direction of the anisotropy vector, $\theta = 0$, in a medium with $\xi > 0$. There is substantial reduction in the rate of broadening, especially at low and intermediate transverse momenta. This reduction is due to increased screening in the medium and means that $\mathcal{C}(\mathbf{p}_\perp) \sim \mathcal{O}(1)$ at small momenta while in equilibrium $\mathcal{C}(\mathbf{p}_\perp) \sim \mathcal{O}(1/\mathbf{p}_\perp^2)$. A substantial reduction is seen even for relatively small values of anisotropy. A qualitatively similar picture is seen for a jet parton travelling transverse to the anisotropy vector, $\theta = \pi/2$, in a medium with $\xi < 0$, see Fig. 4.6. As the medium becomes more anisotropic, screening increases and medium broadening is reduced. Medium effects are less important for higher momentum gluons which propagate nearly like in vacuum, meaning that there is little difference between the equilibrium and anisotropic kernel at higher momenta. We have furthermore explored the dependence on the jet direction which is seen to be fairly mild, see Fig. 4.7.

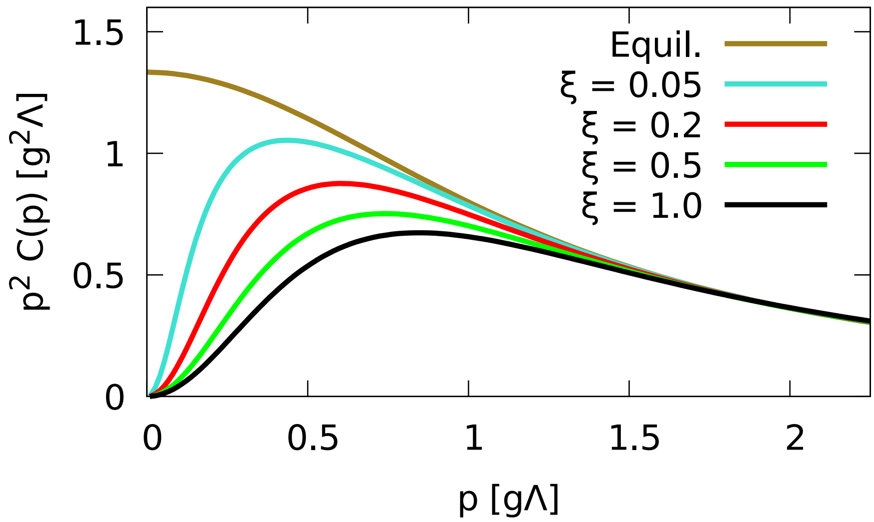

Figure 4.5: Transverse momentum broadening of a parton travelling in the direction of the anisotropy vector, $\theta = 0$, in a medium with positive anisotropy. Additional screening leads to less broadening as the anisotropy is increased.

The collision kernel in Figs. 4.5 and 4.6 incorporates a great deal of physics. It depends on the rate of hard quasiparticles radiating soft gluons, including the angular distribution of the radiated gluons due to medium anisotropy. The collision kernel furthermore depends on the details of how soft gluons propagate in the medium while continuously interacting with quasiparticles. Our numerical calculations show that the most important effect in an anisotropic medium is increased screening of chromomagnetic modes. Very heuristically, one can imagine that the term $1/\mathbf{q}_\perp^2$ in Eq. (2.35) for the equilibrium collision kernel gets screening with angular dependence and becomes $1/(\mathbf{q}_\perp^2 + m^2(\xi,\theta))$. This leads to qualitatively different behaviour at low momenta $\mathbf{q}_\perp$. In particular, $q_\perp^2 \mathcal{C}(\mathbf{q}_\perp)$ is finite as $\mathbf{q}_\perp \to 0$ in equilibrium but goes to zero in that limit in an anisotropic medium.

In an isotropic non-equilibrium plasma, one can obtain an exact, analytic expression for the collision kernel at leading order. This is because there are only longitudinal and transverse gluon modes which commute, allowing one to apply a sum rule from [82], see [81] for further details. One gets a analogous expression to the equilibrium case, see Eq. (2.35), with

$$\mathcal{C}_{\text{iso}}(\mathbf{q}_\perp) = g^2 C_F T_* \left(\frac{1}{\mathbf{q}_\perp^2} - \frac{1}{\mathbf{q}_\perp^2 + \widetilde{m}_D^2} \right) \tag{4.8}$$

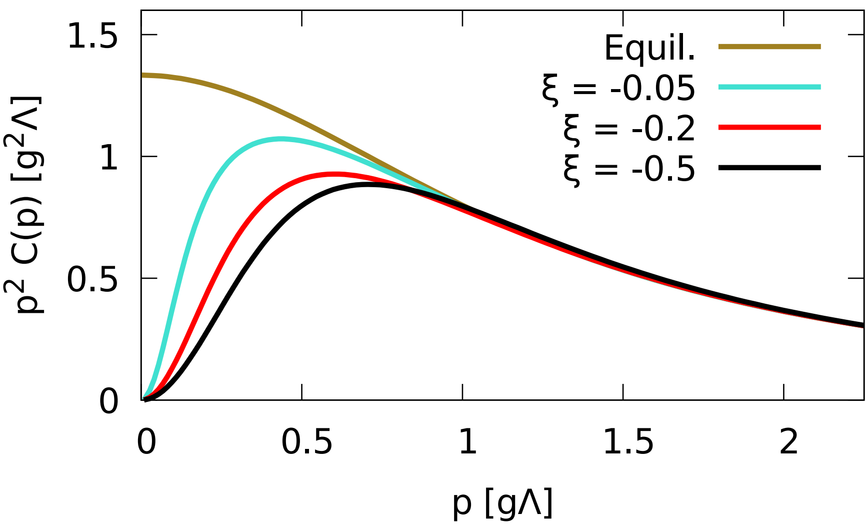

Figure 4.6: Transverse momentum broadening of a parton travelling perpendicularly to the anisotropy vector, $\theta = \pi/2$, in a medium with negative anisotropy. As in Fig. 4.5, additonal screening in an anisotropic medium leads to less broadening.

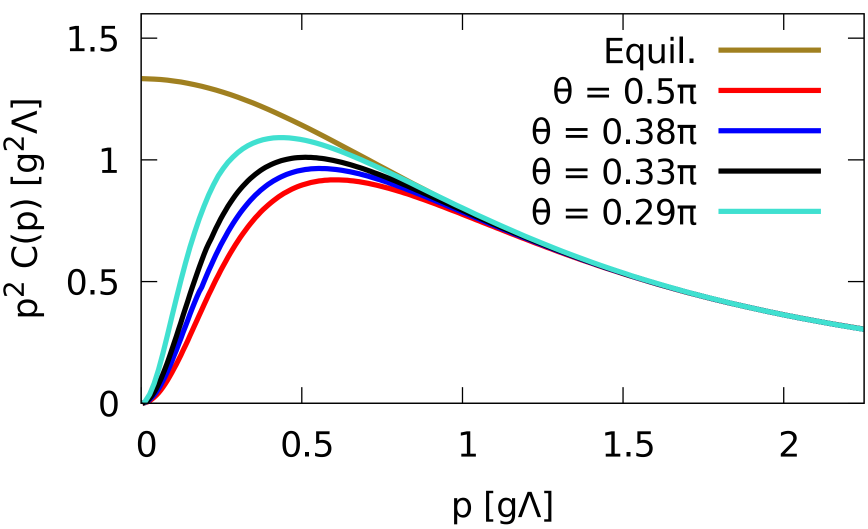

Figure 4.7: The collision kernel for some different values of the angle θ between the jet parton momentum and the anisotropy vector of the medium. Evaluated with $\xi = -0.2$.

where the non-equilibrium Debye mass is

$$\widetilde{m}_D^2 = 2\int \frac{d^3p}{(2\pi)^3 p}\ \left[2N_f f_q(\mathbf{p}) + 2N_c f_g(\mathbf{p})\right] \tag{4.9}$$

and T_* is an effective temperature given by

$$T_* = \frac{\frac{1}{2}\int \frac{d^3p}{(2\pi)^3}\left[2N_f f_q(\mathbf{p})(1-f_q(\mathbf{p})) + 2N_c f_g(\mathbf{p})(1+f_g(\mathbf{p}))\right]}{\int \frac{d^3p}{(2\pi)^3 p}\ \left[2N_f f_q(\mathbf{p}) + 2N_c f_g(\mathbf{p})\right]}. \tag{4.10}$$

The isotropic result in Eq. (4.8) has been used in effective kinetic theory simulations [52, 53] which bridge between glasma physics and relativistic hydrodynamics. There the isotropic kernel is also used for anisotropic momentum distributions. Then it is simply an ansatz with the effective temperature and non-equilibrium Debye mass defined through Eqs. (4.9) and (4.10) for a general momentum distribution $f(\mathbf{p})$ [171, 172]. It is interesting to compare this isotropic ansatz with our full result for the anisotropic collision kernel. Two representative plots are shown in Fig. 4.8, where the isotropic ansatz has been evaluated using the momentum distribution in Eq. (2.36). We see that the isotropic ansatz does not capture the qualitative behaviour of the full result since it lacks the additional screening in an anisotropic medium. The substantial difference between our anisotropic kernel and the isotropic ansatz can lead to differences in the rate of one-to-two quasi-particle scattering. Thus, using a full anisotropic collision kernel could lead to different results in kinetic theory simulations.

4.3 DIRECTIONAL DEPENDENCE IN MOMENTUM BROADENING

In an anisotropic quark-gluon plasma, momentum broadening has directional dependence. In other words, the collision kernel $\mathcal{C}(\mathbf{p}_\perp)$, which describes momentum broadening transverse to a parton's direction of motion, depends not only on the magnitude of a transverse kick $p_\perp$ but also on its direction. This can be quantified by evaluating the total transverse broadening in different directions in the transverse plane. This is quantified by

$$\widehat{q}_{ij} = \int \frac{d^2q_\perp}{(2\pi)^2}\ p_{\perp i} p_{\perp j}\, \mathcal{C}(\mathbf{p}_\perp). \tag{4.11}$$

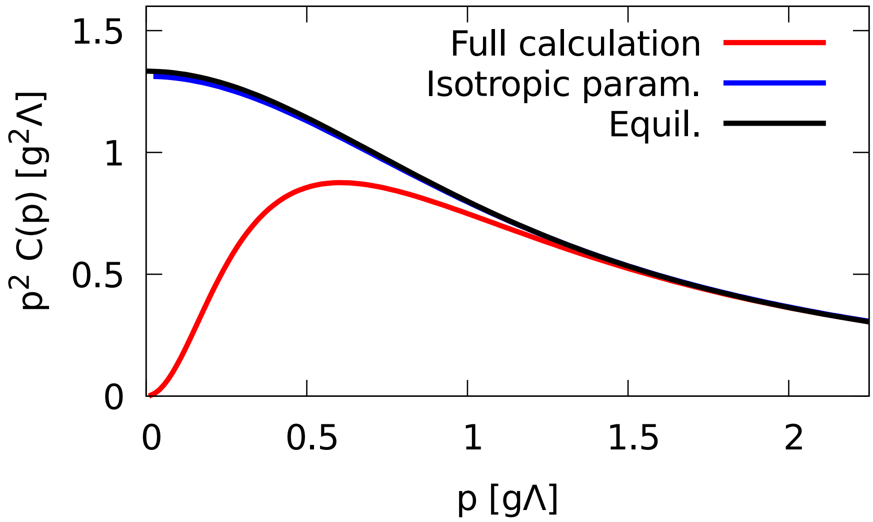

(a) $\xi = 0.2$, $\theta = 0$

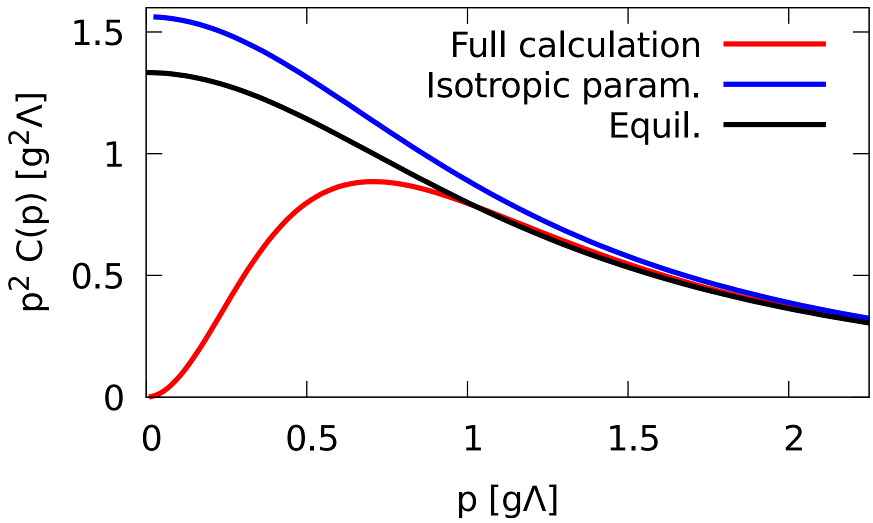

(b) $\xi = -0.5$, $\theta = \pi/2$

Figure 4.8: Comparison of our anisotropic collision kernel with the isotropic ansatz in Eq. (4.8) and the equilibrium result. The isotropic ansatz does not capture the physics of the anisotropic kernel.

The matrix $\hat{q}_{ij}$ is real and symmetric, so one can always find orthogonal axes x and y which diagonalize the matrix so that $\hat{q}_{xy} = 0$. The total momentum broadening from Eq. (2.23) is then $\hat{q} = \hat{q}_{xx} + \hat{q}_{yy}$. For the momentum distribution in Eq. (2.36), one principal axis is in the plane spanned by the jet direction and the anisotropy vector $\mathbf{n}$, with the other one being orthogonal.

The transport coefficients for momentum broadening defined in Eq. (4.11) are UV divergent. This is because for high momenta the collision kernel scales as $\mathcal{C}(\mathbf{p}_\perp) \sim 1/p_\perp^4$, giving a logarithmic divergence. Thus a radial UV cutoff is needed. This cutoff depends on the process being studied. For collinear radiation, it can be estimated as

$$q_{\max} \sim g\Lambda(E/\Lambda)^{1/4}. \tag{4.12}$$

where E is the energy of the jet parton and Λ is the hard medium scale [79]. Roughly speaking, in collinear radiation transverse kicks below $q_{\max}$ are frequent enough to be described by momentum diffusion, while transverse kicks above $q_{\max}$ are infrequent and must be described individually. The scaling relation in Eq. (4.12) becomes better as the energy of the jet E increases.

There have been a number of works measuring $\hat{q}$ in simulations of QGP, as well as momentum broadening of heavy quarks. These include HTL simulations with kinetic theory for hard quasiparticles and classical field theory for soft gluons, which assume thermal equilibrium [135, 173], as well as work in the colour-glass condensate [174–177]. Heavy-quark diffusion has also been measured in classical-statistical field theory [169]. Our work differs in that it is not tied to the detailed setup of a simulation. Instead we have analyzed fluctuating modes in a non-equlibrium plasma described by HTL effective theory, where the fluctuating modes only depend on the momentum distribution of hard particles. We note that [178] considered how temperature and density gradients in local thermal equilibirum affect momentum broadening, working in an opacity expansion and using a simple model for the medium as composed of massive particles.

Figs. 4.9 and 4.10 show total momentum broadening in an anisotropic HTL plasma, using our calculation of $\mathcal{C}(\mathbf{p}_\perp)$. Fig. 4.9 shows momentum broadening of a parton travelling in the direction of the anisotropy vector $\theta = 0$ in a medium with $\xi \geq 0$. In this case $\hat{q}_{xx} = \hat{q}_{yy}$. For a jet parton with fairly high energy, $E \sim 100\Lambda$ or $q_{\max} = \sqrt{10}g\Lambda$, there is a modest reduction of around 15% in momentum broadening due to anisotropy,

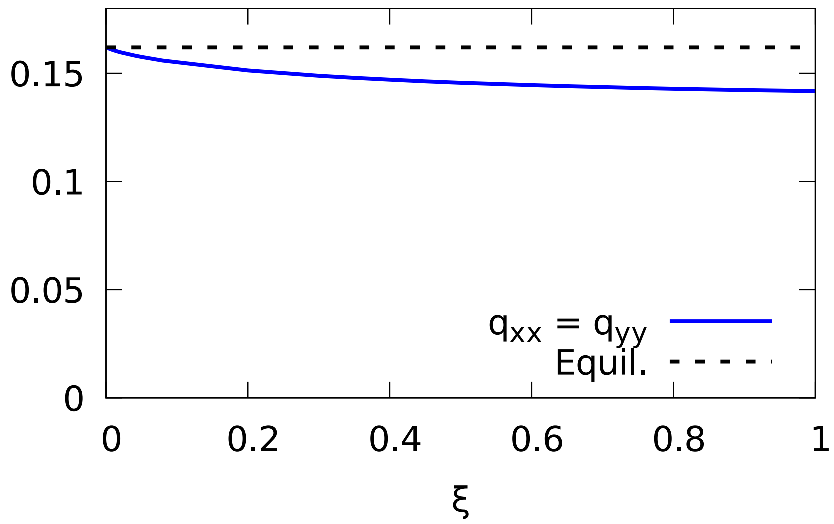

(a) UV cutoff of $q_{\text{max}} = \sqrt{10}g\Lambda$ corresponding to parton energy $E \sim 100\Lambda$.

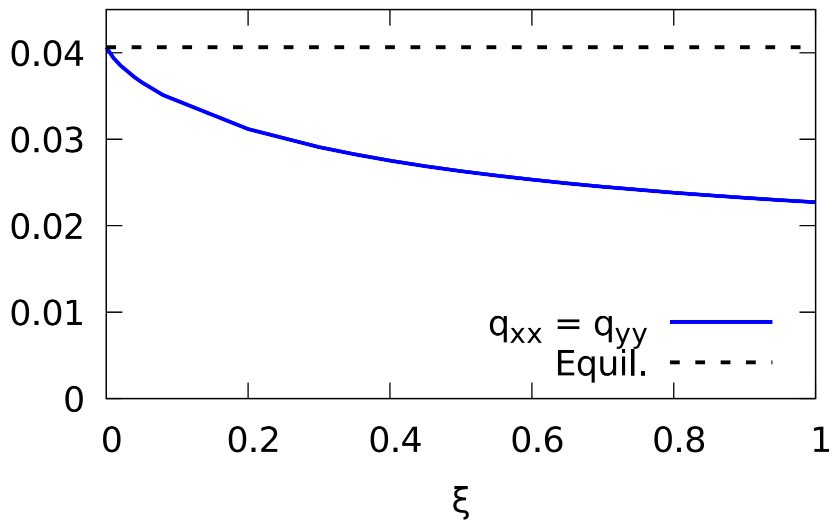

(b) UV cutoff of $q_{\text{max}} = g\Lambda$ corresponding to $E \sim \Lambda$

Figure 4.9: Total momentum broadening, $\widehat{q}_{xx} = \widehat{q}_{yy}$, in units of $g^4\Lambda^3$ for a parton travelling in the direction of the anisotropy vector, $\theta = 0$. For a low energy parton there is substantial reduction due to anisotropy while for an energetic jet parton there is moderate reduction.

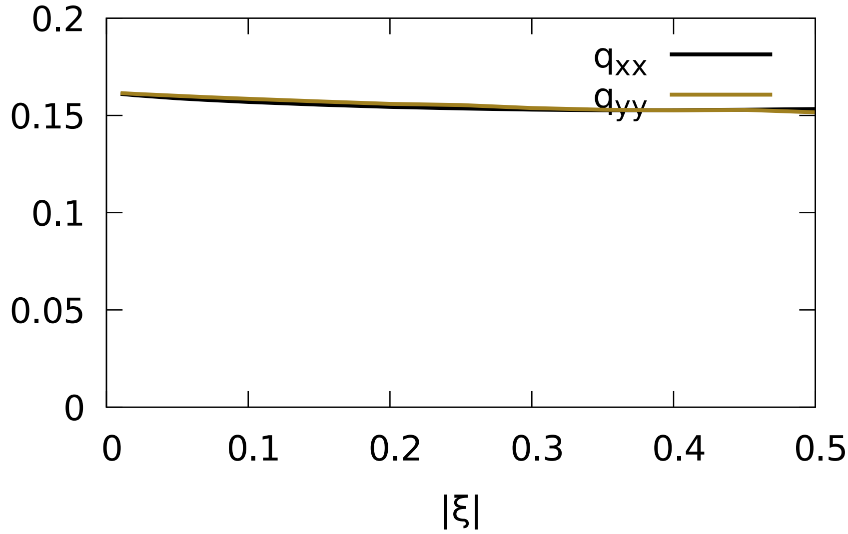

(a) UV cutoff of $q_{\max} = \sqrt{10} g\Lambda$ corresponding to parton energy $E \sim 100\Lambda$.

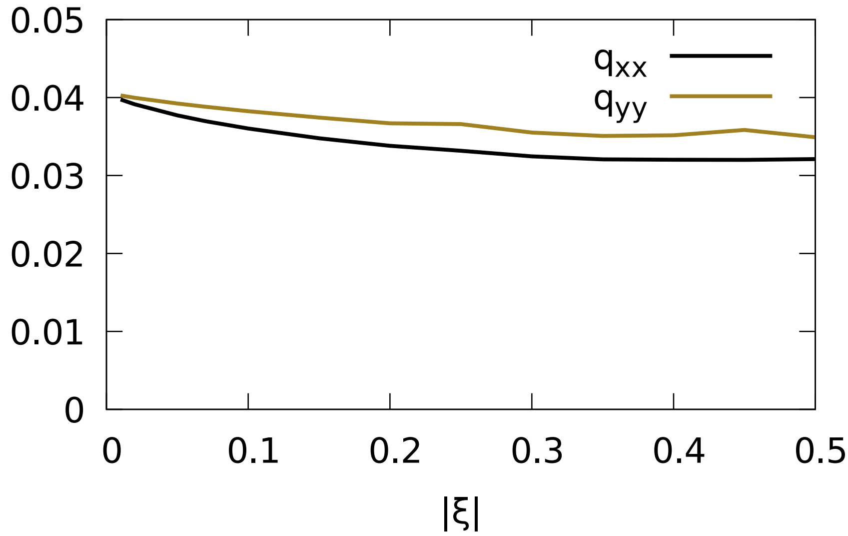

(b) UV cutoff of $q_{\max} = g\Lambda$ corresponding to $E \sim \Lambda$

Figure 4.10: Momentum broadening in units of $g^4\Lambda^3$ for a parton travelling perpendicularly to the direction of the anisotropy vector, $\theta = \pi/2$. We assume a medium with $\xi < 0$. For a low energy parton there is moderate reduction in momentum broadening due to anisotropy as well as angular dependence.

see Fig. 4.9a. This is because the collision kernel decreases with anisotropy at low and intermediate momenta as seen in Fig. 4.5 while momentum broadening of a high-energy jet parton is dominated by high-energy kicks.

For partons at lower energy there is substantially more reduction in momentum broadening. Fig. 4.9b shows momentum broadening for a parton with energy $E \sim \Lambda$, travelling in the direction of the anisotropy vector. This can either be a jet parton with extremely low energy, or a medium quasiparticle in kinetic theory. We see a reduction of around 45%. This can be seen as a very rough estimate of the importance of anisotropic corrections to 1-to-2 processes with collinear radiation for quasiparticles in kinetic theory, as these processes are dominated by momentum broadening. Thus it is clear that anisotropy can change the rate of such processes substantially.

In Fig. 4.10 we show momentum broadening of a jet parton travelling orthogonally to the anisotropy vector, $\theta = \pi/2$. The medium has $\xi < 0$. In this case $\widehat{q}_{xx} \neq \widehat{q}_{yy}$. There is less reduction in momentum broadening here because a jet parton travelling in this direction sees less anisotropic screening. For a jet parton with $E \sim 100\Lambda$ there is little reduction in momentum broadening, see Fig. 4.10a, but for a parton with $E \sim \Lambda$ as in 4.10b there is a 20% reduction in $\widehat{q}_{xx}$ and a 15% reduction in $\widehat{q}_{yy}$. This shows that the overall effect of an anisotropic medium is primarily to reduce momentum broadening due to increased screening, but also to introduce an angular dependence to the broadening.

Part V

PHOTON AND GLUON RADIATION IN AN ANISOTROPIC PLASMA

5

PHOTON AND GLUON RADIATION IN AN ANISOTROPIC PLASMA

5.1 EQUATIONS FOR COLLINEAR SPLITTING

Collinear photon and gluon emission including the LPM effect are central processes in the physics of heavy-ion collisions. Collinear photon production accounts for half of photons emitted during the QGP stage. Furthermore, the physics of jets is dominated by medium-induced gluon radiation which is also one of two interaction channels for quasi-particles in a kinetic theory description of QGP. For consistency, all of these processes should be evaluated in a non-equilibrium plasma as is found in heavy-ion collisions. This furthermore allows for extracting non-equilibrium properties of the QGP using jets and photons.

The rate of collinear radiation of photons and gluons in a non-equilibrium plasma has not been calculated consistently before. In particular, calculations have not included non-equilibrium momentum broadening but rather assumed an equilibrium or isotropic collision kernel $\mathcal{C}$ [52, 53]. Our goal is to evaluate non-equilibrium collinear radiation consistently, using the anisotropic collision kernel from Sec. 4. This is considerably more involved than the equilibrium or isotropic evaluation due to the angular dependence of the collision kernel.

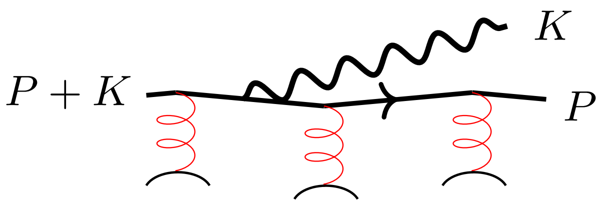

Figure 5.1: Collinear photon emission through bremsstrahlung, including the LPM effect.

Photon production through collinear radiation is shown in Fig. 5.1. During the radiation, the emitting quark can receive arbitrarily many soft kicks from the medium since the quark and photon wavepackets overlap for a long time, see Sec. 1.6 for a qualitative discussion. This diagram can be evaluated, giving that the rate R of emitting photons of energy k collinearly in a QCD plasma is

$$k\frac{dR}{d^3k} = \frac{3Q^2\alpha_{EM}}{4\pi^2}\int \frac{d^3p}{(2\pi)^3}F(P+K)\left[1-F(P)\right]\frac{p^{z\,2}+(p^z+k)^2}{2p^{z\,2}(p^z+k)^2}\,2\mathbf{p}_\perp\cdot\mathrm{Re}\,\mathbf{f}(\mathbf{p};\mathbf{k}), \quad (5.1)$$

see [72, 73], as well as our work in [78] which analyzed these diagrams in detail in a non-equilibrium medium and did not assume the equilibrium KMS condition. We have chosen the photon to emitted along the z axis. The quark's collinear momentum is $p^z \sim \Lambda$ after emission and the transverse momentum it gains through kicks is $\mathbf{p}_\perp \sim g\Lambda$. Furthermore

$$F(P) = f_q(\mathbf{p})\theta(p^0) + (1-f_q(\mathbf{p}))\theta(-p^0) \quad (5.2)$$

gives the momentum distribution of the incoming and outgoing quarks. It is easy to see that the factor $F(P+K)\left[1-F(P)\right]$ corresponds to bremsstrahlung off a quark when $p^0 > 0$, to bremsstrahlung off an antiquark when $p^0 < -k^0$ and to pair annihilation of a quark and an antiquark when $-k^0 < p^0 < 0$. Furthermore, $Q^2e^2 = \sum_{\text{flavour}} q^2$ sums over the different flavours of quarks in the plasma. The factor $(p^{z\,2}+(p^z+k)^2)/(2p^{z\,2}(p^z+k)^2)$ describes the hard splitting where a photon is radiated.

The central ingredient in Eq. (5.1) is the function $\mathbf{f}$ which quantifies how momentum broadening modifies coherence between the partons during photon emission. This function solves the integral equation [73, 78]

$$2\mathbf{p}_\perp = i\delta E\,\mathbf{f}(\mathbf{p}_\perp) + \int\frac{d^2q_\perp}{(2\pi)^2}\,\mathcal{C}(\mathbf{q}_\perp)\left[\mathbf{f}(\mathbf{p}_\perp)-\mathbf{f}(\mathbf{p}_\perp+\mathbf{q}_\perp)\right]. \quad (5.3)$$

The collision kernel $\mathcal{C}(\mathbf{q}_\perp)$ gives the rate of receiving a kick of transverse momentum $\mathbf{q}_\perp$ from the medium. Eq. (5.3) both has a loss term and a gain term for these transverse kicks. Furthermore, $\delta E = k^0 + E_p\mathrm{sgn}(p^z) - E_{p+k}\mathrm{sgn}(p^z+k)$ is the phase difference between the photon and quark after emission, and the quark before emission. Expanding δE using that e.g. $E_p = \sqrt{p_z^2+\mathbf{p}_\perp^2+m_\infty^2} \approx |p_z| + \frac{p_\perp^2+m_\infty^2}{|p_z|}$, gives that

$$\delta E = \frac{k}{2p^z\left(p^z+k\right)}\left(\mathbf{p}_\perp^2+m_\infty^2\right) \quad (5.4)$$

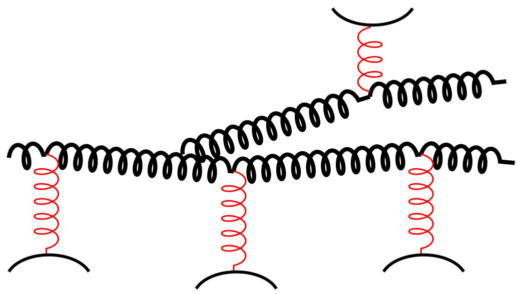

Figure 5.2: Collinear gluon emission off another gluon, including the LPM effect.

where $m_\infty^2 = 4g^2 C_F \int \frac{d^3p}{2p(2\pi)^3} \left(f_q(\mathbf{p}) + f_g(\mathbf{p})\right)$ is the thermal mass of hard quarks. The thermal mass depends on the momentum distribution of hard particles. In Eq. (5.3), the different components of $\mathbf{f}$ correspond to different polarization of the emitted photon. In the absence of medium kicks $\mathcal{C} = 0$ and the single hard splitting gives $\mathbf{f} = -i\mathbf{p}_\perp/\delta E$. This gives vanishing contribution to Eq. (5.1) since $\mathbf{f}$ is purely imaginary, confirming that bremsstrahlung off an on-shell quark is not possible in vacuum. These complicated equations were first solved numerically in thermal equilibrium in [72], see also [82] for an alternative numerical evaluation.

The equations for collinear gluon emission by a jet parton or a quasiparticle are similar to Eqs. (5.1) and (5.3). As an example, the rate of emitting a gluon with energy k by another gluon with energy $p+k$, see Fig. 5.2, is given by

$$k\frac{d\Gamma}{d^3k} = \frac{\alpha_s}{4\pi^2 k}\, n_g(p+k)(1+n_g(p))(1+n_g(k))\frac{1}{k^3}\mathcal{J}(p,k)\int \frac{d^2h}{(2\pi)^2}\, 2\mathbf{h}\cdot \mathrm{Re}\,\mathbf{F} \tag{5.5}$$

where n_g is the momentum distribution of gluons and

$$\mathcal{J}(p,k) = \frac{p^4 + k^4 + (p+k)^4}{8p^3(p+k)^3} \tag{5.6}$$

is the splitting function for gluon emission. The function $\mathbf{F}(\mathbf{h})$ solves

$$\begin{aligned} 2\mathbf{h} = i\delta E\,\mathbf{F} + \int \frac{d^2q_\perp}{(2\pi)^2}\,\tilde{\mathcal{C}}(\mathbf{q}_\perp)\Big[&\left\{\mathbf{F}(\mathbf{h}) - \mathbf{F}(\mathbf{h}+(k+p)\mathbf{q}_\perp)\right\} \\ &+ \left\{\mathbf{F}(\mathbf{h}) - \mathbf{F}(\mathbf{h}-p\mathbf{q}_\perp)\right\} \\ &- \left\{\mathbf{F}(\mathbf{h}) - \mathbf{F}(\mathbf{h}-k\mathbf{q}_\perp)\right\}\Big] \end{aligned} \tag{5.7}$$

Because of different colour factors for gluon emission we use the collision kernel $\tilde{\mathcal{C}} = \frac{C_A}{2C_F}\mathcal{C}$. The phase difference is given by

$$\delta_E = \frac{m_g^2}{2}\left(\frac{1}{k} + \frac{1}{p} - \frac{1}{p+k}\right) + \frac{h^2}{2pk(p+k)} \tag{5.8}$$

where m_g^2 is the gluon thermal mass. The central difference with respect to photon emission is that the produced parton can also have momentum broadening which explains the three different broadening terms in Eq. (5.7). Finally, the transverse momentum $\mathbf{h}$ has been defined as $\mathbf{h} = k_z\mathbf{p}_\perp - p_z\mathbf{k}_\perp$, see [71] for further information. These equations were evaluated numerically in equilibrium for jet partons in [80]. We note that the rate of photon and gluon production has been evaluated at next-to-leading order in [179–181].

There exist a number of other formulations of jet splitting through bremsstrahlung in a quark-gluon plasma. They are mostly equivalent to each other. The earliest calculations were performed by Baier, Dokshitzer, Mueller, Peigné and Schiff (BDMPS) [182–184] and independently by Zakharov using a path-integral formulation [185, 186]. These calculations have been shown to be equivalent to each other [187, 188]. These calculations included the effect of a finite medium and reformulated momentum broadening for high energy jets as diffusion in the transverse plane using the harmonic-oscillator approximation, giving analytic results for the rate of splitting.[1] However, the work by BDMPS and Zhakarov assumed a simple model for the collision kernel $\mathcal{C}$ [190], while the AMY rates which we have discussed give a full leading-order calculation of the kernel. Thus the AMY calculation accurately includes the microscopic details of a weakly-coupled medium, both through the collision kernel as well as through the inclusion of particle thermal masses.

Another widely used formulation of jet splitting in a medium is the work of Gyulassy, Levai and Vitev [191] which assumes a thin medium so that only a finite number of medium kicks need to be taken into account. This can be seen as an expansion in the collision kernel $\mathcal{C}$ in Eq. (5.7) [192]. Such calculations have also been performed for massive quarks [193]. In our work, we will assume a medium that is thick enough to allow for arbitrarily many medium kicks during emission.

1 See [189] for a reformulation of the AMY formalism to allow for a finite medium. See furthermore [79, 105] for analytic solutions in the AMY formalism up to next-to-leading order in $\log(E/T)$ where E is the jet parton energy, which correspond physically to the harmonic-oscillator approximation.

Finally, a completely different treatment of jet splitting was given by Wang and Guo in [194, 195]. Unlike other calculations which assume on-shell jet partons, their calculation is for highly virtual partons where medium-induced splitting is a correction to vacuum radiation in a virtuality-ordered shower. This physics has been implemented in a numerical code called MATTER [196] which describes the early evolution of jets in a medium when the jet partons are still highly virtual.

5.2 NUMERICAL DETAILS

The integral equation in Eq. (5.3) can be solved in an anisotropic medium, given the anisotropic collision kernel $\mathcal{C}(\mathbf{p}_\perp)$ evaluated in Sec. 5. Together with Eq. (5.1) this gives the rate of collinear photon production, including the LPM effect, in an anisotropic, non-equilibrium plasma. To solve the integral equation we will use an expansion in a functional basis, see [72] for the corresponding treatment in equilibrium. The anisotropic case requires different methods than the isotropic case. This is because in an isotropic medium the solution of Eq. (5.3) satisfies $\mathbf{f}(\mathbf{p}_\perp) = \mathbf{p}_\perp \tilde{f}(p_\perp)$ where $\tilde{f}$ only depends on the magnitude of a transverse kick $p_\perp$, while in an anisotropic medium $\mathbf{f}$ need not be in the direction of $\mathbf{p}_\perp$ and has non-trivial dependence on the direction of $\mathbf{p}_\perp$.

For the purposes of this thesis we will focus on photon radiation. All of the methods presented can easily be extended to gluon radiation, which is especially interesting for gluon bremsstrahlung in kinetic theory. For jet partons the effect of anisotropy will be much smaller since momentum broadening of a high-energy jet parton is less sensitive to details of the medium than broadening of partons with energy of order Λ, see Figs. 4.9 and 4.10.

To solve Eq. (5.3), we separate the equations into real and imaginary components. Writing $\mathbf{f} = \mathbf{R} + i\mathbf{J}$, with $\mathbf{R}$ and $\mathbf{J}$ real, the integral equation becomes

$$\begin{aligned} 0 &= \delta E\, \mathbf{R}(\mathbf{p}_\perp) + \int \frac{d^2 q_\perp}{(2\pi)^2}\, \mathcal{C}(\mathbf{q}_\perp)\, [\mathbf{J}(\mathbf{p}_\perp) - \mathbf{J}(\mathbf{p}_\perp + \mathbf{q}_\perp)] \\ 2\mathbf{p}_\perp &= -\delta E\, \mathbf{J}(\mathbf{p}_\perp) + \int \frac{d^2 q_\perp}{(2\pi)^2}\, \mathcal{C}(\mathbf{q}_\perp)\, [\mathbf{R}(\mathbf{p}_\perp) - \mathbf{R}(\mathbf{p}_\perp + \mathbf{q}_\perp)] \end{aligned} \tag{5.9}$$

The function $\mathbf{J}(\mathbf{p}_\perp)$ is $\mathbf{J} = -2\mathbf{p}_\perp/\delta E \sim 1/p_\perp$ at high transverse momentum $\mathbf{p}_\perp$. Because of how slowly $\mathbf{J}$ falls off with $p_\perp$ we prefer to use the the function $\mathbf{I}$ defined by

$$\mathbf{J} = -\frac{2\mathbf{p}_\perp}{\delta E} + \mathbf{I}. \tag{5.10}$$

This gives

$$\begin{aligned} 0 &= \delta E\,\mathbf{R}(\mathbf{p}_\perp) - \frac{4p^z(p^z+k)}{k}\int \frac{d^2q_\perp}{(2\pi)^2}\,\mathcal{C}(\mathbf{q}_\perp)\left[\frac{\mathbf{p}_\perp}{\mathbf{p}_\perp^2+m_\infty^2} - \frac{\mathbf{p}_\perp+\mathbf{q}_\perp}{(\mathbf{p}_\perp+\mathbf{q}_\perp)^2+m_\infty^2}\right] \\ &\qquad + \int \frac{d^2q_\perp}{(2\pi)^2}\,\mathcal{C}(\mathbf{q}_\perp)\left[\mathbf{I}(\mathbf{p}_\perp)-\mathbf{I}(\mathbf{p}_\perp+\mathbf{q}_\perp)\right] \\ 0 &= -\delta E\,\mathbf{I}(\mathbf{p}_\perp) + \int \frac{d^2q_\perp}{(2\pi)^2}\,\mathcal{C}(\mathbf{q}_\perp)\left[\mathbf{R}(\mathbf{p}_\perp)-\mathbf{R}(\mathbf{p}_\perp+\mathbf{q}_\perp)\right]. \end{aligned} \tag{5.11}$$

These are the equations we will solve numerically.[2]

Eq. (5.11) is naturally expressed using the language of functional analysis. We write

$$\begin{bmatrix} \delta E & \hat{\mathcal{C}} \\ \hat{\mathcal{C}} & -\delta E \end{bmatrix} \begin{bmatrix} \mathbf{R} \\ \mathbf{I} \end{bmatrix} = \begin{bmatrix} \boldsymbol{\eta} \\ 0 \end{bmatrix} \tag{5.12}$$

where the integral operator $\hat{\mathcal{C}}$ acts on a function $\mathbf{g}$ through

$$\hat{\mathcal{C}}\mathbf{g} := \int \frac{d^2q_\perp}{(2\pi)^2}\,\mathcal{C}(\mathbf{q}_\perp)\left[\mathbf{g}(\mathbf{p}_\perp)-\mathbf{g}(\mathbf{p}_\perp+\mathbf{q}_\perp)\right] \tag{5.13}$$

and the function $\boldsymbol{\eta}$ is defined through

$$\begin{aligned} \boldsymbol{\eta} &:= \hat{\mathcal{C}}\left[\frac{4p^z(p^z+k)}{k}\frac{\mathbf{p}_\perp}{\mathbf{p}_\perp^2+m_\infty^2}\right] \\ &= \frac{4p^z(p^z+k)}{k}\int \frac{d^2q_\perp}{(2\pi)^2}\,\mathcal{C}(\mathbf{q}_\perp)\left[\frac{\mathbf{p}_\perp}{\mathbf{p}_\perp^2+m_\infty^2} - \frac{\mathbf{p}_\perp+\mathbf{q}_\perp}{(\mathbf{p}_\perp+\mathbf{q}_\perp)^2+m_\infty^2}\right] \end{aligned} \tag{5.14}$$

To measure the overlap of two functions, we define an inner product in the space of functions as

$$(\mathbf{f},\mathbf{g}) = \int \frac{d^2p_\perp}{(2\pi)^2}\,\mathbf{f}(\mathbf{p}_\perp)\cdot\mathbf{g}(\mathbf{p}_\perp) \tag{5.15}$$

for functions that decay sufficiently rapidly for the integral to be convergent.

2 For numerical evaluation we furthermore scale the variables with $g\,\Lambda$. In particular, $\tilde{k} = k/\Lambda$, $\tilde{p}_z = p_z/\Lambda$, $\tilde{p}_\perp = p_\perp/g\Lambda$, $\tilde{m}_\infty = m_\infty/g\Lambda$, $\tilde{\delta E} = \delta E/g^2\Lambda$, $\tilde{\mathcal{C}} = \Lambda\mathcal{C}$, and $\tilde{\mathbf{f}} = g\mathbf{f}$.

When soft gluons are emitted by hard quasiparticles with momentum distribution $f(\mathbf{p}) = f(-\mathbf{p})$, the collision kernel obeys $\mathcal{C}(\mathbf{p}_\perp) = \mathcal{C}(-\mathbf{p}_\perp)$.[3] Then

$$\begin{aligned} &\int \frac{d^2p_\perp}{(2\pi)^2} \int \frac{d^2q_\perp}{(2\pi)^2}\, \mathbf{f}(\mathbf{p}_\perp)\mathcal{C}(\mathbf{q}_\perp)\, [\mathbf{g}(\mathbf{p}_\perp) - \mathbf{g}(\mathbf{p}_\perp + \mathbf{q}_\perp)] \\ = &\int \frac{d^2p_\perp}{(2\pi)^2} \int \frac{d^2q_\perp}{(2\pi)^2}\, [\mathbf{f}(\mathbf{p}_\perp) - \mathbf{f}(\mathbf{p}_\perp + \mathbf{q}_\perp)]\, \mathcal{C}(\mathbf{q}_\perp)\,\mathbf{g}(\mathbf{p}_\perp) \end{aligned} \tag{5.16}$$

which is equivalent to

$$\left(\mathbf{f}, \hat{\mathcal{C}}\mathbf{g}\right) = \left(\hat{\mathcal{C}}\mathbf{f}, \mathbf{g}\right). \tag{5.17}$$

In other words, the integral operator $\hat{\mathcal{C}}$ is Hermitian with respect to the inner product. The multiplicative operator δE is furthermore trivially Hermitian. Thus, the total matrix in Eq. (5.12) is Hermitian which guarantees that the total matrix can be inverted and that there exists a unique solution $\mathbf{R}$, $\mathbf{I}$ of Eq. (5.12).

In order to find the unique solution for the functions $\mathbf{R}$ and $\mathbf{I}$, we will expand them in a basis of functions. In an isotropic system, we have $\mathbf{R}(\mathbf{p}_\perp) = \mathbf{p}_\perp r(p_\perp)$ and $\mathbf{I}(\mathbf{p}_\perp) = \mathbf{p}_\perp i(p_\perp)$ so that only two scalar functions, r and i, need to be solved for. In the more general case of an anisotropic plasma $\mathbf{I}$ and $\mathbf{R}$ have two independent components, giving a total of four unknown functions. We choose to separate the functions in Cartesian components, writing

$$\mathbf{R} = R_x\hat{\mathbf{x}} + R_y\hat{\mathbf{y}} \tag{5.18}$$

and

$$\mathbf{I} = I_x\hat{\mathbf{x}} + I_y\hat{\mathbf{y}} \tag{5.19}$$

This naturally decouples the equations in Eq. (5.12) into two sets of equations,

$$\begin{bmatrix} \delta E & \hat{\mathcal{C}} \\ \hat{\mathcal{C}} & -\delta E \end{bmatrix} \begin{bmatrix} R_x \\ I_x \end{bmatrix} = \begin{bmatrix} \eta_x \\ 0 \end{bmatrix}, \tag{5.20}$$

and

$$\begin{bmatrix} \delta E & \hat{\mathcal{C}} \\ \hat{\mathcal{C}} & -\delta E \end{bmatrix} \begin{bmatrix} R_y \\ I_y \end{bmatrix} = \begin{bmatrix} \eta_y \\ 0 \end{bmatrix} \tag{5.21}$$

3 If $f(\mathbf{p}) \neq f(-\mathbf{p})$ there is a net current in the system. This might e.g. be if one is in a boosted frame relative to the fluid's rest frame. We will always choose to work in the fluid's rest frame.

which can be solved separately.

We expand the four functions in a an infinite basis of functions. We write

$$\begin{cases} R_x(\mathbf{p}_\perp) = \sum_\chi a_\chi \phi_\chi(\mathbf{p}_\perp) \\ R_y(\mathbf{p}_\perp) = \sum_\chi b_\chi \phi_\chi(\mathbf{p}_\perp) \\ I_x(\mathbf{p}_\chi) = \sum_\chi c_\chi \psi_\chi(\mathbf{p}_\perp) \\ I_y(\mathbf{p}_\chi) = \sum_\chi d_\chi \psi_\chi(\mathbf{p}_\perp) \end{cases} \tag{5.22}$$

where we allow for different functions for **R** and **I** since they differ in how fast they decay as $\mathbf{p}_\perp \to \infty$. Unlike in the case of an isotropic medium where $\phi(\mathbf{p}_\perp) = \phi(p_\perp)$, we have functions in two variables. Taking the inner product from Eq. (5.15) with a test function $\tilde{\phi}_\omega$ we can write Eqs. (5.20) and (5.21) as

$$\begin{cases} (\delta E)_{\omega\chi} a_\chi + (\hat{\mathcal{C}})_{\omega\chi} c_\chi = \eta_{x\,\omega} \\ (\hat{\mathcal{C}})_{\omega\chi} a_\chi - (\delta E)_{\omega\chi} c_\chi = 0 \end{cases} \tag{5.23}$$

$$\begin{cases} (\delta E)_{\omega\chi} b_\chi + (\hat{\mathcal{C}})_{\omega\chi} d_\chi = \eta_{y\,\omega} \\ (\hat{\mathcal{C}})_{\omega\chi} b_\chi - (\delta E)_{\omega\chi} d_\chi = 0 \end{cases} \tag{5.24}$$

with an implicit sum over χ. This is a matrix equation for the coefficients. It can in principle be solved if we know

$$(\hat{\mathcal{C}})_{\omega\chi} := \int \frac{d^2p_\perp}{(2\pi)^2} \int \frac{d^2q_\perp}{(2\pi)^2}\, \tilde{\phi}_\omega(\mathbf{p}_\perp)\, \mathcal{C}(\mathbf{q}_\perp)\, [\phi_\chi(\mathbf{p}_\perp) - \phi_\chi(\mathbf{p}_\perp + \mathbf{q}_\perp)]\,, \tag{5.25}$$

$$(\delta E)_{\omega\chi} = \int \frac{d^2p_\perp}{(2\pi)^2}\, \tilde{\phi}_\omega(\mathbf{p}_\perp)\, \delta E(\mathbf{p}_\perp)\phi_\chi(\mathbf{p}_\perp) \tag{5.26}$$

and

$$\eta_\omega := \frac{4p^z(p^z+k)}{k} \int \frac{d^2p_\perp}{(2\pi)^2} \int \frac{d^2q_\perp}{(2\pi)^2}\, \tilde{\phi}_\omega(\mathbf{p}_\perp)\mathcal{C}(\mathbf{q}_\perp) \left[\frac{\mathbf{p}_\perp}{\mathbf{p}_\perp^2 + m_\infty^2} - \frac{\mathbf{p}_\perp + \mathbf{q}_\perp}{(\mathbf{p}_\perp + \mathbf{q}_\perp)^2 + m_\infty^2} \right], \tag{5.27}$$

In practice, we need to truncate the infinite basis of function to a finite number of functions that approximate **R** and **I** well. The finite basis must be chosen wisely so that rapid convergence is achieved when the number of basis functions grows.

The collision kernel $\mathcal{C}(\mathbf{p}_\perp)$ can blow up at small $p_\perp$. To have a better handle on this region, we use radial coordinates for $\mathbf{p}_\perp$. Specifically, we write

$$\mathbf{p}_\perp = \gamma \frac{1-z}{1+z} (\cos\alpha, \sin\alpha) \tag{5.28}$$

where α is the angular variable and $z \in [-1,1]$ stands for the radial variable with $z \to -1$ corresponding to $p_\perp \to \infty$ and $z \to 1$ corresponding to $p_\perp \to 0$. Here, $\gamma = 4.0$ is a numerical coefficient which we choose to make numerical evaluation of integrals as fast as possible. Using these variables we write $\chi = (kl)$ in terms of two indices so that e.g.

$$\phi_\chi(\mathbf{p}_\perp) = \phi_{(kl)}(\mathbf{p}_\perp) = (1+z)^4 P_k(z) B_l(\alpha) \tag{5.29}$$

where we separate the radial and angular dependence of R_x. Then e.g.

$$\begin{aligned} R_x(\mathbf{p}_\perp) &= \sum_\chi a_\chi \phi_\chi(\mathbf{p}_\perp) \\ &= \sum_{kl} a_{kl} (1+z)^4 P_k(z) B_l(\alpha). \end{aligned} \tag{5.30}$$

We have factored out $(1+z)^4$ since $\mathbf{R}$ and $\mathbf{I}$ decay at least as $1/p_\perp^4$ when $\mathbf{p}_\perp \to \infty$. Similarly, we write the test functions as

$$\tilde{\phi}_{kl}(z,\alpha) = (1+z)^2 P_k(z) B_l(\alpha) \tag{5.31}$$

As $\boldsymbol{\eta}$ needs to be in the span of $\tilde{\phi}_{kl}$ and $\eta \sim 1/p_\perp^2$ as $p_\perp \to \infty$, we can only factor out $(1+z)^2$ for the test function.

The functions $P_k(z)$, $B_l(\alpha)$ need to be chosen wisely. Polynomials turn out to give rapidly oscillating integrals with slow convergence. Therefore, for the radial functions we choose Gaussians centered at different points,

$$P_k(z) = \sqrt{\frac{N}{\pi}} \exp\left(-N\left(z - 1 + \frac{2k}{N}\right)^2\right) \tag{5.32}$$

Here $k = 0, ..., N$ for a basis of size N and $-1 \leq z \leq 1$. As N we have more functions, which are more narrowly spread around different points on the interval. Similarly, we write the angular functions as

$$B_l(\alpha) = \frac{M^{1/6}}{\sqrt{\pi}} \exp\left(-M\left(-1 + \cos\left[\alpha - 2\pi\frac{l}{M+1}\right]\right)^2\right) \tag{5.33}$$

where $l = 0, ..., M$ for a basis of size M and $0 \leq \alpha \leq 2\pi$. This function can be seen as a reparametrization of Gaussians to give periodic basis functions. The overall normalization constant $M^{1/6}$ is chosen so that $\int d\alpha B_l^2(\alpha)$ is approximately constant for a wide range of values of M.

Having chosen a basis for functions, the integrals in Eqs. (5.25), (5.26) and (5.27) need to be evaluated numerically. Since $\mathcal{C}(\mathbf{q}_\perp)$ is a complicated general function, integration over all four variables must be done numerically. We discuss this numerical evaluation in more detail in App. C. In particular, the expression for $\left(\hat{\mathcal{C}}\right)_{\alpha\beta}$ expressed in radial coordinates contains rapid oscillations when $\mathbf{p}_\perp \to \mathbf{q}_\perp$ due to the angular variable for $\mathbf{p}_\perp - \mathbf{q}_\perp$ being ill-defined. In App. C, we rewrite the integral to avoid these rapid oscillations. When these integrals have been evaluated, one can solve for the coefficients a_χ, b_χ, c_χ and d_χ in Eqs. (5.23) and (5.24) giving a good approximation for $\mathbf{R}$ and $\mathbf{I}$. Substituting $\mathbf{Re}\,\mathbf{f} = \mathbf{R}$ into Eq. (5.1) and performing the remaining integrals numerically then gives the rate of collinear photon emission in an anisotropic plasma.

5.3 RESULTS

In this thesis, we focus on photon emission in an anisotropic medium. The rate of gluon emission by jet partons is less affected by a medium anisotropy as there is less reduction in momentum broadening, see Sec. 4.3. We note that the anisotropic correction to gluon emission by quasiparticles in kinetic theory should be comparable to the anisotropic correction to photon emission which we evaluate here.

Fig. 5.3 shows our results for the rate of photon production through bremsstrahlung in an anisotropic medium. We consider a photon travelling in the direction of the anisotropy vector $\mathbf{n}$ and compare the rate for two different values of medium anisotropy, as well as in thermal equilibrium. As expected, the rate runs over many orders of magnitude as the number of high-energy quarks is exponentially suppressed, making radiation of high-energy photons less likely. For easier comparison, we show the ratio between the anisotropic and equilibrium result in Fig. 5.4. There is a large suppression in the rate as the anisotropy is increased, especially for higher photon momenta.

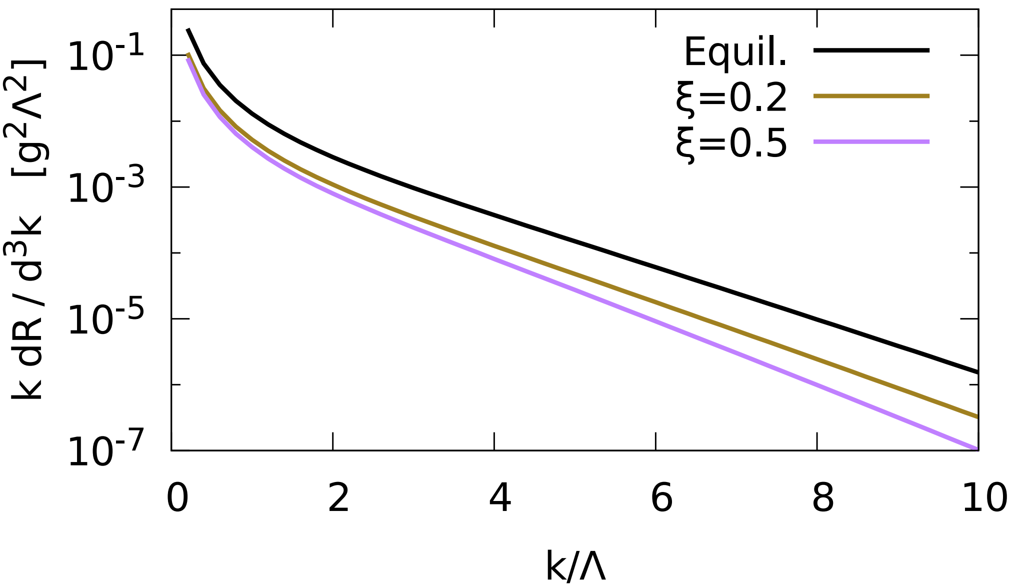

Figure 5.3: Rate of photon production in an anisotropic plasma, $k\frac{dR}{d^3k}$, where k is photon momentum. The rate is given in units of $g^2\Lambda^2$. We consider emission of a photon in the direction of the anisotropy vector $\mathbf{n}$.

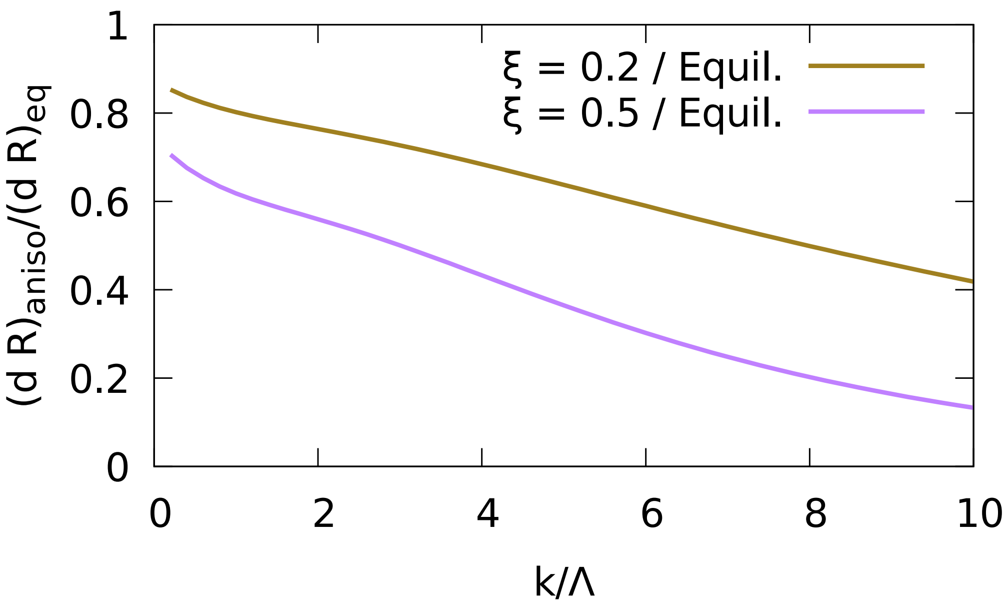

Figure 5.4: Ratio of the anisotropic rate of photon production from Fig. 5.3, $(dR)_{\text{aniso}} := k\frac{dR}{d^3k}\big|_{\text{aniso}}$, with the equilibrium rate, $(dR)_{\text{eq}} := k\frac{dR}{d^3k}\big|_{\text{eq}}$. The rate is substantially reduced by the anisotropy, especially for higher photon momenta.

To understand better the suppression in photon production rate seen in Fig. 5.4 as anisotropy is increased, it is helpful to consider the quantity $k\frac{dR}{d^3kdp_z}$. This gives the rate of photon production where the momentum of one of the quarks is fixed as $|p_z|$. This quantity is given by

$$k\frac{dR}{d^3kdp_z} = \frac{3Q^2\alpha_{EM}}{8\pi^3}F(P+K)\left[1-F(P)\right]\frac{p^{z\,2}+(p^z+k)^2}{2p^{z\,2}(p^z+k)^2}\int\frac{d^2p_\perp}{(2\pi)^2}\,2\mathbf{p}_\perp\cdot\mathrm{Re}\,\mathbf{f}(\mathbf{p};\mathbf{k}), \quad (5.34)$$

see Eq. (5.1). In Fig. 5.5, we show this quantity for pair-annihilation of a quark and an antiquark, and for bremsstrahlung off a quark, both of which are needed for the overall rate of photon production. We fix the photon momentum to be $k = 5\Lambda$. For sizable photon momentum like $k = 5\Lambda$, pair-annihilation is dominant because bremsstrahlung requires more energetic quarks which are fewer in number in the plasma.

There are two ways in which medium anisostropy can change the rate of photon production, both of which are included in Fig. 5.5. Firstly, the density of soft gluons is modified, giving a different collision kernel for momentum broadening $\mathcal{C}(\mathbf{p}_\perp)$. This is a complicated effect. We have shown in Sec. 4 that momentum broadening is reduced in an anisotropic medium. Intuitively, this reduces the rate of photon production, since the emitting quark is brought less off shell by medium kicks, meaning that the medium stimulates less splitting. Secondly, medium anisotropy changes the rate of photon production because the distribution of hard quarks in the medium $f(\mathbf{p})$ is changed. Depending on the momentum direction, there can be more or fewer quarks emitting a photon, leading to either an enhancement or reduction in photon production.

It is important to separate these two contributions of anisotropy to photon production. In Fig. 5.6, we plot the ratio of

$$\int\frac{d^2p_\perp}{(2\pi)^2}\,2\mathbf{p}_\perp\cdot\mathrm{Re}\,\mathbf{f}(\mathbf{p};\mathbf{k}) \quad (5.35)$$

in an anisotropic medium and in equilibrium. This factor from Eq. (5.34) isolates the contribution of the collision kernel to the rate of photon radiation. We see that for pair-annihilation, an anisotropy of $\xi = 0.2$ gives a reduction of around 8 % to the rate due to momentum broadening while the total reduction seen in Fig. 5.5 is around 27 %. Similarly, at $\xi = 0.5$ the reduction due to momentum broadening is around 13 %, while the total reduction is about 50 %. In other words, a larger correction due to anisotropy comes

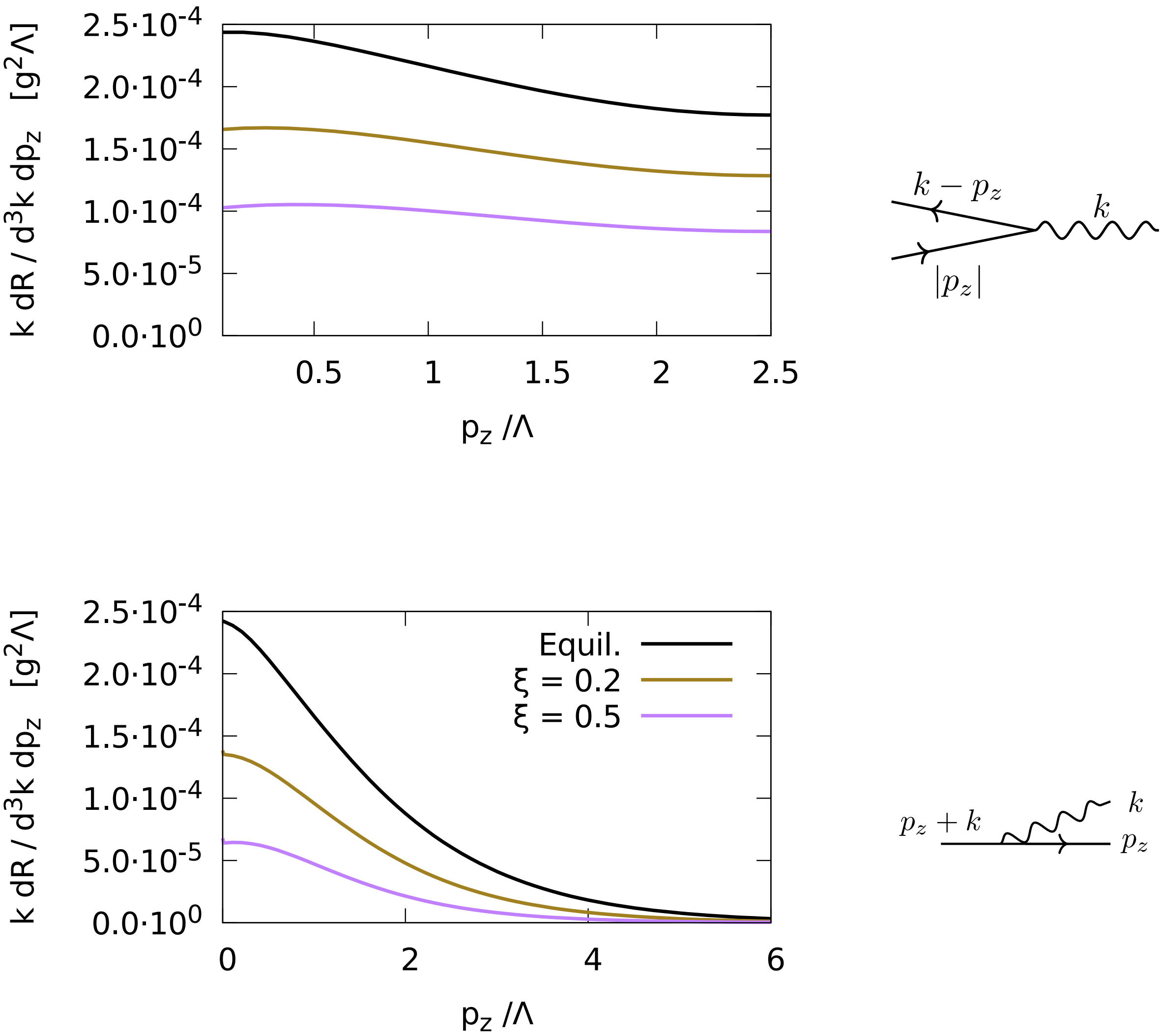

Figure 5.5: The quantity $k\frac{dR}{d^3k dp_z}$ in units of $g^2\Lambda$ for photon momentum $k = 5\Lambda$. This gives the rate of emitting a photon when one quark has fixed momentum $|p_z|$. The upper plot shows photon production through pair annihilation and the lower plot shows photon production through bremsstrahlung. In the Feynman diagrams, we omit showing medium kicks; see Figs. 1.11 and 1.12 for the full diagrams.

from the momentum distribution of quarks but there is also a sizable correction because of the anisotropic collision kernel.

A rough calculation explains how the anisotropic collision kernel affects photon production. Assuming that the quark transverse momentum $p_\perp$ is much greater than the typical momentum kick from the medium, we can rewrite Eq. (5.3) as

$$2\mathbf{p}_\perp = i\frac{k}{2p^z\,(p^z+k)}\mathbf{p}_\perp^2\;\mathbf{f}(\mathbf{p}_\perp) - \frac{\hat{q}}{2}\nabla^2 f(\mathbf{p}_\perp) \tag{5.36}$$

where we expanded $\mathbf{f}(\mathbf{p}_\perp+\mathbf{q}_\perp)$ in $\mathbf{q}_\perp$ and defined

$$\hat{q} = \int \frac{d^2q_\perp}{(2\pi)^2}\,\mathbf{q}_\perp^2\,\mathcal{C}(\mathbf{q}_\perp), \tag{5.37}$$

as usually. This assumption is not rigorously justified for photons but leads to intuitive results. We put the UV cutoff in $\hat{q}$ at the typical value of $p_\perp \sim g\Lambda$. Eq. (5.36) has been much studied, see e.g. [79, 184]. It can be solved analytically, giving that

$$\int \frac{d^2p_\perp}{(2\pi)^2}\,2\mathbf{p}_\perp\cdot\mathrm{Re}\,\mathbf{f}(\mathbf{p};\mathbf{k}) \sim \left(\frac{p_z(p_z+k)}{k}\right)^{3/2}\sqrt{\hat{q}}. \tag{5.38}$$

which can also be seen through dimensional analysis. Therefore, this rough estimate gives that the rate of photon production goes with the square root of momentum broadening. As an example, results from Sec. 4.3 give that at $\xi = 0.5$,

$$\sqrt{\frac{\hat{q}_{\text{aniso}}}{\hat{q}_{\text{eq}}}} \sim 0.8, \tag{5.39}$$

giving an estimate of a 20 % reduction in the rate coming from momentum broadening. This is a decent estimate of the real reduction of 13 %.

The anisotropic collision kernel allows us to evaluate the rate of emitting photons in different directions in an anisotropic plasma. We have already shows results for photon emission in the direction of the anisotropy vector $\mathbf{n}$. For a photon emitted orthogonally to the anisotropy vector, there is substantially less momentum broadening of the emitting quark as seen in Sec. 4.3. At $\xi = 0.5$, we can estimate this reduction to be the same as the reduction due to momentum broadening when a photon is emitted in the direction of $\mathbf{n}$, i.e. around a 15 % from the equilibrium rate. Furthermore, the quark momentum distributions for momentum $\mathbf{p}$ orthogonal to the anisotropy vector $\mathbf{n}$ is

$$\begin{aligned} f(\mathbf{p}) &= \sqrt{1+\xi}\, f_{\text{eq}}(\sqrt{p^2+\xi(\mathbf{p}\cdot\mathbf{n})^2}) \\ &= \sqrt{1+\xi}\, f_{\text{eq}}(p). \end{aligned} \tag{5.40}$$

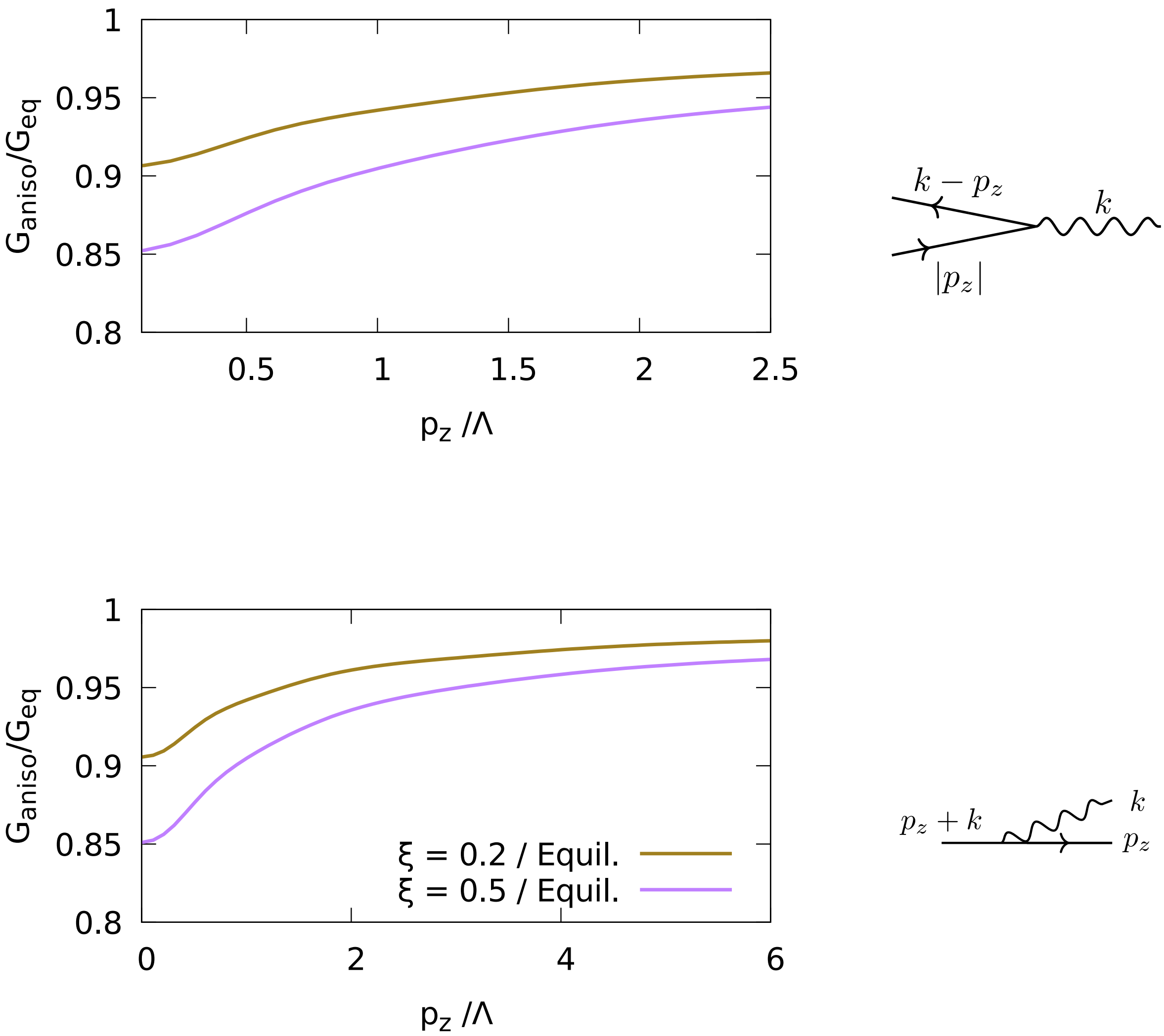

Figure 5.6: The ratio of the quantity $G := \int \frac{d^2 p_\perp}{(2\pi)^2} \, 2\mathbf{p}_\perp \cdot \mathrm{Re}\, \mathbf{f}(\mathbf{p};\mathbf{k})$ in an anisotropic medium and in equilbrium. This quantifies how important the anisotropic modification to momentum broadening is for the modification of the overall rate. We assume a photon momentum of $k = 5\Lambda$. The upper plot shows photon production through pair annihilation and the lower plot shows photon production through bremsstrahlung.

For $\xi = 0.5$ this gives an enhancement of $\sqrt{1+\xi} \approx 1.2$ in the rate with respect to the equilbrium rate due to an increased number of quarks. These two effects mostly cancel out, and therefore we expect the rate orthogonally to the anisotropy vector to be roughly the same as in equilibrium. Then Fig. 5.4 can be used to estimate the difference in photon yield orthogonally and parallel to the anisotropy vector. As an example for photon momentum $k = 10\,\Lambda$ and anisotropy $|\xi| = 0.5$ this suggests a factor six difference in photon yield in these two directions.

This large angular dependence could have interesting phenomenological implications. During the hydrodynamic stage of heavy-ion collision, there are sizable deviation from equilibrium leading to an anisotropic momentum distribution of quarks and gluons in the transverse plane of the collisions. Our results suggest that this could lead to a sizable angular dependence in photon yield from bremsstrahlung in the QGP phase. This gives a change in elliptic flow of photons which might partially explain why theory undershoots measurements of photon elliptic flow. In addition to these anisotropic corrections during the hydrodynamic stages, there are large deviations from equilibrium during early stages of heavy-ion collisions where the effect of anisotropy on photon production needs to be taken into account.

Part VI

CONCLUSIONS

6 CONCLUSIONS

Heavy-ion collisions create hot QCD matter known as the quark-gluon plasma (QGP). The plasma is out of thermal equilibrium at all times, meaning that heavy-ion collisions give a window into non-equilibrium QCD. The non-equilibrium properties of QCD include transport coefficients, like shear viscosity, which describe how a QCD medium relaxes to equilibrium, as well as hydrodynamization in which the initially far-from-equilibrium medium becomes amenable to a hydrodynamic description. Experimental probes are essential to understand the details of this non-equilibrium physics. These probes must be sensitive to microscopic details of the medium and must probe the whole QGP evolution. This makes jets and photons, the focus of this study, ideal candidates.

The collision kernel $\mathcal{C}(\mathbf{p}_\perp)$ is an essential part of the physics of jets and photons in both equilibrium and non-equilibrium QGP. This kernel gives the rate for a jet parton or a medium quasiparticle to receive transverse momentum kicks $\mathbf{p}_\perp$ from soft gluons in the medium. In this thesis, we evaluated the collision kernel microscopically in a non-equilibrium medium using quantum field theory. Specifically, we considered a medium where hard quasiparticle are anisotropically distributed in momentum space and evaluated in detail the density of soft gluons emitted by the quasiparticles by deriving the statistical rr correlator. To our knowledge, this is the first microscopic calculation of the collision kernel for momentum broadening in a non-equilibrium medium.

Evaluating the collision kernel in a non-equilibrium medium is complicated by so-called gauge instabilities. These instabilities are exponential growth in soft gluon density which seemingly leads to divergences in the collision kernel. We analyzed these divergences in detail and showed that they arise when one incorrectly assumes a static medium. For this purpose, we evaluated the time dependence of the retarded and statistical correlators for soft gluons in an unstable plasma.

In heavy-ion collisions, instabilities are important very early on, but classical-statistical simulations suggest that they rapidly become saturated [161, 162]. We proposed a phenomenological prescription in which ultrasoft modes, including instability modes, are subtracted, leaving momentum broadening through fluctuating modes. These fluctuating modes are sourced at every instance by quasiparticles and do not depend on the detailed history of the medium. This phenomenological prescription is justified during the kinetic theory and hydrodynamic stage of collisions, given that the ultrasoft modes are not too heavily occupied.

Using this prescription, our results show that the rate of momentum broadening is reduced in an anisotropic medium because of increased medium screening. This is especially true for low-momentum transverse kicks. The reduction is particularly pronounced for the momentum broadening of quasiparticles but also present for jet parton broadening. This leads to an anisotropic collision kernel which is qualitatively different from the equilibrium kernel or the ansatz that has been employed in non-equilibrium kinetic theory simulations. In addition to increased screening, the anisotropic collision kernel has a dependence on the momentum direction of the parton, as well as on the direction of a transverse kick.

Momentum broadening is the central ingredient for a host of different processes in the quark-gluon plasma. Specifically, the collinear emission of a gluon or a photon is made possible when an on-shell emitter is brough slightly off shell by transverse momentum kicks. Thus our anisotropic collision kernel can be used to evaluate consistently processes in a non-equilibrium plasma that include medium-induced gluon radiation in a jet, one-to-two processes in kinetic theory and the collinear emission of photons, which accounts for around half of the emitted photons in the QGP phase.

In this thesis, we focused on the collinear emission of photons in an anisotropic plasma. We devised a numerical procedure to solve the non-equilibrium integral equation for photon emission including the LPM effect. This procedure can easily be extended to gluon emission. Solving the integral equation, we showed that the rate of photon production in the direction of an anisotropy vector is reduced, both due less momentum broadening and due to the redistribution of hard particles in the medium.

Our work raises two outstanding questions. Firstly, it is important to understand how our results affect the phenomenology of heavy-ion collisions. This is especially relevant for the kinetic theory stage and the early hydrodynamic stage of heavy-ion collisions where there is large anisotropy along the beam axis. This could introduce additional rapidity dependence in observables such as photon yield and jet substructure. Furthermore, one of the two main processes in kinetic theory simulations is the bremsstrahlung of gluon quasiparticles. Including the effect of anisotropic momentum broadening on gluon bremsstrahlung will affect the whole space-time evolution of the kinetic theory medium.

An additional phenomenological question is the effect on jets and photons of the sizable deviations from equilibrium during the later hydrodynamic evolution in heavy-ion collisions. The size of these deviations depends on transport coefficients of the plasma. Therefore, one might be able to use jets and photons to study transport coefficients of the plasma. This is a difficult task which requires evaluating shear viscous corrections to photon and gluon production, as well as a detailed phenomenological analysis. Lastly, we note that small collisional systems have large deviations from thermal equilibrium which makes the inclusion of non-equilibrium effects especially important.

The other main question raised by our work is the role of ultrasoft modes in the physics of non-equilibrium QGP. When calculating the rate of momentum broadening, we cut off ultrasoft modes below a certain energy scale. For some parton direction and values of anisotropy there is moderate dependence on the cut, suggesting that our calculation needs to be complemented by a description of ultrasoft modes. This can in principle be achieved by measuring the collision kernel as defined in terms of Wilson lines [170] in classical-statistical simulations. However, the assumption of classical field dynamics breaks down in the regime we are interested in where the occupation density of hard modes is $\mathcal{O}(1)$. Therefore, we believe it is important to have a more rigorous description of the deep infrared in a non-equilibrium quark-gluon plasma. The development and use of functional methods in non-equilibrium QCD might shed some light on that complicated question.

Part VII

APPENDICES

A

REAL-TIME FORMALISM

In this appendix, we give an overview of the real-time formalism in non-equilibrium quantum field theory. This is also known as the Keldysh-Schwinger or closed-time path formalism. Further details can be found in reviews such as [106, 197, 198].

Any system is determined by an initial density matrix ρ. As an example, in vacuum the initial density matrix is $\rho = |0\rangle\langle 0|$ and in thermal equilibrium it is

$$\rho = e^{-\beta H}/Z \tag{A.1}$$

where H is the Hamiltonian, $\beta = 1/T$ is the inverse temperature and Z is a normalization factor so that $\mathrm{Tr}\,\rho = 1$. In general, the density matrix can be any operator as long as $\mathrm{Tr}\,\rho = 1$ so that the total probability is one.

We are interested in probing the system by calculating the average of observables at different times in its evolution. A typical observable is

$$\langle \mathcal{O}_2(t_2)\mathcal{O}_1(t_1)\rangle := \mathrm{Tr}\left[\rho\, \mathcal{O}_2(t_2)\mathcal{O}_1(t_1)\right] \tag{A.2}$$

for two operators $\mathcal{O}_1$ and $\mathcal{O}_2$ in the Heisenberg picture, where the trace sums over all possible states of the system. By going from Heisenberg operators $\mathcal{O}(t)$ to time-independent Schrodinger operators $\mathcal{O}$, this can be rewritten as

$$\begin{aligned}
&\mathrm{Tr}\left[\rho\, \mathcal{O}_2(t_2)\mathcal{O}_1(t_1)\right] \\
=&\mathrm{Tr}\left[\rho\, U(t_0,t_2)\, \mathcal{O}_2\, U(t_2,t_0)\, U(t_0,t_1)\, \mathcal{O}_1\, U(t_1,t_0)\right] \\
=&\mathrm{Tr}\left[\rho\, U(t_0,t_2)\, \mathcal{O}_2\, U(t_2,t_f)\, U(t_f,t_1)\, \mathcal{O}_1\, U(t_1,t_0)\right] .
\end{aligned} \tag{A.3}$$

Here $U(t_1, t_2)$ is the unitary time-evolution operator which satisfies $U(t_1,t_2)U(t_2,t_3) = U(t_1,t_3)$. Furthermore, t_0 is the initial time of the system and t_f is some arbitrarily chosen final time. By inserting a complete set of states, this can be written more explicitly as

$$\begin{aligned}
&\langle \mathcal{O}_2(t_2)\mathcal{O}_1(t_1)\rangle \\
&= \sum_{\phi_1^0}\sum_{\phi_2^0}\sum_{\phi_f} \langle \phi_1^0|\rho|\phi_2^0\rangle\, \langle \phi_2^0|\, U(t_0,t_2)\, \mathcal{O}_2\, U(t_2,t_f)\, |\phi_f\rangle\, \langle \phi_f| U(t_f,t_1)\, \mathcal{O}_1\, U(t_1,t_0)|\phi_1^0\rangle
\end{aligned} \tag{A.4}$$

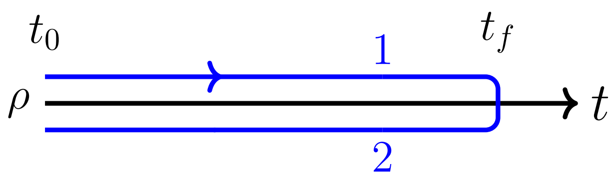

Figure A.1: Closed time path contour. There are two branches, labelled 1 and 2, both of which have one end at the initial density matrix ρ at time t_0 and the other end at the final time t_f.

Eq. (A.4) can be expressed with path integrals. This relies on the well-known procedure in vacuum where the amplitude for initial particles $|\phi_i\rangle$ to scatter into final particles $|\phi_f\rangle$ is expressed as

$$\langle\phi_f|U(t_f,t_0)|\phi_i\rangle = \int \mathcal{D}\phi\, e^{iS[\phi]} \tag{A.5}$$

However, here we have both an element $\langle\phi_1^0|\,U(t_0,t_f)\,|\phi_f\rangle$ going from the initial time to the final time and an element $\langle\phi_f|U(t_f,t_0)|\phi_2^0\rangle$ going from the final time to the initial time. This can be represented as a closed time contour, see Fig. A.1, with the ends of the contour being at the time t_i of the initial condition. The relevant path integral to calculate Eq. (A.4) is therefore

$$Z[J_1,J_2] = \int d\phi_f\, d\phi_1^0\, d\phi_2^0 \int_{\phi_1^0}^{\phi_f} \mathcal{D}\phi_1 \int_{\phi_2^0}^{\phi_f} \mathcal{D}\phi_2\, \langle\phi_1^0|\rho|\phi_2^0\rangle\, e^{iS[\phi_1]-iS[\phi_2]+iJ_1\phi_1-iJ_2\phi_2}. \tag{A.6}$$

Here, we have two path integrals with field ϕ_1 living on branch 1 and field ϕ_2 living on branch 2 on the closed time contour in Fig. A.1. The action S is the same as in vacuum with a relative minus sign for $S[\phi_2]$ since $\langle\phi_f|U(t_f,t_0)|\phi_2^0\rangle = \langle\phi_2^0|U(t_0,t_f)|\phi_f\rangle^\dagger$. We have included currents J_1 and J_2 on each contour. By taking deriviatives with respect to the currents, one can obtain the expectation value of operators $\mathcal{O}_1$ and $\mathcal{O}_2$. The path integral in Eq. (A.6) depends explicitly on the density matrix ρ.

The most important observable to consider are two-point correlators. Because of the closed time contour there are four possible correlators. As an example

$$D_{11}(x,y) := \langle\mathcal{T}_C\phi_1(x)\phi_1(y)\rangle = \langle T\phi(x)\phi(y)\rangle \tag{A.7}$$

where $\mathcal{T}_C$ is time-ordering along the closed time-path contour in Fig. A.1. For two fields living on branch 1 it reduces to the usual time ordering T defined by

$$\langle T\phi(x)\phi(y)\rangle := \theta(x^0-y^0)\langle\phi(x)\phi(y)\rangle + \theta(y^0-x^0)\langle\phi(y)\phi(x)\rangle. \tag{A.8}$$

Similarly,

$$D_{12}(x,y) := \langle \mathcal{T}_{\mathcal{C}}\phi_1(x)\phi_2(y)\rangle = \langle \phi(y)\phi(x)\rangle \tag{A.9}$$

since a field with index 2 always comes after a field with index 1. The other two propagators are

$$D_{21}(x,y) := \langle \mathcal{T}_{\mathcal{C}}\phi_2(x)\phi_1(y)\rangle = \langle \phi(x)\phi(y)\rangle \tag{A.10}$$

and

$$D_{22} := \langle \mathcal{T}_{\mathcal{C}}\phi_1(x)\phi_2(y)\rangle = \langle \bar{T}\phi(x)\phi(y)\rangle \tag{A.11}$$

where $\bar{T}$ orders backwards in time

$$\langle \bar{T}\phi(x)\phi(y)\rangle := \theta(y^0 - x^0)\langle \phi(x)\phi(y)\rangle + \theta(x^0 - y^0)\langle \phi(y)\phi(x)\rangle. \tag{A.12}$$

These propagators depend on both the action S as well as the initial density matrix $\langle \phi_2^0|\rho|\phi_1^0\rangle$.

A redefinition of the fields gives more intuitive two-point correlators. We define

$$\phi_r = \frac{\phi_1 + \phi_2}{2} \tag{A.13}$$

and

$$\phi_a = \phi_1 - \phi_2. \tag{A.14}$$

The propagator

$$\begin{aligned} D_{aa}(x,y) &:= \langle \mathcal{T}_{\mathcal{C}}\phi_a(x)\phi_a(y)\rangle \\ &= D_{11}(x,y) - D_{12}(x,y) - D_{21}(x,y) + D_{22}(x,y) \end{aligned} \tag{A.15}$$

vanishes identically. This can be seen by an explicit calculation, as well as by noting that if, say, $x^0 > y^0$ then $\langle \mathcal{T}_{\mathcal{C}}\phi_1(x)\phi_a(y)\rangle = \langle \mathcal{T}_{\mathcal{C}}\phi_2(x)\phi_a(y)\rangle$ as changing the index does not change the time ordering and thus $D_{aa} = \langle \mathcal{T}_{\mathcal{C}}\phi_1(x)\phi_a(y)\rangle - \langle \mathcal{T}_{\mathcal{C}}\phi_2(x)\phi_a(y)\rangle$ vanishes. Furthermore,

$$D_{ra}(x,y) = D_{\text{ret}}(x,y) := \theta(x^0 - y^0)\langle [\phi(x), \phi(y)]\rangle \tag{A.16}$$

and

$$D_{ar}(x,y) = D_{\text{adv}}(x,y) := -\theta(y^0 - x^0)\langle[\phi(x), \phi(y)]\rangle. \tag{A.17}$$

These correlators are also known as the retarded correlator D_{ret} and the advanced correlator D_{adv}. They describe propagation of modes in the system. The retarded correlator gives propagation forward in time, while the advanced propagator gives propagation backwards in time. The final correlator is

$$D_{rr}(x,y) = \frac{1}{2}\langle\{\phi(x), \phi(y)\}\rangle. \tag{A.18}$$

It is non-vanishing for classical fields and describes the density of modes in the system. As $D_{aa} = 0$ and $D_{\text{ret}}(x,y) = D_{\text{adv}}(y,x)$, there are only two independent propagators in the system, which can be chosen to be D_{rr} and D_{ret}.

In thermal equilibrium, the two independent propagators, D_{ret} and D_{rr}, can be related by the Kubo-Martin-Schwinger (KMS) relation. This is seen by noting that

$$\begin{aligned} D_{12}(t + i\beta, \mathbf{x}) &= \frac{1}{Z}\text{Tr}[e^{-\beta H}\phi(0)\phi(t+i\beta, \mathbf{x})] \\ &= \frac{1}{Z}\text{Tr}[e^{-\beta H}\phi(0)e^{-\beta H}\phi(t,\mathbf{x})e^{\beta H}] \\ &= \frac{1}{Z}\text{Tr}[e^{-\beta H}\phi(t,\mathbf{x})\phi(0)] \\ &= D_{21}(t,\mathbf{x}) \end{aligned} \tag{A.19}$$

where we used the cyclic property of the trace and the fact that the Hamiltonian H generates time translation. Fourier transforming gives that

$$D_{12}(P) = e^{-\beta p^0} D_{21}(P). \tag{A.20}$$

which implies

$$D_{rr}(P) = \left(\frac{1}{2} + f_B(p^0)\right)[D_{\text{ret}}(P) - D_{\text{adv}}(P)] \tag{A.21}$$

where

$$f_B(p^0) = \frac{1}{e^{\beta p^0} - 1} \tag{A.22}$$

is the equilibrium Bose-Einstein distribution. The interpretation is clear. The density of a propagating mode with energy p^0 is $\frac{1}{2} + f_B(p^0)$ where f_B is the thermal density and $\frac{1}{2}$ is the density of fluctuations in vacuum. Out-of-equilibrium the two propagators, D_{rr} and $D_{\rm ret}$ are independent of each other.

In perturbative calculations, we need the Feynman rules generated by the path integral in Eq. (A.6). They are given in terms of bare propagators and vertices. For concreteness, we assume an action

$$S[\phi] = \int d^x \left(\frac{1}{2}\partial_\mu \phi \partial^\mu \phi + \frac{\lambda}{3!}\phi^3 \right) \tag{A.23}$$

The bare retarded propagator in momentum space can easily be shown to be

$$D^0_{\rm ret}(P) = \frac{i}{P^2 + i\epsilon p^0} \tag{A.24}$$

[106] where ϵ is an infinitesimal quantity and the term $i\epsilon p^0$ guarantees that all poles are in the lower-half complex plane. This is the same as in vacuum. Similarly,

$$D^0_{\rm adv}(P) = \frac{i}{P^2 - i\epsilon p^0}. \tag{A.25}$$

In thermal equilibrium, the KMS relation in Eq. (A.21) can be used to show that

$$D^0_{rr}(P) = \left(\frac{1}{2} + f_B(p) \right) 2\pi\delta(P^2). \tag{A.26}$$

Out-of-equilibrium, the rr correlator depends on the details of the initial density matrix ρ. In [199] it was shown that one can always choose a density matrix so that the rr propagator is

$$D^0_{rr}(P) = \left(\frac{1}{2} + f(\mathbf{p}) \right) 2\pi\delta(P^2) \tag{A.27}$$

for some momentum distribution $f(\mathbf{p})$. This is the parametrization we will use in this thesis. We note that out of equilibrium, all resummed propagators in momentum space are Wigner transforms

$$D(P,X) = \int d^4(x-y)\, e^{iP\cdot(x-y)} D(x,y) \tag{A.28}$$

which depend on position in the system $X = (x+y)/2$.

The vertices in the Feynman rules come from the action in Eq. (A.6). In the 12 basis there are two separate vertices, one only with indices 1 and the other only with indices 2, see Fig. A.2. Since

$$\frac{\lambda}{3!}\left(\phi_1^3 - \phi_2^3\right) = \frac{\phi_r^2}{2!}\phi_a + \frac{1}{4}\frac{\phi_a^3}{3!}, \tag{A.29}$$

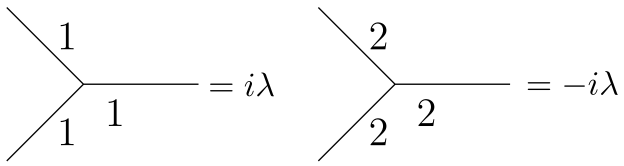

Figure A.2: Vertices in the 12 basis of the real-time formalism.

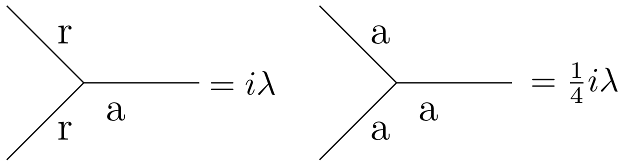

Figure A.3: Vertices in the *ra* basis of the real-time formalism.

in the *ra* basis, there is an odd number of *a* labels at each vertex, see Fig. A.3.

A main task of this thesis is to calculated resummed propagators using perturbation theory. We will derive general equations for these propagators. In general, a resummed propagator D can be written as

$$D(x,y) = D^0(x,y) + \int d^4z \int d^4w \; D^0(x,z)\Pi(z,w)D(w,y) \tag{A.30}$$

where D^0 is a bare propagator and Π is a self-energy. We write this schematically as

$$D = D^0 + D^0\,\Pi\, D. \tag{A.31}$$

We need to find the right ordering of *ra* indices in these equations. Since $D_{aa} = D^0_{aa} = 0$, we immediately see that

$$0 = D^0_{ar}\Pi_{rr}D_{ra} \tag{A.32}$$

which gives that $\Pi_{rr} = 0$. Here we define Π_{cd}, with $c, d \in \{r, a\}$ as in Fig. **??**. Using this, it is easy to show that the resummed retarded propagator is

$$D_{ra} = D^0_{ra} + D^0_{ra}\Pi_{ar}D_{ra} \tag{A.33}$$

For instance, other potential terms like $D^0_{rr}\Pi_{rr}D_{ra}$ or $D^0_{ra}\Pi_{aa}D_{aa}$ vanish identically. Eq. (A.33) is reproduced in Eq. (2.41) in the main text, where we call $\Pi_{ar} = \Pi_{\text{ret}}$. Similarly,

$$D_{ar} = D^0_{ar} + D^0_{ar}\Pi_{ra}D_{ar}. \tag{A.34}$$

The resummed equation for D_{rr} is slightly more complicated. It is fairly easy to see that all terms are of the form

$$D_{rr} = D_{ra}\Pi_{aa}D_{ar} + D^0_{rr} + D^0_{rr}\Pi_{ra}D_{ar} + D_{ra}\Pi_{ar}D^0_{rr} + D_{ra}\Pi_{ar}D^0_{rr}\Pi_{ra}D_{ar}. \tag{A.35}$$

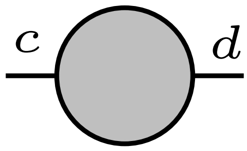

Figure A.4: Definition of Π_{cd} where c, d are either a or r indices.

The first term on the right hand side contains Π_{aa}, while all the other terms contain the bare propagator D^0_{rr} exactly once. Using that

$$\Pi_{ra} D_{ar} = \underrightarrow{\left(D^0_{ar}\right)^{-1}} D_{ar} - 1 \tag{A.36}$$

where the arrow tells us in which direction the operator $\left(D^0_{ar}\right)^{-1}$ acts, this can be written more succinctly as

$$D_{rr} = D_{ra} \Pi_{aa} D_{ar} + D_{ra} \underleftarrow{\left(D^0_{ra}\right)^{-1}} D^0_{rr} \underrightarrow{\left(D^0_{ar}\right)^{-1}} D_{ar} \tag{A.37}$$

This equation for rr propagator has a simple interpretation. The first term describes the occupation density of particles that were sourced after the system was initialized. The rate of sourcing a pair of excitations is Π_{aa} and then these two excitations evolve in time with the retarded and advanced propagators. This is the term reproduced in Eq. (2.37). The second term describes particles that were already present in the initial condition. That term contains the bare propagator D^0_{rr} which solely depends on the initial density matrix, as well as retarded and advanced correlators for evolution in time.

B

EVALUATION OF INTEGRALS FOR CORRELATORS IN AN UNSTABLE PLASMA

In this section we show some details in the derivation of the retarded and rr correlators in an unstable plasma with initial time $t_0 = 0$. The end results for the retarded correlator is given by Eq. (3.18) and the one for the rr correlator is given by Eqs. (3.37) and Eq. (3.46).

To complete the derivation of the retarded correlator we need to shows that the expression in Eq. (3.13), i.e.

$$\int \frac{dk_1}{2\pi} \int \frac{dk_2}{2\pi} \int_\alpha \frac{dk_3}{2\pi}\, D^0_{\text{ret}}(k_1)\, \Pi_{\text{ret}}(k_2)\, D_{\text{ret}}(k_3)\; f(k_1,k_2,k_3) \tag{B.1}$$

with

$$\begin{aligned} f(k_1,k_2,k_3) = &-\frac{e^{-ik_1(x-y)}}{(k_1-k_2)(k_1-k_3)} \\ &-\frac{e^{-ik_2(x-y)}}{(k_2-k_1)(k_2-k_3)} - \frac{e^{-ik_3(x-y)}}{(k_3-k_1)(k_3-k_2)}. \end{aligned} \tag{B.2}$$

and

$$\begin{aligned} &f(k_1,k_2,k_3) \longrightarrow \\ &\frac{1}{8} \sum_{\substack{\{k_1\to k_1+i\epsilon_1\}\\ \{k_1\to k_1-i\epsilon_1\}}} \sum_{\substack{\{k_2\to k_2+i\epsilon_2\}\\ \{k_2\to k_2-i\epsilon_2\}}} \sum_{\substack{\{k_3\to k_3+i\epsilon_3\}\\ \{k_3\to k_3-i\epsilon_3\}}} f(k_1,k_2,k_3). \end{aligned} \tag{B.3}$$

is identical to the expression in Eq. (3.16), i.e.

$$\int_\alpha \frac{dk}{2\pi}\, e^{-ik(x-y)}\, D^0_{\text{ret}}(k)\, \Pi_{\text{ret}}(k)\, D_{\text{ret}}(k) \tag{B.4}$$

The contribution of the first term in Eq. (B.2) to Eq. (B.1) is

$$
\begin{aligned}
&-\int \frac{dk_1}{2\pi} \int \frac{dk_2}{2\pi} \int_\alpha \frac{dk_3}{2\pi}\, D^0_{\text{ret}}(k_1)\, \Pi_{\text{ret}}(k_2)\, D_{\text{ret}}(k_3)\, e^{-ik_1(x-y)} \\
&\times \frac{1}{8}\Bigg[\left(\frac{i}{k_1 - k_2 + i\epsilon_1 - i\epsilon_2} + \frac{i}{k_1 - k_2 + i\epsilon_1 + i\epsilon_2} \right) \\
&\qquad \times \left(\frac{i}{k_1 - k_3 + i\epsilon_1 - i\epsilon_3} + \frac{i}{k_1 - k_3 + i\epsilon_1 + i\epsilon_3} \right) \\
&\quad + \left(\frac{i}{k_1 - k_2 - i\epsilon_1 - i\epsilon_2} + \frac{i}{k_1 - k_2 - i\epsilon_1 + i\epsilon_2} \right) \\
&\qquad \times \left(\frac{i}{k_1 - k_3 - i\epsilon_1 - i\epsilon_3} + \frac{i}{k_1 - k_3 - i\epsilon_1 + i\epsilon_3} \right) \Bigg]
\end{aligned}
\tag{B.5}
$$

The k_3 integral can be evaluated by closing the integration contour in the upper half complex plane, see Fig. B.1a. Since all the poles of D_{ret} are below the contour α, only poles in the square bracket will contribute. The k_1 integral can be evaluated similarly. This gives

$$
\begin{aligned}
&\int_{\mathbb{R}} \frac{dk_1}{2\pi}\, G^0_{\text{ret}}(k_1)\, \Pi_{\text{ret}}(k_1)\, G_{\text{ret}}(k_1)\, e^{-ik_1(x-y)} \\
&\times \frac{1}{8}\left[\theta(\epsilon_2 - \epsilon_1)\theta(\epsilon_3 - \epsilon_1) + \big(1 + \theta(\epsilon_1 - \epsilon_2)\big)\big(1 + \theta(\epsilon_1 - \epsilon_3)\big)\right].
\end{aligned}
\tag{B.6}
$$

A similar calculation shows that substituting the second term of Eq. (B.2) into Eq. (B.1) gives

$$
\begin{aligned}
&\int_{\mathbb{R}} \frac{dk}{2\pi}\, G^0_{\text{ret}}(k)\, \Pi_{\text{ret}}(k)\, G_{\text{ret}}(k)\, e^{-ik(x-y)} \\
&\times \frac{1}{8}\left[\theta(\epsilon_1 - \epsilon_2)\theta(\epsilon_3 - \epsilon_2) + \big(1 + \theta(\epsilon_2 - \epsilon_1)\big)\big(1 + \theta(\epsilon_2 - \epsilon_3)\big)\right].
\end{aligned}
\tag{B.7}
$$

We finally evaluate the integral in Eq. (B.1) with the third term of Eq. (B.2) substituted for $f(k_1, k_2, k_3)$. This is slightly more difficult and requires us to write the integration contour for k_3 as $\int_\alpha = \int_{\mathbb{R}} + \sum_i \int_{\gamma_i}$ where γ_i go around poles in the upper half plane, see Fig. B.1b. The part where k_3 is integrated over the real line can be evaluated as before, giving

$$
\begin{aligned}
&\int_{\mathbb{R}} \frac{dk_3}{2\pi}\, G^0_{\text{ret}}(k_3)\, \Pi_{\text{ret}}(k_3)\, G_{\text{ret}}(k_3)\, e^{-ik_3(x-y)} \\
&\times \frac{1}{8}\left[(1 + \theta(\epsilon_3 - \epsilon_1))\,(1 + \theta(\epsilon_3 - \epsilon_2)) + \theta(\epsilon_1 - \epsilon_3)\theta(\epsilon_2 - \epsilon_3)\right].
\end{aligned}
\tag{B.8}
$$

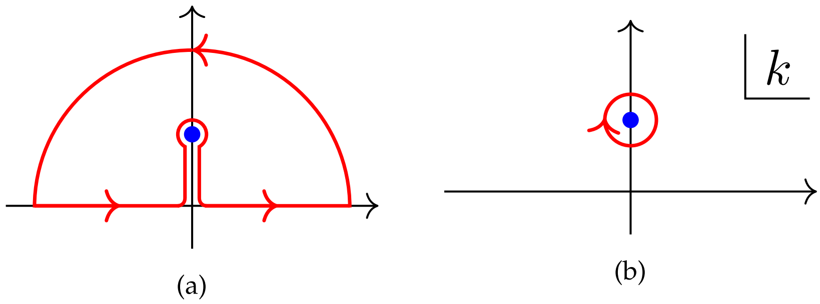

Figure B.1: Different contours used for the evaluation of the retarded function in an unstable system.

Finally, in the part where k_3 is integrated over γ_i, the k_1 and k_2 integrals can be done explicitly without using the principal value prescription since k_3 is always in the upper half plane. This gives

$$\sum_i \int_{\gamma_i} \frac{dk}{2\pi}\, G^0_{\text{ret}}(k)\, \Pi_{\text{ret}}(k)\, G_{\text{ret}}(k) e^{-ik(x-y)}. \tag{B.9}$$

By adding up Eqs. (B.6), (B.7), (B.8) and (B.9), we finally get the value of Eq. (B.1), namely

$$\int_\alpha \frac{dk}{2\pi}\, G^0_{\text{ret}}(k)\, \Pi_{\text{ret}}(k)\, G_{\text{ret}}(k) e^{-ik(x-y)} \tag{B.10}$$

which is what we wanted to show.

We now turn to the evaluation of the rr correlator, i.e. Eq. (3.37), in full detail. As discussed in the main text, averaging over oscillations allows us to drop terms e^{-iax} where $\operatorname{Re} a \sim g\Lambda$, and waiting until correlation with the initial condition has decayed allows us to drop terms with e^{-iax} with $\operatorname{Im} a < 0$, $\operatorname{Re} a \sim g\Lambda$. Together, these approximations allow us to drop all terms of the form e^{-iax} where $a \sim g\Lambda$ is a pole in the fluctuating part of the retarded function $\widehat{G}_{\text{ret}}$.

Using the separation of G_{ret} and G_{adv} into a fluctuating part and an exponentially growing instability part, see Eqs. (3.35) and (3.36), we get that Eq. (3.33) is

$$\begin{aligned}
G_{rr}(x,y) = &\int_{\alpha} \frac{dk_1}{2\pi} \int \frac{dk_2}{2\pi} \int_{\tilde{\alpha}} \frac{dk_3}{2\pi} \left[e^{-ik_2(x-y)} - e^{-ik_1x}e^{ik_2y} - e^{-ik_2x}e^{ik_3y} + e^{-ik_1x}e^{ik_3y}\right] \\
&\times \frac{1}{8}\Bigg[\left(\frac{1}{k_2-k_1+i\epsilon_2-i\epsilon_1} + \frac{1}{k_2-k_1+i\epsilon_2+i\epsilon_1}\right)\left(\frac{1}{k_2-k_3+i\epsilon_2-i\epsilon_3} + \frac{1}{k_2-k_3+i\epsilon_2+i\epsilon_3}\right) \\
&+ \left(\frac{1}{k_2-k_1-i\epsilon_2-i\epsilon_1} + \frac{1}{k_2-k_1-i\epsilon_2+i\epsilon_1}\right)\left(\frac{1}{k_2-k_3-i\epsilon_2-i\epsilon_3} + \frac{1}{k_2-k_3-i\epsilon_2+i\epsilon_3}\right)\Bigg] \\
&\times \left(\widehat{G}_{\text{ret}}(k_1) + \sum_i \frac{A_i}{k_1-a_i}\right) \Pi_{aa}(k_2) \left(\widehat{G}_{\text{adv}}(k_3) + \sum_j \frac{A_j^*}{k_3-a_j^*}\right).
\end{aligned} \tag{B.11}$$

We have furthermore substituted principal values as in Eq. (3.15). This is justified as there are no poles when $k_1 = k_2$ or $k_2 = k_3$ due to the exponentials.

We start by evaluating Eq. (B.11) for the fluctuating contribution from $\widehat{G}_{\text{ret}}(k_1)\,\Pi_{aa}(k_2)\,\widehat{G}_{\text{adv}}(k_3)$. This must be done term by term for the exponentials in the square bracket. The first exponential term can be evaluated exactly by continuing the k_1 integral to the upper half complex plane and the k_3 integral to the lower half complex plane, avoiding all poles of $\widehat{G}_{\text{ret}}$ and $\widehat{G}_{\text{adv}}$. This gives

$$\begin{aligned}
&\int \frac{dk_2}{2\pi}\, \widehat{G}_{\text{ret}}(k_2)\,\Pi_{aa}(k_2)\,\widehat{G}_{\text{adv}}(k_3)\;\; e^{-ik_2(x-y)} \\
&\times \frac{1}{8}\left[\theta(\epsilon_3-\epsilon_2)\left(1+\theta(\epsilon_2-\epsilon_1)\right) + \theta(\epsilon_1-\epsilon_2)\left(1+\theta(\epsilon_2-\epsilon_3)\right)\right].
\end{aligned} \tag{B.12}$$

The term with the second exponential in Eq. (B.11) is trickier to evaluate, requiring the use of our controlled approximations. We first continue the k_3 integral to the lower half plane, giving

$$\begin{aligned}
&-i\int_{\alpha} \frac{dk_1}{2\pi} \int \frac{dk_2}{2\pi}\, \widehat{G}_{\text{ret}}(k_1)\,\Pi_{aa}(k_2)\,\widehat{G}_{\text{adv}}(k_2)\;\; e^{-ik_1x}\,e^{ik_2y} \\
&\times \frac{1}{8}\Bigg[\theta(\epsilon_3-\epsilon_2)\left(\frac{1}{k_2-k_1+i\epsilon_2-i\epsilon_1} + \frac{1}{k_2-k_1+i\epsilon_2+i\epsilon_1}\right) \\
&+ \left(1+\theta(\epsilon_2-\epsilon_3)\right) \\
&\times \left(\frac{1}{k_2-k_1-i\epsilon_2-i\epsilon_1} + \frac{1}{k_2-k_1-i\epsilon_2+i\epsilon_1}\right)\Bigg].
\end{aligned} \tag{B.13}$$

When evaluating the k_1 integral we must continue the integration contour to the lower half plane because of the exponential $e^{-ik_1 x}$. Our approximations allow us to omit poles coming from $\widehat{G}_{\text{ret}}$. Thus the only contributions are the poles $k_1 = k_2$ leaving

$$\begin{aligned}&\int \frac{dk_2}{2\pi}\, \widehat{G}_{\text{ret}}(k_2)\, \Pi_{aa}(k_2)\, \widehat{G}_{\text{adv}}(k_2)\;\; e^{-ik_2(x-y)} \\ &\times \frac{1}{8}\Big[\theta(\epsilon_1-\epsilon_2)\theta(\epsilon_3-\epsilon_2) \\ &\qquad\qquad + \big(1+\theta(\epsilon_2-\epsilon_3)\big)\big(1+\theta(\epsilon_2-\epsilon_1)\big)\Big].\end{aligned} \tag{B.14}$$

Using the same set of approximations, we get that the term with the third exponential in Eq. (B.11) gives

$$\begin{aligned}&\int \frac{dk_2}{2\pi}\, \widehat{G}_{\text{ret}}(k_2)\, \Pi_{aa}(k_2)\, \widehat{G}_{\text{adv}}(k_2)\;\; e^{-ik_2(x-y)} \\ &\times \frac{1}{8}\Big[\theta(\epsilon_1-\epsilon_2)\theta(\epsilon_3-\epsilon_2) \\ &\qquad\qquad + \big(1+\theta(\epsilon_2-\epsilon_1)\big)\big(1+\theta(\epsilon_2-\epsilon_3)\big)\Big]\end{aligned} \tag{B.15}$$

and the fourth exponential gives

$$\begin{aligned}&\int \frac{dk_2}{2\pi}\, \widehat{G}_{\text{ret}}(k_2)\, \Pi_{aa}(k_2)\, \widehat{G}_{\text{adv}}(k_2)\;\; e^{-ik_2(x-y)} \\ &\times \frac{1}{8}\Big[\theta(\epsilon_1-\epsilon_2)\big(1+\theta(\epsilon_2-\epsilon_3)\big) \\ &\qquad\qquad + \theta(\epsilon_3-\epsilon_2)\big(1+\theta(\epsilon_2-\epsilon_1)\big)\Big].\end{aligned} \tag{B.16}$$

Adding up Eqs. (B.12), (B.14), (B.15) and (B.16), we finally get the contribution of the fluctuating functions, $\widehat{G}_{\text{ret}}$ and $\widehat{G}_{\text{adv}}$, to Eq. (B.11). It is

$$\approx \int \frac{dk}{2\pi}\, \widehat{G}_{\text{ret}}(k)\, \Pi_{aa}(k)\, \widehat{G}_{\text{adv}}(k)\;\; e^{-ik(x-y)}. \tag{B.17}$$

This strikingly simple form has no mention of the initial time. It is expressed as a Fourier transform of $\widehat{G}_{\text{ret}}\,\Pi_{aa}\,\widehat{G}_{\text{adv}}$ which has the same form as the equilibrium result, even though the functions look different.

We now turn to evaluating the contribution of the instability parts

$$\sum_i \frac{A_i}{k_1 - a_i}\, \Pi_{aa}(k_2) \sum_j \frac{A_j^*}{k_3 - a_j^*} \tag{B.18}$$

to Eq. (B.11). In the same manner as above, the contribution of the first exponential in Eq. (B.11) is

$$\begin{aligned}
&\sum_{i,j} \int \frac{dk_2}{2\pi} \frac{A_i}{k_2 - a_i} \Pi_{aa}(k_2) \frac{A_j^*}{k_2 - a_j^*} \quad e^{-ik_2(x-y)} \\
&\quad \times \frac{1}{8}\Big[\theta(\epsilon_3 - \epsilon_2)\big(1 + \theta(\epsilon_2 - \epsilon_1)\big) \\
&\qquad\qquad + \theta(\epsilon_1 - \epsilon_2)\big(1 + \theta(\epsilon_2 - \epsilon_3)\big)\Big].
\end{aligned} \tag{B.19}$$

When evaluating the contribution of the second exponential, we continue the k_3 integral to the lower half plane giving

$$\begin{aligned}
&-i \sum_{i,j} \int_{\alpha} \frac{dk_1}{2\pi} \int \frac{dk_2}{2\pi} \frac{A_i}{k_1 - a_i} \Pi_{aa}(k_2) \frac{A_j^*}{k_2 - a_j^*} \quad e^{-ik_1 x} e^{ik_2 y} \\
&\quad \times \frac{1}{8}\left[\theta(\epsilon_3 - \epsilon_2)\left(\frac{1}{k_2 - k_1 + i\epsilon_2 - i\epsilon_1} + \frac{1}{k_2 - k_1 + i\epsilon_2 + i\epsilon_1}\right)\right. \\
&\qquad \left.\big(1 + \theta(\epsilon_2 - \epsilon_3)\big)\left(\frac{1}{k_2 - k_1 - i\epsilon_2 - i\epsilon_1} + \frac{1}{k_2 - k_1 - i\epsilon_2 + i\epsilon_1}\right)\right].
\end{aligned} \tag{B.20}$$

The k_1 integral is similarly continued to the lower half plane but now both the poles at $k_1 = k_2$ and at $k_1 = a_i$ contribute. This gives

$$\begin{aligned}
&\sum_{i,j} \int \frac{dk_2}{2\pi} \frac{A_i}{k_2 - a_i} \Pi_{aa}(k_2) \frac{A_j^*}{k_2 - a_j^*} e^{-ik_2(x-y)} \\
&\times \frac{1}{8}\left[\theta(\epsilon_1 - \epsilon_2)\theta(\epsilon_3 - \epsilon_2) + (1 + \theta(\epsilon_2 - \epsilon_3))(1 + \theta(\epsilon_2 - \epsilon_1))\right] \\
&- \frac{1}{2} \sum_{i,j} \int \frac{dk_2}{2\pi} \frac{A_i}{k_2 - a_i} \Pi_{aa}(k_2) \frac{A_j^*}{k_2 - a_j^*} \quad e^{-ia_i x} e^{ik_2 y}
\end{aligned} \tag{B.21}$$

In the same way, the third exponential gives

$$\begin{aligned}
&\sum_{i,j} \int \frac{dk_2}{2\pi} \frac{A_i}{k_2 - a_i} \Pi_{aa}(k_2) \frac{A_j^*}{k_2 - a_j^*} \quad e^{-ik_2(x-y)} \\
&\times \frac{1}{8}\left[\theta(\epsilon_1 - \epsilon_2)\theta(\epsilon_3 - \epsilon_2) + (1 + \theta(\epsilon_2 - \epsilon_1))(1 + \theta(\epsilon_2 - \epsilon_3))\right] \\
&- \frac{1}{2} \sum_{i,j} \int \frac{dk_2}{2\pi} \frac{A_i}{k_2 - a_i} \Pi_{aa}(k_2) \frac{A_j^*}{k_2 - a_j^*} \quad e^{-ik_2 x} e^{ia_j^* y}
\end{aligned} \tag{B.22}$$

and the fourth exponential gives

$$
\begin{aligned}
&\sum_{i,j}\int \frac{dk_2}{2\pi}\,\frac{A_i}{k_2-a_i}\,\Pi_{aa}(k_2)\,\frac{A_j^*}{k_2-a_j^*}\quad e^{-ik_2(x-y)}\\
&\qquad\times\frac{1}{8}\Big[\theta(\epsilon_1-\epsilon_2)(1+\theta(\epsilon_2-\epsilon_3))\\
&\qquad\qquad+\theta(\epsilon_3-\epsilon_2)(1+\theta(\epsilon_2-\epsilon_1))\Big]\\
&-\frac{1}{2}\sum_{i,j}\int \frac{dk_2}{2\pi}\,\frac{A_i}{k_2-a_i}\,\Pi_{aa}(k_2)\,\frac{A_j^*}{k_2-a_j^*}\quad e^{-ik_2x}\,e^{ia_j^*y}\\
&-\frac{1}{2}\sum_{i,j}\int \frac{dk_2}{2\pi}\,\frac{A_i}{k_2-a_i}\,\Pi_{aa}(k_2)\,\frac{A_j^*}{k_2-a_j^*}\quad e^{-ia_ix}\,e^{ik_2y}\\
&+\sum_{i,j}\int \frac{dk_2}{2\pi}\,\frac{A_i}{k_2-a_i}\,\Pi_{aa}(k_2)\,\frac{A_j^*}{k_2-a_j^*}\quad e^{-ia_ix}\,e^{ia_j^*y}.
\end{aligned}
\tag{B.23}
$$

Summing up Eqs. (B.19), (B.21), (B.22) and (B.23) finally gives

$$
\begin{aligned}
&\sum_{i,j}\int \frac{dk}{2\pi}\,\frac{A_i}{k-a_i}\,\Pi_{aa}(k)\,\frac{A_j^*}{k-a_j^*}\\
&\times\left(e^{-ikx}-e^{-ia_ix}\right)\left(e^{iky}-e^{ia_j^*y}\right)
\end{aligned}
\tag{B.24}
$$

for the contribution of instabilities to Eq. (B.11).

In addition to the fluctuating contributions and instability contributions to Eq. (B.11) that have been evaluated, there are cross terms between fluctuations and instabilities such as

$$
\sum_i \frac{A_i}{k_1-a_i}\,\Pi_{aa}(k_2)\,\widehat{G}_{\mathrm{adv}}(k_3).
\tag{B.25}
$$

They can be evaluated using the same methods. The final result is shown in Eq. (3.37)

C

NUMERICAL EVALUATION OF INTEGRALS FOR COLLINEAR SPLITTING

In this appendix we explain in more detail how the integrals in Eqs. (5.25), (5.26) and (5.27) are evaluated numerically. These integrals are needed to evaluate the rate of photon production through bremsstrahlung in an anisotropic medium.

To evaluate Eq. (5.25) it is more convenient to write it as

$$(\hat{\mathcal{C}})_{\chi\omega} := \int \frac{d^2p_\perp}{(2\pi)^2} \int \frac{d^2q_\perp}{(2\pi)^2} \left[\tilde{\phi}_\chi(\mathbf{p}_\perp) - \tilde{\phi}_\chi(\mathbf{p}_\perp - \mathbf{q}_\perp)\right] \mathcal{C}(\mathbf{q}_\perp)\phi_\omega(\mathbf{p}_\perp). \tag{C.1}$$

since ϕ decays faster than $\tilde{\phi}$ at high $\mathbf{p}_\perp$. We write

$$\mathbf{p}_\perp = \gamma \frac{1-z}{1+z} (\cos\alpha, \sin\alpha) \tag{C.2}$$

$$\mathbf{q}_\perp = \gamma \frac{1-w}{1+w} (\cos\beta, \sin\beta) \tag{C.3}$$

where z, w are in the interval $[-1, 1]$ and α and β are angular variables. We see that e.g. $\mathbf{p}_\perp \to 0$ when $z \to 1$ and $\mathbf{p}_\perp \to \infty$ when $z \to -1$. The parameter $\gamma = 4.0$ is a number chosen to make convergence as fast as possible.

We need to write the integral in Eq. (C.1) in terms of the variables z, w, α, β. When doing so a problem arises. In Eq. (C.1) we have $\tilde{\phi}(\mathbf{p}_\perp - \mathbf{q}_\perp)$ which should be expressed in terms of radial and angular functions. This requries writing $\mathbf{p}_\perp - \mathbf{q}_\perp$ in radial coordinates as

$$\mathbf{p}_\perp - \mathbf{q}_\perp = \gamma \frac{1-u}{1+u} (\cos\delta, \sin\delta) \tag{C.4}$$

where u and δ should be expressed in terms of the integration variables z, w, α, β. However, δ is undefined as $\mathbf{p}_\perp \to \mathbf{q}_\perp$ so that the integrand becomes oscillatory in that limit, making numerical integration in terms of our variables difficult.

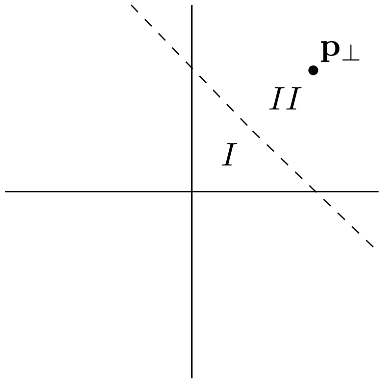

Figure C.1: Integration region for $\mathbf{q}_\perp$. The boundary between regions *I* and *II* is midway between the point $\mathbf{0}$ and $\mathbf{p}_\perp$.

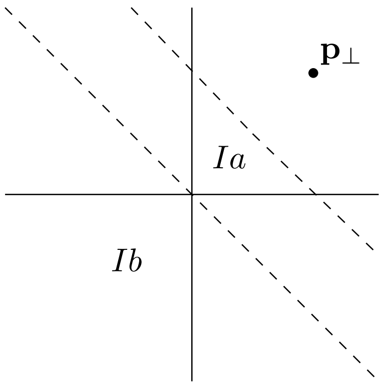

Figure C.2: Integration region for $\mathbf{q}_\perp$. Region *I* is divided into regions *Ia* and *Ib*.

We solve this problem by dividing the integration region of $\mathbf{q}_\perp$ into two regions, see Fig. C.1. The difficult limit occurs in region II. By mapping region II onto region I by a change of variables $\mathbf{q}_\perp \to \mathbf{p}_\perp - \mathbf{q}_\perp$ the oscillatory behaviour can be avoided. Thus we write

$$\begin{aligned}(\hat{\mathcal{C}})_{(nk)(ml)} = &\int \frac{d^2 p_\perp}{(2\pi)^2} \int_I \frac{d^2 q_\perp}{(2\pi)^2} \left[\tilde{\phi}_{nk}(\mathbf{p}_\perp) - \tilde{\phi}_{nk}(\mathbf{p}_\perp - \mathbf{q}_\perp)\right] \mathcal{C}(\mathbf{q}_\perp)\phi_{ml}(\mathbf{p}_\perp) \\ &+ \int \frac{d^2 p_\perp}{(2\pi)^2} \int_I \frac{d^2 q_\perp}{(2\pi)^2} \left[\tilde{\phi}_{nk}(\mathbf{p}_\perp) - \tilde{\phi}_{nk}(\mathbf{q}_\perp\right] \mathcal{C}(\mathbf{q}_\perp - \mathbf{p}_\perp)\phi_{ml}(\mathbf{p}_\perp)\end{aligned} \tag{C.5}$$

where both terms are only integrated over region I. The boundaries of region I can be seen by dividing it up into two regions, see Fig. C.2. Region Ia is determined by $\beta \in \left[\alpha + \frac{\pi}{2}, \alpha + \frac{3\pi}{2}\right]$, while region Ib is determined by $\beta \in \left[\alpha - \frac{\pi}{2}, \alpha + \frac{\pi}{2}\right]$ and $q_\perp \in \left[0, \frac{p_\perp}{2\cos(\alpha-\beta)}\right]$. This last condition is equivalent to $w \in [w_{\min}(\alpha, \beta, z), 1.0]$ where

$$w_{\min}(\alpha, \beta, z) = \frac{(2\cos(\alpha-\beta) - 1) + (2\cos(\alpha-\beta)+1)z}{(2\cos(\alpha-\beta) + 1) + (2\cos(\alpha-\beta)-1)z} \tag{C.6}$$

Using all of this, the first term in Eq. (C.5) can be written as

$$\begin{aligned}\hat{\mathcal{C}}^{(I)}_{(nk)(ml)} = \frac{\gamma^4}{4\pi^4} \int_{-1}^{1} dz \int_0^{2\pi} d\alpha \left(\int_{\alpha+\pi/2}^{\alpha+3\pi/2} \int_{-1}^{1} dw + \int_{\alpha-\pi/2}^{\alpha+\pi/2} \int_{w_{\min}(\alpha,\beta,z)}^{1} dw \right) \\ \times (1-z)(1+z)(1+w) P_m(z) B_l(\alpha) \overline{\mathcal{C}}(w, \beta) \\ \times \frac{1}{1-w} \left[(1+z)^2 P_n(z) B_k(\alpha) - (1+u)^2 P_n(u) B_k(\delta)\right].\end{aligned} \tag{C.7}$$

and the second term as

$$\begin{aligned}\hat{\mathcal{C}}^{(II)}_{(nk)(ml)} = \frac{\gamma^4}{4\pi^4} \int_{-1}^{1} dz \int_0^{2\pi} d\alpha \left(\int_{\alpha+\pi/2}^{\alpha+3\pi/2} \int_{-1}^{1} dw + \int_{\alpha-\pi/2}^{\alpha+\pi/2} \int_{w_{\min}(\alpha,\beta,z)}^{1} dw \right) \\ \times (1+z)(1+u) \left(\frac{1+u}{1+w}\right)^3 P_m(z) B_l(\alpha) \overline{\mathcal{C}}(w, \beta) \\ \times \frac{(1-z)(1-w)}{(1-u)^2} \left[(1+z)^2 P_n(z) B_k(\alpha) - (1+w)^2 P_n(w) B_k(\beta)\right]\end{aligned} \tag{C.8}$$

Here we have defined

$$\overline{\mathcal{C}}(w, \beta) = \frac{(1-w)^2}{(1+w)^4} \mathcal{C}(w, \beta) \tag{C.9}$$

to factor out behaviour in the limits $w \to 1$ and $w \to -1$.

A few numerical issues remain when evaluating Eqs. (C.7) and (C.8). In Eq. (C.7) there seems to be a divergence in the last line as $w \to 1$, i.e. as $\mathbf{q}_\perp \to 1$. However, in this limit

$|\mathbf{p}_\perp - \mathbf{q}_\perp| \to p_\perp$ so that $u \to z$ and $\delta \to \alpha$ and the square bracket vanishes. Thus the last line becomes the ratio of two nearly vanishing numbers in the limit $w \to 1$. This needs to be rewritten for numerical purposes. As an example, we can write

$$u = z + (1-w)A \tag{C.10}$$

which allows for more accurate evaluation when $u \to z$. Noting that

$$u = \frac{1 - |\mathbf{p}_\perp - \mathbf{q}_\perp|/\gamma}{1 + |\mathbf{p}_\perp - \mathbf{q}_\perp|/\gamma} \tag{C.11}$$

where

$$|\mathbf{p}_\perp - \mathbf{q}_\perp|/\gamma = \sqrt{\left(\frac{1-z}{1+z}\right)^2 + \left(\frac{1-w}{1+w}\right)^2 - 2\frac{1-z}{1+z}\frac{1-w}{1+w}\cos(\alpha-\beta)}, \tag{C.12}$$

it is easy to check that

$$A = \frac{2(1-z)(1+w)\cos(\alpha-\beta) - (1-w)(1+z)}{(1-z)(1+w)+\Omega}\,\frac{(1+z)^2}{(1+z)(1+w)+\Omega} \tag{C.13}$$

and

$$\Omega = \sqrt{(1-z)^2(1+w)^2 + (1-w)^2(1+z)^2 - 2(1-z)(1-w)(1+z)(1+w)\cos(\alpha-\beta)}. \tag{C.14}$$

A similar expression can be found for the difference between δ and α.

In Eq. (C.8) there are furthermore two factors that might seemingly lead to divergences. Firstly, there is the limit $u \to 1$ corresponding to $\mathbf{p}_\perp \to \mathbf{q}_\perp$, or in other words $z \to w$ and $\alpha \to \beta$. This limit is not in our integration region and does not cause any problems. Secondly, there is the limit $w \to -1$, i.e. $q_\perp \to \infty$. In this case, we expect $|\mathbf{p}_\perp - \mathbf{q}_\perp| \to \infty$ so that $u \to -1$ at the same time, meaning that $(1+u)/(1+w)$ is finite. For numerical evaluation, it is convenient to write

$$\frac{1+u}{1+w} = \frac{2(1+z)}{(1+z)(1+w)+\Omega} \tag{C.15}$$

with Ω in Eq. (C.14).

We now turn to the other coefficients in matrix equation. We can write Eq. (5.26) as

$$(\delta E)_{(nk)(ml)} = \frac{k}{2p^z(p^z+k)}\frac{\gamma^2}{2\pi^2}\int_{-1}^{1} dz \int_0^{2\pi} d\alpha\; (1-z)(1+z)\left(\gamma^2(1-z)^2 + m_\infty^2(1+z)^2\right)$$
$$\times P_n(z)B_k(\alpha)P_m(z)B_l(\alpha)$$

(C.16)

Similarly, a long derivation gives that Eq. (C.1) is

$$\begin{aligned}\eta_{y\ (nk)} = \frac{4p^z(p^z+k)}{k}\frac{\gamma^3}{4\pi^4}\int_{-1}^{1}dz\int_{-1}^{1}dw\int_0^{2\pi}d\alpha\int_0^{2\pi}d\beta(1-z)(1+z)(1+w) \\ \times P_n(z)\,B_k(\alpha)\,\overline{C}(w,\beta)\,\chi_y(z,w,\alpha,\beta)\end{aligned} \tag{C.17}$$

where

$$\chi_y(z,w,\alpha,\beta) = \chi_{1y}/\chi_{2y} \tag{C.18}$$

with

$$\begin{aligned}\chi_{1y}(z,w,\alpha,\beta) = &\sin\alpha(1-z)\left[2(1-z)(1+w)\cos(\alpha-\beta)+(1-w)(1+z)\right] \\ &-\sin\beta\left[(1-z)^2(1+w)+m_\infty^2/\gamma^2(1+w)(1+z)^2\right]\end{aligned} \tag{C.19}$$

and

$$\begin{aligned}\chi_{2y}(z,w,\alpha,\beta) = &\left[(1-z)^2+m_\infty^2/\gamma^2(1+z)^2\right] \\ \times &\Bigg[(1-z)^2(1+w)^2+(1-w)^2(1+z)^2+2(1-z)(1+z)(1-w)(1+w)\cos(\alpha-\beta) \\ &+(1+z)^2(1+w)^2m_\infty^2\Bigg]\end{aligned} \tag{C.20}$$

Furthermore,

$$\begin{aligned}\eta_{x\ (nk)} = \frac{4p^z(p^z+k)}{k}\frac{\gamma^3}{4\pi^4}\int_{-1}^{1}dz\int_{-1}^{1}dw\int_0^{2\pi}d\alpha\int_0^{2\pi}d\beta(1-z)(1+z)(1+w) \\ \times P_n(z)\,B_k(\alpha)\,\overline{C}(w,\beta)\,\chi_x(z,w,\alpha,\beta)\end{aligned} \tag{C.21}$$

where χ_x has the same expression as χ_y except that $\sin\alpha \to \cos\alpha$, $\sin\beta \to \cos\beta$, while $\cos(\alpha-\beta)$ stays the same.

BIBLIOGRAPHY

[1] Sigtryggur Hauksson, Sangyong Jeon, and Charles Gale. "Probes of the quark-gluon plasma and plasma instabilities." In: *Phys. Rev. C* 103 (2021), p. 064904. DOI: 10.1103/PhysRevC.103.064904. arXiv: 2012.03640 [hep-ph].

[2] Sigtryggur Hauksson, Sangyong Jeon, and Charles Gale. "The momentum broadening of energetic partons in an anisotropic plasma." In: (Sept. 2021). arXiv: 2109.04575 [hep-ph].

[3] P. Bicudo. "QCD confinement and chiral crossovers, two critical points?" In: *PoS* FACESQCD (2010), p. 015. DOI: 10.22323/1.117.0015. arXiv: 1102.5531 [hep-lat].

[4] R. Abbott et al. "Observation of Gravitational Waves from Two Neutron Star–Black Hole Coalescences." In: *Astrophys. J. Lett.* 915.1 (2021), p. L5. DOI: 10.3847/2041-8213/ac082e. arXiv: 2106.15163 [astro-ph.HE].

[5] Xiaofeng Luo, Shusu Shi, Nu Xu, and Yifei Zhang. "A Study of the Properties of the QCD Phase Diagram in High-Energy Nuclear Collisions." In: *Particles* 3.2 (2020), pp. 278–307. DOI: 10.3390/particles3020022. arXiv: 2004.00789 [nucl-ex].

[6] Wit Busza, Krishna Rajagopal, and Wilke van der Schee. "Heavy Ion Collisions: The Big Picture, and the Big Questions." In: *Ann. Rev. Nucl. Part. Sci.* 68 (2018), pp. 339–376. DOI: 10.1146/annurev-nucl-101917-020852. arXiv: 1802.04801 [hep-ph].

[7] Chun Shen, Ulrich W Heinz, Jean-Francois Paquet, and Charles Gale. "Thermal photons as a quark-gluon plasma thermometer reexamined." In: *Phys. Rev. C* 89.4 (2014), p. 044910. DOI: 10.1103/PhysRevC.89.044910. arXiv: 1308.2440 [nucl-th].

[8] P Soding and G Wolf. "Experimental Evidence on QCD." In: *Annual Review of Nuclear and Particle Science* 31.1 (1981), pp. 231–293. DOI: 10.1146/annurev.ns.31.120181.001311. eprint: https://doi.org/10.1146/annurev.ns.31.120181.001311. URL: https://doi.org/10.1146/annurev.ns.31.120181.001311.

[9] S. R. Beane, E. Chang, S. D. Cohen, William Detmold, H. W. Lin, T. C. Luu, K. Orginos, A. Parreno, M. J. Savage, and A. Walker-Loud. "Light Nuclei and Hypernuclei from Quantum Chromodynamics in the Limit of SU(3) Flavor Symmetry." In: *Phys. Rev. D* 87.3 (2013), p. 034506. DOI: 10.1103/PhysRevD.87.034506. arXiv: 1206.5219 [hep-lat].

[10] Michael E. Peskin and Daniel V. Schroeder. *An Introduction to quantum field theory*. Reading, USA: Addison-Wesley, 1995. ISBN: 978-0-201-50397-5.

[11] David J. Gross and Frank Wilczek. "Ultraviolet Behavior of Non-Abelian Gauge Theories." In: *Phys. Rev. Lett.* 30 (26 1973), pp. 1343–1346. DOI: 10.1103/PhysRevLett.30.1343. URL: https://link.aps.org/doi/10.1103/PhysRevLett.30.1343.

[12] H. David Politzer. "Reliable Perturbative Results for Strong Interactions?" In: *Phys. Rev. Lett.* 30 (26 1973), pp. 1346–1349. DOI: 10.1103/PhysRevLett.30.1346. URL: https://link.aps.org/doi/10.1103/PhysRevLett.30.1346.

[13] A.D. Linde. "Infrared problem in the thermodynamics of the Yang-Mills gas." In: *Physics Letters B* 96.3 (1980), pp. 289–292. ISSN: 0370-2693. DOI: https://doi.org/10.1016/0370-2693(80)90769-8. URL: https://www.sciencedirect.com/science/article/pii/0370269380907698.

[14] Alexander M. Polyakov. "Thermal Properties of Gauge Fields and Quark Liberation." In: *Phys. Lett. B* 72 (1978), pp. 477–480. DOI: 10.1016/0370-2693(78)90737-2.

[15] Rajan Gupta. "Introduction to lattice QCD: Course." In: *Les Houches Summer School in Theoretical Physics, Session 68: Probing the Standard Model of Particle Interactions*. July 1997. arXiv: hep-lat/9807028.

[16] E. Laermann and O. Philipsen. "LATTICE QCD AT FINITE TEMPERATURE." In: *Annual Review of Nuclear and Particle Science* 53.1 (2003), pp. 163–198. DOI: 10.1146/annurev.nucl.53.041002.110609.

[17] J. I. Kapusta and Charles Gale. *Finite-temperature field theory: Principles and applications*. Cambridge Monographs on Mathematical Physics. Cambridge University Press, 2011. ISBN: 978-0-521-17322-3, 978-0-521-82082-0, 978-0-511-22280-1. DOI: 10.1017/CBO9780511535130.

[18] A. Bazavov et al. "Equation of state in (2+1)-flavor QCD." In: *Phys. Rev. D* 90 (2014), p. 094503. arXiv: 1407.6387 [hep-lat].

[19] Volodymyr Vovchenko. "Hadron resonance gas with van der Waals interactions." In: *Int. J. Mod. Phys. E* 29.05 (2020), p. 2040002. DOI: 10.1142/S0218301320400029. arXiv: 2004.06331 [nucl-th].

[20] Guy D. Moore. "Shear viscosity in QCD and why it's hard to calculate." In: *Criticality in QCD and the Hadron Resonance Gas*. Oct. 2020. arXiv: 2010.15704 [hep-ph].

[21] Harvey B. Meyer. "Transport Properties of the Quark-Gluon Plasma: A Lattice QCD Perspective." In: *Eur. Phys. J. A* 47 (2011), p. 86. DOI: 10.1140/epja/i2011-11086-3. arXiv: 1104.3708 [hep-lat].

[22] Arthur M. Poskanzer and S. A. Voloshin. "Methods for analyzing anisotropic flow in relativistic nuclear collisions." In: *Phys. Rev. C* 58 (1998), pp. 1671–1678. DOI: 10.1103/PhysRevC.58.1671. arXiv: nucl-ex/9805001.

[23] Sangyong Jeon and Ulrich Heinz. "Introduction to Hydrodynamics." In: *Int. J. Mod. Phys. E* 24.10 (2015), p. 1530010. DOI: 10.1142/S0218301315300106. arXiv: 1503.03931 [hep-ph].

[24] Jean-Yves Ollitrault. "Relativistic hydrodynamics for heavy-ion collisions." In: *Eur. J. Phys.* 29 (2008), pp. 275–302. DOI: 10.1088/0143-0807/29/2/010. arXiv: 0708.2433 [nucl-th].

[25] L. D. Landau. "On the multiparticle production in high-energy collisions." In: *Izv. Akad. Nauk Ser. Fiz.* 17 (1953), pp. 51–64.

[26] Bjoern Schenke, Sangyong Jeon, and Charles Gale. "(3+1)D hydrodynamic simulation of relativistic heavy-ion collisions." In: *Phys. Rev. C* 82 (2010), p. 014903. DOI: 10.1103/PhysRevC.82.014903. arXiv: 1004.1408 [hep-ph].

[27] Bjorn Schenke, Sangyong Jeon, and Charles Gale. "Elliptic and triangular flow in event-by-event (3+1)D viscous hydrodynamics." In: *Phys. Rev. Lett.* 106 (2011), p. 042301. DOI: 10.1103/PhysRevLett.106.042301. arXiv: 1009.3244 [hep-ph].

[28] Pavel Kovtun. "First-order relativistic hydrodynamics is stable." In: *JHEP* 10 (2019), p. 034. DOI: 10.1007/JHEP10(2019)034. arXiv: 1907.08191 [hep-th].

[29] G. Policastro, Dan T. Son, and Andrei O. Starinets. "The Shear viscosity of strongly coupled N=4 supersymmetric Yang-Mills plasma." In: *Phys. Rev. Lett.* 87 (2001), p. 081601. DOI: 10.1103/PhysRevLett.87.081601. arXiv: hep-th/0104066.

[30] D. Everett et al. "Phenomenological constraints on the transport properties of QCD matter with data-driven model averaging." In: *Phys. Rev. Lett.* 126.24 (2021), p. 242301. DOI: 10.1103/PhysRevLett.126.242301. arXiv: 2010.03928 [hep-ph].

[31] Paul Romatschke and Ulrike Romatschke. "Viscosity Information from Relativistic Nuclear Collisions: How Perfect is the Fluid Observed at RHIC?" In: *Phys. Rev. Lett.* 99 (2007), p. 172301. DOI: 10.1103/PhysRevLett.99.172301. arXiv: 0706.1522 [nucl-th].

[32] S. A. Bass et al. "Microscopic models for ultrarelativistic heavy ion collisions." In: *Prog. Part. Nucl. Phys.* 41 (1998), pp. 255–369. DOI: 10.1016/S0146-6410(98)00058-1. arXiv: nucl-th/9803035.

[33] J. Weil et al. "Particle production and equilibrium properties within a new hadron transport approach for heavy-ion collisions." In: *Phys. Rev. C* 94.5 (2016), p. 054905. DOI: 10.1103/PhysRevC.94.054905. arXiv: 1606.06642 [nucl-th].

[34] Fred Cooper and Graham Frye. "Comment on the Single Particle Distribution in the Hydrodynamic and Statistical Thermodynamic Models of Multiparticle Production." In: *Phys. Rev. D* 10 (1974), p. 186. DOI: 10.1103/PhysRevD.10.186.

[35] Michael L. Miller, Klaus Reygers, Stephen J. Sanders, and Peter Steinberg. "Glauber modeling in high energy nuclear collisions." In: *Ann. Rev. Nucl. Part. Sci.* 57 (2007), pp. 205–243. DOI: 10.1146/annurev.nucl.57.090506.123020. arXiv: nucl-ex/0701025.

[36] F. Gelis. "Color Glass Condensate and Glasma." In: *Int. J. Mod. Phys. A* 28 (2013), p. 1330001. DOI: 10.1142/S0217751X13300019. arXiv: 1211.3327 [hep-ph].

[37] Francois Gelis, Edmond Iancu, Jamal Jalilian-Marian, and Raju Venugopalan. "The Color Glass Condensate." In: *Ann. Rev. Nucl. Part. Sci.* 60 (2010), pp. 463–489. DOI: 10.1146/annurev.nucl.010909.083629. arXiv: 1002.0333 [hep-ph].

[38] Chun Shen and Ulrich Heinz. "The road to precision: Extraction of the specific shear viscosity of the quark-gluon plasma." In: *Nucl. Phys. News* 25.2 (2015), pp. 6–11. DOI: 10.1080/10619127.2015.1006502. arXiv: 1507.01558 [nucl-th].

[39] Larry D. McLerran and Raju Venugopalan. "Computing quark and gluon distribution functions for very large nuclei." In: *Phys. Rev. D* 49 (1994), pp. 2233–2241. DOI: 10.1103/PhysRevD.49.2233. arXiv: hep-ph/9309289.

[40] Larry D. McLerran and Raju Venugopalan. "Gluon distribution functions for very large nuclei at small transverse momentum." In: *Phys. Rev. D* 49 (1994), pp. 3352–3355. DOI: 10.1103/PhysRevD.49.3352. arXiv: hep-ph/9311205.

[41] J. Bartels, Krzysztof J. Golec-Biernat, and H. Kowalski. "A modification of the saturation model: DGLAP evolution." In: *Phys. Rev. D* 66 (2002), p. 014001. DOI: 10.1103/PhysRevD.66.014001. arXiv: hep-ph/0203258.

[42] Henri Kowalski and Derek Teaney. "An Impact parameter dipole saturation model." In: *Phys. Rev. D* 68 (2003), p. 114005. DOI: 10.1103/PhysRevD.68.114005. arXiv: hep-ph/0304189.

[43] Alex Kovner, Larry D. McLerran, and Heribert Weigert. "Gluon production from nonAbelian Weizsacker-Williams fields in nucleus-nucleus collisions." In: *Phys. Rev. D* 52 (1995), pp. 6231–6237. DOI: 10.1103/PhysRevD.52.6231. arXiv: hep-ph/9502289.

[44] Alex Kovner, Larry D. McLerran, and Heribert Weigert. "Gluon production at high transverse momentum in the McLerran-Venugopalan model of nuclear structure functions." In: *Phys. Rev. D* 52 (1995), pp. 3809–3814. DOI: 10.1103/PhysRevD.52.3809. arXiv: hep-ph/9505320.

[45] T. Lappi. "Wilson line correlator in the MV model: Relating the glasma to deep inelastic scattering." In: *Eur. Phys. J. C* 55 (2008), pp. 285–292. DOI: 10.1140/epjc/s10052-008-0588-4. arXiv: 0711.3039 [hep-ph].

[46] Alex Krasnitz and Raju Venugopalan. "Nonperturbative computation of gluon minijet production in nuclear collisions at very high-energies." In: *Nucl. Phys. B* 557 (1999), p. 237. DOI: 10.1016/S0550-3213(99)00366-1. arXiv: hep-ph/9809433.

[47] Paul Romatschke and Raju Venugopalan. "The Unstable Glasma." In: *Phys. Rev. D* 74 (2006), p. 045011. DOI: 10.1103/PhysRevD.74.045011. arXiv: hep-ph/0605045.

[48] Bjoern Schenke, Prithwish Tribedy, and Raju Venugopalan. "Fluctuating Glasma initial conditions and flow in heavy ion collisions." In: *Phys. Rev. Lett.* 108 (2012), p. 252301. DOI: 10.1103/PhysRevLett.108.252301. arXiv: 1202.6646 [nucl-th].

[49] Bjoern Schenke, Prithwish Tribedy, and Raju Venugopalan. "Event-by-event gluon multiplicity, energy density, and eccentricities in ultrarelativistic heavy-ion collisions." In: *Phys. Rev. C* 86 (2012), p. 034908. DOI: 10.1103/PhysRevC.86.034908. arXiv: 1206.6805 [hep-ph].

[50] Bjoern Schenke and Soeren Schlichting. "3D glasma initial state for relativistic heavy ion collisions." In: *Phys. Rev. C* 94.4 (2016), p. 044907. DOI: 10.1103/PhysRevC.94.044907. arXiv: 1605.07158 [hep-ph].

[51] Scott McDonald, Sangyong Jeon, and Charles Gale. "Exploring Longitudinal Observables with 3+1D IP-Glasma." In: *Nucl. Phys. A* 1005 (2021). Ed. by Feng Liu, Enke Wang, Xin-Nian Wang, Nu Xu, and Ben-Wei Zhang, p. 121771. DOI: 10.1016/j.nuclphysa.2020.121771. arXiv: 2001.08636 [nucl-th].

[52] Aleksi Kurkela, Aleksas Mazeliauskas, Jean-François Paquet, Sören Schlichting, and Derek Teaney. "Effective kinetic description of event-by-event pre-equilibrium dynamics in high-energy heavy-ion collisions." In: *Phys. Rev. C* 99.3 (2019), p. 034910. DOI: 10.1103/PhysRevC.99.034910. arXiv: 1805.00961 [hep-ph].

[53] Aleksi Kurkela, Aleksas Mazeliauskas, Jean-François Paquet, Sören Schlichting, and Derek Teaney. "Matching the Nonequilibrium Initial Stage of Heavy Ion Collisions to Hydrodynamics with QCD Kinetic Theory." In: *Phys. Rev. Lett.* 122.12 (2019), p. 122302. DOI: 10.1103/PhysRevLett.122.122302. arXiv: 1805.01604 [hep-ph].

[54] Gabor David. "Direct real photons in relativistic heavy ion collisions." In: *Rept. Prog. Phys.* 83.4 (2020), p. 046301. DOI: 10.1088/1361-6633/ab6f57. arXiv: 1907.08893 [nucl-ex].

[55] Charles Gale. "Photon Production in Hot and Dense Strongly Interacting Matter." In: *Landolt-Bornstein* 23 (2010). Ed. by R. Stock, p. 445. DOI: 10.1007/978-3-642-01539-7_15. arXiv: 0904.2184 [hep-ph].

[56] Jessica Churchill, Li Yan, Sangyong Jeon, and Charles Gale. "Emission of electromagnetic radiation from the early stages of relativistic heavy-ion collisions." In: *Phys. Rev. C* 103.2 (2021), p. 024904. DOI: 10.1103/PhysRevC.103.024904. arXiv: 2008.02902 [hep-ph].

[57] Jean-François Paquet, Chun Shen, Gabriel S. Denicol, Matthew Luzum, Björn Schenke, Sangyong Jeon, and Charles Gale. "Production of photons in relativistic heavy-ion collisions." In: *Phys. Rev. C* 93.4 (2016), p. 044906. DOI: 10.1103/PhysRevC.93.044906. arXiv: 1509.06738 [hep-ph].

[58] R. Keith Ellis, W. James Stirling, and B. R. Webber. *QCD and collider physics*. Vol. 8. Cambridge University Press, Feb. 2011. ISBN: 978-0-511-82328-2, 978-0-521-54589-1.

[59] Serguei Chatrchyan et al. "Modification of Jet Shapes in PbPb Collisions at $\sqrt{s_{NN}} = 2.76$ TeV." In: *Phys. Lett. B* 730 (2014), pp. 243–263. DOI: 10.1016/j.physletb.2014.01.042. arXiv: 1310.0878 [nucl-ex].

[60] Morad Aaboud et al. "Measurement of jet fragmentation in Pb+Pb and pp collisions at $\sqrt{s_{NN}} = 5.02$ TeV with the ATLAS detector." In: *Phys. Rev. C* 98.2 (2018), p. 024908. DOI: 10.1103/PhysRevC.98.024908. arXiv: 1805.05424 [nucl-ex].

[61] Serguei Chatrchyan et al. "Study of high-pT charged particle suppression in PbPb compared to pp collisions at $\sqrt{s_{NN}} = 2.76$ TeV." In: *Eur. Phys. J. C* 72 (2012), p. 1945. DOI: 10.1140/epjc/s10052-012-1945-x. arXiv: 1202.2554 [nucl-ex].

[62] Chanwook Park, Sangyong Jeon, and Charles Gale. "Jet modification with medium recoil in quark-gluon plasma." In: *Nucl. Phys. A* 982 (2019). Ed. by Federico Antinori, Andrea Dainese, Paolo Giubellino, Vincenzo Greco, Maria Paola Lombardo,

and Enrico Scomparin, pp. 643–646. DOI: 10.1016/j.nuclphysa.2018.10.057. arXiv: 1807.06550 [nucl-th].

[63] Eric Braaten and Robert D. Pisarski. "Soft Amplitudes in Hot Gauge Theories: A General Analysis." In: *Nucl. Phys. B* 337 (1990), pp. 569–634. DOI: 10.1016/0550-3213(90)90508-B.

[64] Eric Braaten and Robert D. Pisarski. "Deducing Hard Thermal Loops From Ward Identities." In: *Nucl. Phys. B* 339 (1990), pp. 310–324. DOI: 10.1016/0550-3213(90)90351-D.

[65] Eric Braaten and Robert D. Pisarski. "Simple effective Lagrangian for hard thermal loops." In: *Phys. Rev. D* 45.6 (1992), R1827. DOI: 10.1103/PhysRevD.45.R1827.

[66] R. Baier, H. Nakkagawa, A. Niegawa, and K. Redlich. "Production rate of hard thermal photons and screening of quark mass singularity." In: *Z. Phys. C* 53 (1992), pp. 433–438. DOI: 10.1007/BF01625902.

[67] Joseph I. Kapusta, P. Lichard, and D. Seibert. "High-energy photons from quark - gluon plasma versus hot hadronic gas." In: *Phys. Rev. D* 44 (1991). [Erratum: Phys.Rev.D 47, 4171 (1993)], pp. 2774–2788. DOI: 10.1103/PhysRevD.47.4171.

[68] P. Aurenche, F. Gelis, R. Kobes, and H. Zaraket. "Bremsstrahlung and photon production in thermal QCD." In: *Phys. Rev. D* 58 (1998), p. 085003. DOI: 10.1103/PhysRevD.58.085003. arXiv: hep-ph/9804224.

[69] P. Aurenche, F. Gelis, R. Kobes, and E. Petitgirard. "Enhanced photon production rate on the light cone." In: *Phys. Rev. D* 54 (1996), pp. 5274–5279. DOI: 10.1103/PhysRevD.54.5274. arXiv: hep-ph/9604398.

[70] P. Aurenche, F. Gelis, R. Kobes, and E. Petitgirard. "Breakdown of the hard thermal loop expansion near the light cone." In: *Z. Phys. C* 75 (1997), pp. 315–332. DOI: 10.1007/s002880050475. arXiv: hep-ph/9609256.

[71] Peter Brockway Arnold, Guy D. Moore, and Laurence G. Yaffe. "Photon and gluon emission in relativistic plasmas." In: *JHEP* 06 (2002), p. 030. DOI: 10.1088/1126-6708/2002/06/030. arXiv: hep-ph/0204343.

[72] Peter Brockway Arnold, Guy D. Moore, and Laurence G. Yaffe. "Photon emission from quark gluon plasma: Complete leading order results." In: *JHEP* 12 (2001), p. 009. DOI: 10.1088/1126-6708/2001/12/009. arXiv: hep-ph/0111107.

[73] Peter Brockway Arnold, Guy D. Moore, and Laurence G. Yaffe. "Photon emission from ultrarelativistic plasmas." In: *JHEP* 11 (2001), p. 057. DOI: 10.1088/1126-6708/2001/11/057. arXiv: hep-ph/0109064.

[74] L. D. Landau and I. Pomeranchuk. "Electron cascade process at very high-energies." In: *Dokl. Akad. Nauk Ser. Fiz.* 92 (1953), pp. 735–738.

[75] L. D. Landau and I. Pomeranchuk. "Limits of applicability of the theory of bremsstrahlung electrons and pair production at high-energies." In: *Dokl. Akad. Nauk Ser. Fiz.* 92 (1953), pp. 535–536.

[76] Arkady B. Migdal. "Quantum kinetic equation for multiple scattering." In: *Dokl. Akad. Nauk SSSR* 105.1 (1955), pp. 77–79.

[77] A. B. Migdal. "Bremsstrahlung and pair production in condensed media at high-energies." In: *Phys. Rev.* 103 (1956), pp. 1811–1820. DOI: 10.1103/PhysRev.103.1811.

[78] Sigtryggur Hauksson, Sangyong Jeon, and Charles Gale. "Photon emission from quark-gluon plasma out of equilibrium." In: *Phys. Rev. C* 97.1 (2018), p. 014901. DOI: 10.1103/PhysRevC.97.014901. arXiv: 1709.03598 [nucl-th].

[79] Peter Brockway Arnold and Caglar Dogan. "QCD Splitting/Joining Functions at Finite Temperature in the Deep LPM Regime." In: *Phys. Rev. D* 78 (2008), p. 065008. DOI: 10.1103/PhysRevD.78.065008. arXiv: 0804.3359 [hep-ph].

[80] Sangyong Jeon and Guy D. Moore. "Energy loss of leading partons in a thermal QCD medium." In: *Phys. Rev. C* 71 (2005), p. 034901. DOI: 10.1103/PhysRevC.71.034901. arXiv: hep-ph/0309332.

[81] Peter Brockway Arnold, Guy D. Moore, and Laurence G. Yaffe. "Effective kinetic theory for high temperature gauge theories." In: *JHEP* 01 (2003), p. 030. DOI: 10.1088/1126-6708/2003/01/030. arXiv: hep-ph/0209353.

[82] P. Aurenche, F. Gelis, and H. Zaraket. “A Simple sum rule for the thermal gluon spectral function and applications.” In: *JHEP* 05 (2002), p. 043. DOI: 10.1088/1126-6708/2002/05/043. arXiv: hep-ph/0204146.

[83] Simon Caron-Huot. “O(g) plasma effects in jet quenching.” In: *Phys. Rev. D* 79 (2009), p. 065039. DOI: 10.1103/PhysRevD.79.065039. arXiv: 0811.1603 [hep-ph].

[84] Bjoern Schenke, Charles Gale, and Sangyong Jeon. “MARTINI: An Event generator for relativistic heavy-ion collisions.” In: *Phys. Rev. C* 80 (2009), p. 054913. DOI: 10.1103/PhysRevC.80.054913. arXiv: 0909.2037 [hep-ph].

[85] Guang-You Qin, Jorg Ruppert, Charles Gale, Sangyong Jeon, Guy D. Moore, and Munshi G. Mustafa. “Radiative and collisional jet energy loss in the quark-gluon plasma at RHIC.” In: *Phys. Rev. Lett.* 100 (2008), p. 072301. DOI: 10.1103/PhysRevLett.100.072301. arXiv: 0710.0605 [hep-ph].

[86] Bjoern Schenke, Charles Gale, and Guang-You Qin. “The Evolving distribution of hard partons traversing a hot strongly interacting plasma.” In: *Phys. Rev. C* 79 (2009), p. 054908. DOI: 10.1103/PhysRevC.79.054908. arXiv: 0901.3498 [hep-ph].

[87] Guang-You Qin, Jorg Ruppert, Simon Turbide, Charles Gale, Chiho Nonaka, and Steffen A. Bass. “Radiative jet energy loss in a three-dimensional hydrodynamical medium and high pT azimuthal asymmetry of pi0 suppression at mid and forward rapidity in Au+Au collisions at sNN=200 GeV.” In: *Phys. Rev. C* 76 (2007), p. 064907. DOI: 10.1103/PhysRevC.76.064907. arXiv: 0705.2575 [hep-ph].

[88] Torbjörn Sjöstrand, Stefan Ask, Jesper R. Christiansen, Richard Corke, Nishita Desai, Philip Ilten, Stephen Mrenna, Stefan Prestel, Christine O. Rasmussen, and Peter Z. Skands. “An introduction to PYTHIA 8.2.” In: *Comput. Phys. Commun.* 191 (2015), pp. 159–177. DOI: 10.1016/j.cpc.2015.01.024. arXiv: 1410.3012 [hep-ph].

[89] Chanwook Park, Chun Shen, Sangyong Jeon, and Charles Gale. “Rapidity-dependent jet energy loss in small systems with finite-size effects and running coupling.” In: *Nucl. Part. Phys. Proc.* 289-290 (2017). Ed. by Guang-You Qin, Xin-Nian Wang, Ya-Ping Wang, Ben-Wei Zhang, and Dai-Cui Zhou, pp. 289–292. DOI: 10.1016/j.nuclphysbps.2017.05.066. arXiv: 1612.06754 [nucl-th].

[90] Clint Young, Bjorn Schenke, Sangyong Jeon, and Charles Gale. "Dijet asymmetry at the energies available at the CERN Large Hadron Collider." In: *Phys. Rev. C* 84 (2011), p. 024907. DOI: 10.1103/PhysRevC.84.024907. arXiv: 1103.5769 [nucl-th].

[91] R. Baier, M. Dirks, K. Redlich, and D. Schiff. "Thermal photon production rate from nonequilibrium quantum field theory." In: *Phys. Rev. D* 56 (1997), pp. 2548–2554. DOI: 10.1103/PhysRevD.56.2548. arXiv: hep-ph/9704262.

[92] Bjoern Schenke and Michael Strickland. "Photon production from an anisotropic quark-gluon plasma." In: *Phys. Rev. D* 76 (2007), p. 025023. DOI: 10.1103/PhysRevD.76.025023. arXiv: hep-ph/0611332.

[93] Chun Shen, Jean-Francois Paquet, Ulrich Heinz, and Charles Gale. "Photon Emission from a Momentum Anisotropic Quark-Gluon Plasma." In: *Phys. Rev. C* 91.1 (2015), p. 014908. DOI: 10.1103/PhysRevC.91.014908. arXiv: 1410.3404 [nucl-th].

[94] Sigtryggur Hauksson, Chun Shen, Sangyong Jeon, and Charles Gale. "Bulk viscous corrections to photon production in the quark–gluon plasma." In: *Nucl. Part. Phys. Proc.* 289-290 (2017). Ed. by Guang-You Qin, Xin-Nian Wang, Ya-Ping Wang, Ben-Wei Zhang, and Dai-Cui Zhou, pp. 169–172. DOI: 10.1016/j.nuclphysbps.2017.05.036. arXiv: 1612.05517 [nucl-th].

[95] Jean-Paul Blaizot and Edmond Iancu. "The Quark gluon plasma: Collective dynamics and hard thermal loops." In: *Phys. Rept.* 359 (2002), pp. 355–528. DOI: 10.1016/S0370-1573(01)00061-8. arXiv: hep-ph/0101103.

[96] V. P. Silin. "On the electronmagnetic properties of a relativistic plasma." In: *Sov. Phys. JETP* 11.5 (1960), pp. 1136–1140.

[97] P. F. Kelly, Q. Liu, C. Lucchesi, and C. Manuel. "Deriving the hard thermal loops of QCD from classical transport theory." In: *Phys. Rev. Lett.* 72 (1994), pp. 3461–3463. DOI: 10.1103/PhysRevLett.72.3461. arXiv: hep-ph/9403403.

[98] Stanislaw Mrowczynski and Markus H. Thoma. "Hard loop approach to anisotropic systems." In: *Phys. Rev. D* 62 (2000), p. 036011. DOI: 10.1103/PhysRevD.62.036011. arXiv: hep-ph/0001164.

[99] Simon Caron-Huot. "Hard thermal loops in the real-time formalism." In: *JHEP* 04 (2009), p. 004. DOI: 10.1088/1126-6708/2009/04/004. arXiv: 0710.5726 [hep-ph].

[100] Stanislaw Mrowczynski, Anton Rebhan, and Michael Strickland. "Hard loop effective action for anisotropic plasmas." In: *Phys. Rev. D* 70 (2004), p. 025004. DOI: 10.1103/PhysRevD.70.025004. arXiv: hep-ph/0403256.

[101] Margaret E. Carrington and Stanislaw Mrowczynski. "Effective Coupling Constant of Plasmons." In: *Phys. Rev. D* 100.5 (2019), p. 056020. DOI: 10.1103/PhysRevD.100.056020. arXiv: 1907.03131 [hep-ph].

[102] Rolf Baier and Yacine Mehtar-Tani. "Jet quenching and broadening: The Transport coefficient q-hat in an anisotropic plasma." In: *Phys. Rev. C* 78 (2008), p. 064906. DOI: 10.1103/PhysRevC.78.064906. arXiv: 0806.0954 [hep-ph].

[103] Paul Romatschke. "Momentum broadening in an anisotropic plasma." In: *Phys. Rev. C* 75 (2007), p. 014901. DOI: 10.1103/PhysRevC.75.014901. arXiv: hep-ph/0607327.

[104] Abhijit Majumder, Berndt Muller, and Stanislaw Mrowczynski. "Momentum Broadening of a Fast Parton in a Perturbative Quark-Gluon Plasma." In: *Phys. Rev. D* 80 (2009), p. 125020. DOI: 10.1103/PhysRevD.80.125020. arXiv: 0903.3683 [hep-ph].

[105] Peter Brockway Arnold and Wei Xiao. "High-energy jet quenching in weakly-coupled quark-gluon plasmas." In: *Phys. Rev. D* 78 (2008), p. 125008. DOI: 10.1103/PhysRevD.78.125008. arXiv: 0810.1026 [hep-ph].

[106] Michel Le Bellac. *Thermal Field Theory*. Cambridge Monographs on Mathematical Physics. Cambridge University Press, Mar. 2011. ISBN: 978-0-511-88506-8, 978-0-521-65477-7. DOI: 10.1017/CBO9780511721700.

[107] Jacopo Ghiglieri and Derek Teaney. "Parton energy loss and momentum broadening at NLO in high temperature QCD plasmas." In: *International Journal of Modern Physics E* 24.11 (2015), p. 1530013. ISSN: 1793-6608. DOI: 10.1142/s0218301315300131. URL: http://dx.doi.org/10.1142/S0218301315300131.

[108] S. Mrowczynski. "Energy loss of a high-energy parton in the quark - gluon plasma." In: *Phys. Lett. B* 269 (1991), pp. 383–388. DOI: 10.1016/0370-2693(91)90188-V.

[109] Markus H. Thoma and Miklos Gyulassy. "Quark Damping and Energy Loss in the High Temperature QCD." In: *Nucl. Phys. B* 351 (1991), pp. 491–506. DOI: 10.1016/S0550-3213(05)80031-8.

[110] Margaret E. Carrington, Katarzyna Deja, and Stanislaw Mrowczynski. "Energy Loss in Unstable Quark-Gluon Plasma." In: *Phys. Rev. C* 92.4 (2015), p. 044914. DOI: 10.1103/PhysRevC.92.044914. arXiv: 1506.09082 [hep-ph].

[111] Ryogo Kubo. "Statistical mechanical theory of irreversible processes. 1. General theory and simple applications in magnetic and conduction problems." In: *J. Phys. Soc. Jap.* 12 (1957), pp. 570–586. DOI: 10.1143/JPSJ.12.570.

[112] Paul C. Martin and Julian S. Schwinger. "Theory of many particle systems. 1." In: *Phys. Rev.* 115 (1959). Ed. by K. A. Milton, pp. 1342–1373. DOI: 10.1103/PhysRev.115.1342.

[113] Marco Panero, Kari Rummukainen, and Andreas Schäfer. "Lattice Study of the Jet Quenching Parameter." In: *Phys. Rev. Lett.* 112.16 (2014), p. 162001. DOI: 10.1103/PhysRevLett.112.162001. arXiv: 1307.5850 [hep-ph].

[114] Guy D. Moore, Soeren Schlichting, Niels Schlusser, and Ismail Soudi. "Non-perturbative determination of collisional broadening and medium induced radiation in QCD plasmas." In: (May 2021). arXiv: 2105.01679 [hep-ph].

[115] Paul Romatschke and Michael Strickland. "Collective modes of an anisotropic quark gluon plasma." In: *Phys. Rev. D* 68 (2003), p. 036004. arXiv: hep-ph/0304092.

[116] Paul Romatschke and Michael Strickland. "Collective modes of an anisotropic quark-gluon plasma II." In: *Phys. Rev. D* 70 (2004), p. 116006. DOI: 10.1103/PhysRevD.70.116006. arXiv: hep-ph/0406188.

[117] Peter Brockway Arnold, Jonathan Lenaghan, and Guy D. Moore. "QCD plasma instabilities and bottom up thermalization." In: *JHEP* 08 (2003), p. 002. DOI: 10.1088/1126-6708/2003/08/002. arXiv: hep-ph/0307325.

[118] Margaret E. Carrington, Katarzyna Deja, and Stanislaw Mrowczynski. "Plasmons in Anisotropic Quark-Gluon Plasma." In: *Phys. Rev. C* 90.3 (2014), p. 034913. DOI: 10.1103/PhysRevC.90.034913. arXiv: 1407.2764 [hep-ph].

[119] Margaret E. Carrington, Bailey M. Forster, and Sofiya Makar. "Collective modes in anisotropic plasmas." In: (July 2021). arXiv: 2107.08229 [hep-ph].

[120] Bjoern Schenke and Michael Strickland. "Fermionic Collective Modes of an Anisotropic Quark-Gluon Plasma." In: *Phys. Rev. D* 74 (2006), p. 065004. DOI: 10.1103/PhysRevD.74.065004. arXiv: hep-ph/0606160.

[121] Babak S. Kasmaei, Mohammad Nopoush, and Michael Strickland. "Quark self-energy in an ellipsoidally anisotropic quark-gluon plasma." In: *Phys. Rev. D* 94.12 (2016), p. 125001. DOI: 10.1103/PhysRevD.94.125001. arXiv: 1608.06018 [hep-ph].

[122] Mohammad Nopoush, Yun Guo, and Michael Strickland. "The static hard-loop gluon propagator to all orders in anisotropy." In: *JHEP* 09 (2017), p. 063. DOI: 10.1007/JHEP09(2017)063. arXiv: 1706.08091 [hep-ph].

[123] Babak S. Kasmaei and Michael Strickland. "Parton self-energies for general momentum-space anisotropy." In: *Phys. Rev. D* 97.5 (2018), p. 054022. DOI: 10.1103/PhysRevD.97.054022. arXiv: 1801.00863 [hep-ph].

[124] Stanislaw Mrowczynski, Bjoern Schenke, and Michael Strickland. "Color instabilities in the quark–gluon plasma." In: *Phys. Rept.* 682 (2017), pp. 1–97. DOI: 10.1016/j.physrep.2017.03.003. arXiv: 1603.08946 [hep-ph].

[125] Stanislaw Mrowczynski. "Stream Instabilities of the Quark - Gluon Plasma." In: *Phys. Lett. B* 214 (1988). [Erratum: Phys.Lett.B 656, 273 (2007)], p. 587. DOI: 10.1016/0370-2693(88)90124-4.

[126] S. Mrowczynski. "Plasma instability at the initial stage of ultrarelativistic heavy ion collisions." In: *Phys. Lett. B* 314 (1993), pp. 118–121. DOI: 10.1016/0370-2693(93)91330-P.

[127] Stanislaw Mrowczynski. "Color filamentation in ultrarelativistic heavy ion collisions." In: *Phys. Lett. B* 393 (1997), pp. 26–30. DOI: 10.1016/S0370-2693(96)01621-8. arXiv: hep-ph/9606442.

[128] Aleksi Kurkela and Guy D. Moore. "Thermalization in Weakly Coupled Non-abelian Plasmas." In: *JHEP* 12 (2011), p. 044. DOI: 10.1007/JHEP12(2011)044. arXiv: 1107.5050 [hep-ph].

[129] Eric Braaten and Markus H. Thoma. "Energy loss of a heavy quark in the quark - gluon plasma." In: *Phys. Rev. D* 44.9 (1991), R2625. DOI: 10.1103/PhysRevD.44.R2625.

[130] Eric Braaten and Markus H. Thoma. "Energy loss of a heavy fermion in a hot plasma." In: *Phys. Rev. D* 44 (1991), pp. 1298–1310. DOI: 10.1103/PhysRevD.44.1298.

[131] Paul Romatschke and Michael Strickland. "Energy loss of a heavy fermion in an anisotropic QED plasma." In: *Phys. Rev. D* 69 (2004), p. 065005. DOI: 10.1103/PhysRevD.69.065005. arXiv: hep-ph/0309093.

[132] Paul Romatschke and Michael Strickland. "Collisional energy loss of a heavy quark in an anisotropic quark-gluon plasma." In: *Phys. Rev. D* 71 (2005), p. 125008. DOI: 10.1103/PhysRevD.71.125008. arXiv: hep-ph/0408275.

[133] Aleksi Kurkela and Urs Achim Wiedemann. "Analytic structure of nonhydrodynamic modes in kinetic theory." In: *Eur. Phys. J. C* 79.9 (2019), p. 776. DOI: 10.1140/epjc/s10052-019-7271-9. arXiv: 1712.04376 [hep-ph].

[134] Ivan Dadić, Dubravko Klabučar, and Domagoj Kuić. "Direct Photons from Hot Quark Matter in Renormalized Finite-Time-Path QED." In: *Particles* 3.4 (2020), pp. 676–692. DOI: 10.3390/particles3040044. arXiv: 2012.00863 [hep-ph].

[135] Adrian Dumitru, Yasushi Nara, Bjoern Schenke, and Michael Strickland. "Jet broadening in unstable non-Abelian plasmas." In: *Phys. Rev. C* 78 (2008), p. 024909. DOI: 10.1103/PhysRevC.78.024909. arXiv: 0710.1223 [hep-ph].

[136] Jürgen Berges, Michal P. Heller, Aleksas Mazeliauskas, and Raju Venugopalan. "QCD thermalization: Ab initio approaches and interdisciplinary connections." In: *Rev. Mod. Phys.* 93.3 (2021), p. 035003. DOI: 10.1103/RevModPhys.93.035003. arXiv: 2005.12299 [hep-th].

[137] Erich S. Weibel. "Spontaneously Growing Transverse Waves in a Plasma Due to an Anisotropic Velocity Distribution." In: *Phys. Rev. Lett.* 2 (3 1959), pp. 83–84. DOI: 10.1103/PhysRevLett.2.83. URL: https://link.aps.org/doi/10.1103/PhysRevLett.2.83.

[138] Anton Rebhan, Paul Romatschke, and Michael Strickland. “Dynamics of quark-gluon-plasma instabilities in discretized hard-loop approximation.” In: *JHEP* 09 (2005), p. 041. DOI: 10.1088/1126-6708/2005/09/041. arXiv: hep-ph/0505261.

[139] Anton Rebhan, Paul Romatschke, and Michael Strickland. “Hard-loop dynamics of non-Abelian plasma instabilities.” In: *Phys. Rev. Lett.* 94 (2005), p. 102303. DOI: 10.1103/PhysRevLett.94.102303. arXiv: hep-ph/0412016.

[140] Peter Brockway Arnold and Jonathan Lenaghan. “The Abelianization of QCD plasma instabilities.” In: *Phys. Rev. D* 70 (2004), p. 114007. DOI: 10.1103/PhysRevD.70.114007. arXiv: hep-ph/0408052.

[141] Peter Brockway Arnold, Guy D. Moore, and Laurence G. Yaffe. “The Fate of non-Abelian plasma instabilities in 3+1 dimensions.” In: *Phys. Rev. D* 72 (2005), p. 054003. DOI: 10.1103/PhysRevD.72.054003. arXiv: hep-ph/0505212.

[142] Peter Brockway Arnold and Guy D. Moore. “The Turbulent spectrum created by non-Abelian plasma instabilities.” In: *Phys. Rev. D* 73 (2006), p. 025013. DOI: 10.1103/PhysRevD.73.025013. arXiv: hep-ph/0509226.

[143] Peter Brockway Arnold and Guy D. Moore. “QCD plasma instabilities: The Non-Abelian cascade.” In: *Phys. Rev. D* 73 (2006), p. 025006. DOI: 10.1103/PhysRevD.73.025006. arXiv: hep-ph/0509206.

[144] Andreas Ipp, Anton Rebhan, and Michael Strickland. “Non-Abelian plasma instabilities: SU(3) vs. SU(2).” In: *Phys. Rev. D* 84 (2011), p. 056003. DOI: 10.1103/PhysRevD.84.056003. arXiv: 1012.0298 [hep-ph].

[145] Dietrich Bodeker and Kari Rummukainen. “Non-abelian plasma instabilities for strong anisotropy.” In: *JHEP* 07 (2007), p. 022. DOI: 10.1088/1126-6708/2007/07/022. arXiv: 0705.0180 [hep-ph].

[146] Peter Brockway Arnold and Guy D. Moore. “Non-Abelian plasma instabilities for extreme anisotropy.” In: *Phys. Rev. D* 76 (2007), p. 045009. DOI: 10.1103/PhysRevD.76.045009. arXiv: 0706.0490 [hep-ph].

[147] Paul Romatschke and Anton Rebhan. “Plasma Instabilities in an Anisotropically Expanding Geometry.” In: *Phys. Rev. Lett.* 97 (2006), p. 252301. DOI: 10.1103/PhysRevLett.97.252301. arXiv: hep-ph/0605064.

[148] Anton Rebhan and Dominik Steineder. “Collective modes and instabilities in anisotropically expanding ultrarelativistic plasmas.” In: *Phys. Rev. D* 81 (2010), p. 085044. DOI: 10.1103/PhysRevD.81.085044. arXiv: 0912.5383 [hep-ph].

[149] Anton Rebhan, Michael Strickland, and Maximilian Attems. “Instabilities of an anisotropically expanding non-Abelian plasma: 1D+3V discretized hard-loop simulations.” In: *Phys. Rev. D* 78 (2008), p. 045023. DOI: 10.1103/PhysRevD.78.045023. arXiv: 0802.1714 [hep-ph].

[150] Maximilian Attems, Anton Rebhan, and Michael Strickland. “Instabilities of an anisotropically expanding non-Abelian plasma: 3D+3V discretized hard-loop simulations.” In: *Phys. Rev. D* 87.2 (2013), p. 025010. DOI: 10.1103/PhysRevD.87.025010. arXiv: 1207.5795 [hep-ph].

[151] S. K. Wong. “Field and particle equations for the classical Yang-Mills field and particles with isotopic spin.” In: *Nuovo Cim. A* 65 (1970), pp. 689–694. DOI: 10.1007/BF02892134.

[152] Guy D. Moore, Chao-ran Hu, and Berndt Muller. “Chern-Simons number diffusion with hard thermal loops.” In: *Phys. Rev. D* 58 (1998), p. 045001. DOI: 10.1103/PhysRevD.58.045001. arXiv: hep-ph/9710436.

[153] Adrian Dumitru and Yasushi Nara. “QCD plasma instabilities and isotropization.” In: *Phys. Lett. B* 621 (2005), pp. 89–95. DOI: 10.1016/j.physletb.2005.06.041. arXiv: hep-ph/0503121.

[154] Adrian Dumitru, Yasushi Nara, and Michael Strickland. “Ultraviolet avalanche in anisotropic non-Abelian plasmas.” In: *Phys. Rev. D* 75 (2007), p. 025016. DOI: 10.1103/PhysRevD.75.025016. arXiv: hep-ph/0604149.

[155] Juergen Berges, Sebastian Scheffler, and Denes Sexty. “Bottom-up isotropization in classical-statistical lattice gauge theory.” In: *Phys. Rev. D* 77 (2008), p. 034504. DOI: 10.1103/PhysRevD.77.034504. arXiv: 0712.3514 [hep-ph].

[156] Juergen Berges, Daniil Gelfand, Sebastian Scheffler, and Denes Sexty. “Simulating plasma instabilities in SU(3) gauge theory.” In: *Phys. Lett. B* 677 (2009), pp. 210–213. DOI: 10.1016/j.physletb.2009.05.008. arXiv: 0812.3859 [hep-ph].

[157] Paul Romatschke and Raju Venugopalan. "Collective non-Abelian instabilities in a melting color glass condensate." In: *Phys. Rev. Lett.* 96 (2006), p. 062302. DOI: 10.1103/PhysRevLett.96.062302. arXiv: hep-ph/0510121.

[158] Kenji Fukushima. "Initial fields and instability in the classical model of the heavy-ion collision." In: *Phys. Rev. C* 76 (2007). [Erratum: Phys.Rev.C 77, 029901 (2007)], p. 021902. DOI: 10.1103/PhysRevC.76.021902. arXiv: 0711.2634 [hep-ph].

[159] Jurgen Berges, Kirill Boguslavski, and Soren Schlichting. "Nonlinear amplification of instabilities with longitudinal expansion." In: *Phys. Rev. D* 85 (2012), p. 076005. DOI: 10.1103/PhysRevD.85.076005. arXiv: 1201.3582 [hep-ph].

[160] Jürgen Berges and Sören Schlichting. "The nonlinear glasma." In: *Phys. Rev. D* 87.1 (2013), p. 014026. DOI: 10.1103/PhysRevD.87.014026. arXiv: 1209.0817 [hep-ph].

[161] J. Berges, K. Boguslavski, S. Schlichting, and R. Venugopalan. "Turbulent thermalization process in heavy-ion collisions at ultrarelativistic energies." In: *Phys. Rev. D* 89.7 (2014), p. 074011. DOI: 10.1103/PhysRevD.89.074011. arXiv: 1303.5650 [hep-ph].

[162] Juergen Berges, Kirill Boguslavski, Soeren Schlichting, and Raju Venugopalan. "Universal attractor in a highly occupied non-Abelian plasma." In: *Phys. Rev. D* 89.11 (2014), p. 114007. DOI: 10.1103/PhysRevD.89.114007. arXiv: 1311.3005 [hep-ph].

[163] J. Berges, K. Boguslavski, S. Schlichting, and R. Venugopalan. "Basin of attraction for turbulent thermalization and the range of validity of classical-statistical simulations." In: *JHEP* 05 (2014), p. 054. DOI: 10.1007/JHEP05(2014)054. arXiv: 1312.5216 [hep-ph].

[164] J. Berges, K. Boguslavski, S. Schlichting, and R. Venugopalan. "Universality far from equilibrium: From superfluid Bose gases to heavy-ion collisions." In: *Phys. Rev. Lett.* 114.6 (2015), p. 061601. DOI: 10.1103/PhysRevLett.114.061601. arXiv: 1408.1670 [hep-ph].

[165] J. Berges, K. Boguslavski, S. Schlichting, and R. Venugopalan. "Nonequilibrium fixed points in longitudinally expanding scalar theories: infrared cascade, Bose

condensation and a challenge for kinetic theory." In: *Phys. Rev. D* 92.9 (2015), p. 096006. DOI: 10.1103/PhysRevD.92.096006. arXiv: 1508.03073 [hep-ph].

[166] K. Boguslavski, A. Kurkela, T. Lappi, and J. Peuron. "Highly occupied gauge theories in 2+1 dimensions: A self-similar attractor." In: *Phys. Rev. D* 100.9 (2019), p. 094022. DOI: 10.1103/PhysRevD.100.094022. arXiv: 1907.05892 [hep-ph].

[167] Kirill Boguslavski and Asier Piñeiro Orioli. "Unraveling the nature of universal dynamics in $O(N)$ theories." In: *Phys. Rev. D* 101.9 (2020), p. 091902. DOI: 10.1103/PhysRevD.101.091902. arXiv: 1911.04506 [hep-ph].

[168] K. Boguslavski, A. Kurkela, T. Lappi, and J. Peuron. "Spectral function for overoccupied gluodynamics from real-time lattice simulations." In: *Phys. Rev. D* 98.1 (2018), p. 014006. DOI: 10.1103/PhysRevD.98.014006. arXiv: 1804.01966 [hep-ph].

[169] K. Boguslavski, A. Kurkela, T. Lappi, and J. Peuron. "Heavy quark diffusion in an overoccupied gluon plasma." In: *JHEP* 09 (2020), p. 077. DOI: 10.1007/JHEP09(2020)077. arXiv: 2005.02418 [hep-ph].

[170] Jorge Casalderrey-Solana and Derek Teaney. "Transverse Momentum Broadening of a Fast Quark in a N=4 Yang Mills Plasma." In: *JHEP* 04 (2007), p. 039. DOI: 10.1088/1126-6708/2007/04/039. arXiv: hep-th/0701123.

[171] Aleksi Kurkela and Yan Zhu. "Isotropization and hydrodynamization in weakly coupled heavy-ion collisions." In: *Phys. Rev. Lett.* 115.18 (2015), p. 182301. DOI: 10.1103/PhysRevLett.115.182301. arXiv: 1506.06647 [hep-ph].

[172] Mark C. Abraao York, Aleksi Kurkela, Egang Lu, and Guy D. Moore. "UV cascade in classical Yang-Mills theory via kinetic theory." In: *Phys. Rev. D* 89.7 (2014), p. 074036. DOI: 10.1103/PhysRevD.89.074036. arXiv: 1401.3751 [hep-ph].

[173] Bjoern Schenke, Michael Strickland, Adrian Dumitru, Yasushi Nara, and Carsten Greiner. "Transverse momentum diffusion and jet energy loss in non-Abelian plasmas." In: *Phys. Rev. C* 79 (2009), p. 034903. DOI: 10.1103/PhysRevC.79.034903. arXiv: 0810.1314 [hep-ph].

[174] Stanislaw Mrowczynski. "Heavy Quarks in Turbulent QCD Plasmas." In: *Eur. Phys. J. A* 54.3 (2018), p. 43. DOI: 10.1140/epja/i2018-12478-5. arXiv: 1706.03127 [nucl-th].

[175] Andreas Ipp, David I. Müller, and Daniel Schuh. "Jet momentum broadening in the pre-equilibrium Glasma." In: *Phys. Lett. B* 810 (2020), p. 135810. DOI: 10.1016/j.physletb.2020.135810. arXiv: 2009.14206 [hep-ph].

[176] Andreas Ipp, David I. Müller, and Daniel Schuh. "Anisotropic momentum broadening in the 2+1D Glasma: analytic weak field approximation and lattice simulations." In: *Phys. Rev. D* 102.7 (2020), p. 074001. DOI: 10.1103/PhysRevD.102.074001. arXiv: 2001.10001 [hep-ph].

[177] Margaret E. Carrington, Alina Czajka, and Stanislaw Mrowczynski. "Heavy Quarks Embedded in Glasma." In: *Nucl. Phys. A* 1001 (2020), p. 121914. DOI: 10.1016/j.nuclphysa.2020.121914. arXiv: 2001.05074 [nucl-th].

[178] Andrey V. Sadofyev, Matthew D. Sievert, and Ivan Vitev. "Ab Initio Coupling of Jets to Collective Flow in the Opacity Expansion Approach." In: (Apr. 2021). arXiv: 2104.09513 [hep-ph].

[179] Jacopo Ghiglieri, Juhee Hong, Aleksi Kurkela, Egang Lu, Guy D. Moore, and Derek Teaney. "Next-to-leading order thermal photon production in a weakly coupled quark-gluon plasma." In: *JHEP* 05 (2013), p. 010. DOI: 10.1007/JHEP05(2013)010. arXiv: 1302.5970 [hep-ph].

[180] Jacopo Ghiglieri, Guy D. Moore, and Derek Teaney. "Jet-Medium Interactions at NLO in a Weakly-Coupled Quark-Gluon Plasma." In: *JHEP* 03 (2016), p. 095. DOI: 10.1007/JHEP03(2016)095. arXiv: 1509.07773 [hep-ph].

[181] Jacopo Ghiglieri and Derek Teaney. "Parton energy loss and momentum broadening at NLO in high temperature QCD plasmas." In: *Int. J. Mod. Phys. E* 24.11 (2015). Ed. by Xin-Nian Wang, p. 1530013. DOI: 10.1142/S0218301315300131. arXiv: 1502.03730 [hep-ph].

[182] R. Baier, Yuri L. Dokshitzer, S. Peigne, and D. Schiff. "Induced gluon radiation in a QCD medium." In: *Phys. Lett. B* 345 (1995), pp. 277–286. DOI: 10.1016/0370-2693(94)01617-L. arXiv: hep-ph/9411409.

[183] R. Baier, Yuri L. Dokshitzer, Alfred H. Mueller, S. Peigne, and D. Schiff. "Radiative energy loss and p(T) broadening of high-energy partons in nuclei." In: *Nucl.*

Phys. B 484 (1997), pp. 265–282. DOI: 10.1016/S0550-3213(96)00581-0. arXiv: hep-ph/9608322.

[184] R. Baier, Yuri L. Dokshitzer, Alfred H. Mueller, S. Peigne, and D. Schiff. "Radiative energy loss of high-energy quarks and gluons in a finite volume quark - gluon plasma." In: *Nucl. Phys. B* 483 (1997), pp. 291–320. DOI: 10.1016/S0550-3213(96)00553-6. arXiv: hep-ph/9607355.

[185] B. G. Zakharov. "Fully quantum treatment of the Landau-Pomeranchuk-Migdal effect in QED and QCD." In: *JETP Lett.* 63 (1996), pp. 952–957. DOI: 10.1134/1.567126. arXiv: hep-ph/9607440.

[186] B. G. Zakharov. "Radiative energy loss of high-energy quarks in finite size nuclear matter and quark - gluon plasma." In: *JETP Lett.* 65 (1997), pp. 615–620. DOI: 10.1134/1.567389. arXiv: hep-ph/9704255.

[187] R. Baier, Yuri L. Dokshitzer, Alfred H. Mueller, and D. Schiff. "Medium induced radiative energy loss: Equivalence between the BDMPS and Zakharov formalisms." In: *Nucl. Phys. B* 531 (1998), pp. 403–425. DOI: 10.1016/S0550-3213(98)00546-X. arXiv: hep-ph/9804212.

[188] Urs Achim Wiedemann. "Gluon radiation off hard quarks in a nuclear environment: Opacity expansion." In: *Nucl. Phys. B* 588 (2000), pp. 303–344. DOI: 10.1016/S0550-3213(00)00457-0. arXiv: hep-ph/0005129.

[189] Simon Caron-Huot and Charles Gale. "Finite-size effects on the radiative energy loss of a fast parton in hot and dense strongly interacting matter." In: *Phys. Rev. C* 82 (2010), p. 064902. DOI: 10.1103/PhysRevC.82.064902. arXiv: 1006.2379 [hep-ph].

[190] Miklos Gyulassy and Xin-nian Wang. "Multiple collisions and induced gluon Bremsstrahlung in QCD." In: *Nucl. Phys. B* 420 (1994), pp. 583–614. DOI: 10.1016/0550-3213(94)90079-5. arXiv: nucl-th/9306003.

[191] M. Gyulassy, P. Levai, and I. Vitev. "Reaction operator approach to nonAbelian energy loss." In: *Nucl. Phys. B* 594 (2001), pp. 371–419. DOI: 10.1016/S0550-3213(00)00652-0. arXiv: nucl-th/0006010.

[192] Simon Wicks. “Up to and beyond ninth order in opacity: Radiative energy loss with GLV.” In: (Apr. 2008). arXiv: 0804.4704 [nucl-th].

[193] Nestor Armesto, Carlos A. Salgado, and Urs Achim Wiedemann. “Medium induced gluon radiation off massive quarks fills the dead cone.” In: *Phys. Rev. D* 69 (2004), p. 114003. DOI: 10.1103/PhysRevD.69.114003. arXiv: hep-ph/0312106.

[194] Xin-Nian Wang and Xiao-feng Guo. “Multiple parton scattering in nuclei: Parton energy loss.” In: *Nucl. Phys. A* 696 (2001), pp. 788–832. DOI: 10.1016/S0375-9474(01)01130-7. arXiv: hep-ph/0102230.

[195] Xiao-feng Guo and Xin-Nian Wang. “Multiple scattering, parton energy loss and modified fragmentation functions in deeply inelastic e A scattering.” In: *Phys. Rev. Lett.* 85 (2000), pp. 3591–3594. DOI: 10.1103/PhysRevLett.85.3591. arXiv: hep-ph/0005044.

[196] Abhijit Majumder. “Incorporating Space-Time Within Medium-Modified Jet Event Generators.” In: *Phys. Rev. C* 88 (2013), p. 014909. DOI: 10.1103/PhysRevC.88.014909. arXiv: 1301.5323 [nucl-th].

[197] Kuang-chao Chou, Zhao-bin Su, Bai-lin Hao, and Lu Yu. “Equilibrium and Nonequilibrium Formalisms Made Unified.” In: *Phys. Rept.* 118 (1985), pp. 1–131. DOI: 10.1016/0370-1573(85)90136-X.

[198] Jacopo Ghiglieri, Aleksi Kurkela, Michael Strickland, and Aleksi Vuorinen. “Perturbative Thermal QCD: Formalism and Applications.” In: *Phys. Rept.* 880 (2020), pp. 1–73. DOI: 10.1016/j.physrep.2020.07.004. arXiv: 2002.10188 [hep-ph].

[199] Sangyong Jeon. “The Boltzmann equation in classical and quantum field theory.” In: *Phys. Rev. C* 72 (2005), p. 014907. DOI: 10.1103/PhysRevC.72.014907. arXiv: hep-ph/0412121.